

Functional “Backpacks” for Cellular Engineering

by

ALBERT JOSEPH SWISTON JR.

Bachelor of Science, Materials Science and Engineering
Johns Hopkins University, 2005

Masters of Science in Engineering, Materials Science and Engineering
Johns Hopkins University, 2005

Submitted to the Department of Materials Science and Engineering
in partial fulfillment of the requirements for the degree of

DOCTOR OF PHILOSOPHY IN MATERIALS SCIENCE AND ENGINEERING
at the
MASSACHUSETTS INSTITUTE OF TECHNOLOGY

June 2010

© Massachusetts Institute of Technology, 2010. All rights reserved.

Signature of Author: _____
Department of Materials Science and Engineering
April 29, 2010

Certified by: _____
Michael F. Rubner
TDK Professor of Materials Science and Engineering
Thesis Co-Advisor

Certified by: _____
Robert E. Cohen
St. Laurent Professor of Chemical Engineering
Thesis Co-Advisor

Accepted by: _____
Christine Ortiz
Associate Professor of Materials Science and Engineering
Chair, Departmental Committee on Graduate Students

Functional “Backpacks” for Cellular Engineering

by

ALBERT JOSEPH SWISTON JR.

Submitted to the Department of Materials Science and Engineering
On April 29th, 2010 in partial fulfillment of the requirements for the degree of
Doctor of Philosophy in Materials Science and Engineering

ABSTRACT

Polymer multilayers may be built through the sequential (“layer-by-layer”) adsorption of species (polymers, nanoparticles) with specific interactions (electrostatic, hydrogen-bonding). Multilayered heterostructures – films comprised of multiple lamellar regions or strata, each of which consisting of several bilayers of electrostatically complexed or hydrogen-bonded materials – may be assembled and patterned into precise geometries. These heterostructures maintain the functions and capabilities of each lamellar region, and thus complex, stimuli-responsive films with multiple functionalities may be fabricated and patterned with high fidelity.

This thesis describes a method to fabricate such heterostructured devices for single-cell functionalization. These devices may be attached to the surface of living immune system cells, conferring new functions without impairing native cellular behaviors.

The first part of this thesis focuses on the techniques to create a heterostructured backpack. Photolithographic methods were developed to geometrically pattern multilayer films into a desired size and shape. A host of polymer multilayer systems labile at physiologically relevant pH’s were built and tested as a way to release the backpack from its fabrication substrate. Therapeutically and diagnostically interesting materials, such as magnetic nanoparticles, biodegradable polymers, and quantum dots were built into the backpack’s payload region. Finally, a film that non-cytotoxically adheres the backpack to the cell surface was developed and optimized as the cell-adhesive region.

How backpack attachment affect native cell behavior is of utmost importance. Backpack attachment was found to be non-cytotoxic to B lymphocytes, and T cells were still able to migrate on ICAM-coated surfaces. Backpacks could be made with specific chemistries that could activate desirable cell behavior, such as activating dendritic cells, which demonstrates that backpacks need not be passive objects but rather actively engage with the attached cell to create hybrid bio-synthetic devices.

The last part of this thesis describes how backpacks can be used as functional phagocytosis-resistant particles that may be used to increase *in vivo* circulation time or functionalize phagocytic cells. This presents exciting opportunities for immunoen지니어ing applications, such as using immune cells to invade solid tumors and deliver cytotoxic payloads.

Thesis Supervisors: Michael F. Rubner and Robert E. Cohen
Respective Titles: TDK Professor of Materials Science and Engineering, St. Laurent
Professor of Chemical Engineering

Acknowledgments

I am deeply grateful to my thesis advisors Prof. Michael Rubner and Prof. Robert Cohen. Both have been invaluable sources of guidance and support during my time at MIT, and I have benefited a great deal academically and professionally by being a part of their research groups. The opportunity to work with two of the most talented scientists at MIT has been an incredible opportunity that I cannot fully appreciate now. I am also indebted for the advice and guidance of Prof. Darrell Irvine, without whom this work would have never gotten off the ground. Every discussion with Prof. Irvine led to great insights and moved this project forward by leaps and bounds. I also thank Prof. Hamad-Schifferli, my final thesis committee member, for valuable discussions and suggestions.

Great advisors attract great groups, and I owe a great deal of gratitude to my incredibly talented colleagues and lab mates in the Rubner, Cohen, and Irvine groups. In particular, I would like to thank Jungsang Doh, Andy Miller, Ryan Bennett, Zhizhong Wu, Xiaoxia Sheng, Solar Olugebefola, Daeyeon Lee, Jenny Lichter, Anna Bershteyn, Hiroomi Shimomura, Soong Ho Um, Mike Tambe, Wui Siew Tan, Gary Chia, Zekeriyya Gemici, Erik Williamson, and Jon Gilbert. The Rubner Group has had the incredible opportunity to collaborate with the Beppu Group in the Department of Thermofluidynamics, State University of Campinas, Campinas, Brasil. I have had the great fortune of working with Prof. Marisa Beppu, Grinia Nogueira, and Fernando C. Vasconcellos on much of the all-biopolymer multilayer work. Finally, we have had the opportunity to begin a very fruitful collaboration with the Mitragotri Group at the University of California at Santa Barbara – I thank Nishit Doshi for sharing his time and talents for the phagocytosis-resistant particle work.

MIT offers a wealth of resources to students, and I acknowledge the Center for Materials Science and Engineering (CMSE) Shared Experimental Facilities, and the Institute for Soldier Nanotechnology for use of their equipment. The research in this thesis was made possible by the DuPont-MIT Alliance (first year Presidential Fellowship), the CMSE as part of a NSF MRSEC program, and a NSF Graduate Research Fellowship.

Additionally, I thank the undergraduate students I've had the opportunity to work with: Kimberly Kam, Lindsay Wilhelmus, Kathy Tompkins, and Connie Cheng. In particular, Connie was a driving force at the early stages of this project, and I am incredibly fortunate to have had such talent on the team.

I co-founded the MIT Science Policy Initiative (SPI) during my stay at MIT, and have had the chance to work alongside some of the most talented young scientists interested in public policy. Countless Science Policy "Bootcamps" and Congressional Visits were enjoyed with Gerry Ostheimer, Wayne Blaylock, Scott Carlson, Bridget Dolan, Dina Faddah, Anna Bershteyn, Megan Palmer, Mike Henninger, and Megan Brewster. An enormous debt of gratitude goes to Bill Bonvillian, the MIT DC Office Director – not

only has his wisdom and guidance made SPI possible, but he has also been an enormous source of insight and personal support. While brought together over our interest in the intersection of policy and science, I count everyone in SPI as close friends.

I thank Jei Lee Friedman, Dianne Brooks, Jessica Landry, Susan Rosevear, Susan Dalton, Karyn Jones, and Ed Kruzel for administrative support and keeping me out of trouble. I also thank Angelita Mireles in the DMSE office for all the advice and guidance over the years.

I also want to acknowledge my advisors at Johns Hopkins who encouraged me to embark on the graduate school journey in the first place: Tim Weihs, Todd Hufnagel, and Hai-Quan Mao. Thank you for the opportunity to begin my science career and the advice on how to continue it.

Above all, I value the friendships I've made in the past few years, which have gotten me through thick and thin. Many of my closest friends I've met through The Most Informal Running Club Ever (TMIRCE), which seems to attract some of the best folks from in and around Cambridge. Thanks to JP Lewicke and Tree Bernstein for many a potluck; Chris Collins for late night runs and the most hyperbolic stories; Rich Whitcomb for inviting folks to TMIRCE events; and Carol Powers for always a good story and a good laugh. Zach Einterz, Tim Connelly, Evan Dana, Brian Fallik, Lora Reams, Ryan McMahon: you all really made Boston home.

I especially thank Adriane Musgrave for her unending support and kindness. I could not have made it without you.

Last, I acknowledge the support and love from my family, now and always. To my parents, Albert "Big Al" Sr. and Nancy, I am ever grateful for the wisdom, patience, and love you've given over the years. This thesis may finally be the last "Board of Review." I thank my sister Colleen and my brother-in-law Bryan for all their good advice and support. I also thank my grandfather Albert Feehely for showing Colleen and me more love than either of us could appreciate at the time.

I dedicate this thesis to Linda Trinh, a life so full of promise and so tragically cut short.

Table of Contents

List of Figures	7
List of Tables.....	15
Chapter 1: Introduction and Background.....	17
Motivation	17
Cellular Surface Modification and Bio-hybrid Materials.....	17
Patterned Polymer Multilayers as Cellular “Backpacks”	20
Introduction to Polymer Multilayer Assemblies	22
Attaching Backpacks to Cellular Surfaces	25
Cellular Backpack Applications.....	26
Thesis Scope.....	29
References.....	32
Chapter 2: Backpack Fabrication and Multilayer Systems Developed	36
Overview of Fabrication Methods	36
Photolithographic Fabrication	37
Hydrogen-bonded Polymer Multilayer Release Regions	41
(PAA / PEG).....	45
(PMAA / PEG).....	47
(PMAA / PVPON).....	47
(PMAA / PNIPAAm).....	49
(PMAA / PVCL)	51
Composition of a Released Backpack’s Outer Face.....	52
Rhodamine-labeled PMAA Release Regions.....	53
XPS analysis of the Backpack’s Outer Face	55
Barriers Against Polycation Diffusion	58
Conclusions on the Composition of the Backpack’s Outer Face.....	58
Payload Regions	60
Poly(allylamine hydrochloride) (PAH) / Magnetic Nanoparticle (MNP) Regions....	60
Quantum Dot Payloads.....	61
Payloads containing Poly(lactic-co-glycolic acid) (PLGA)	63
Cell-Adhesive Regions.....	67
Conclusions	73
Experimental Details	75
References.....	81
Chapter 3: Cellular Behavior with Attached Backpacks	84
Introduction.....	84
Backpack Attachment to Cell Surfaces	85
CH27 B Lymphocyte Cytotoxicity and CD44 Migration	87
HuT78 T Lymphocyte Migration.....	91
Magnetic Manipulation of B cells.....	94
DC2.4 Dendritic Cell Activation	95
Conclusions	99
Experimental Details	101
References.....	104

Chapter 4: Cellular Aggregation Behavior Led by Freely Suspended Backpacks	105
.....	
Introduction	105
Flow Cytometry and Confocal Microscopy Studies	108
Laser Diffraction Studies	116
Nylon Mesh Filtering: A Model for Extravasation	119
Conclusions	121
Experimental Details	122
References	125
Chapter 5: All-Biopolymer Multilayer Systems	127
HA/CHI Multilayers	127
Multilayer Assembly.....	130
CH27 B-Cell Binding.....	131
Lymphocyte Binding to PEM Arrays.....	133
Determination of HA Carboxylates and CHI Amines.....	139
Quartz Crystal Microbalance.....	142
Discussion on HA/CHI Multilayers.....	145
Conclusions and Future Work on HA/CHI Multilayers.....	148
CMC/CHI Multilayers	149
Growth Behavior and Crosslinking.....	151
Hydrophilicity and Mechanical Robustness.....	152
Transparency of CMC/CHI Films.....	154
Conclusions and Future Work on CMC/CHI films.....	155
ALG/CHI Multilayers	156
Atomic Force Microscopy (AFM).....	157
Conclusions and Future Work on CHI/ALG Films.....	157
Conclusions	160
Experimental Details	161
References	166
Chapter 6: Cellular Backpacks as Functional Phagocytosis-Resistant Materials	169
.....	
Phagocytosis-Resistance by Dendritic Cells	171
Phagocytosis-Resistance by Macrophages	173
Conclusions	176
Experimental Details	178
References	180
Chapter 7: Summary and Future Work	181
Thesis Summary	181
Future Research Directions	183
References	188
Appendix A: Photolithography Photomask Designs	189
Appendix B: Batch ID Definitions	192

List of Figures

Chapter 1

- Figure 1.1: Prior surface modification techniques – primarily encapsulation – focused on coating the entire surface of one or more cells with a protective coating, allowing nutrients and stimuli across the barrier while precluding immune system components from de-activating the cells. From Reference 3. 18
- Figure 1.2: Schematic of a model backpack system still attached to the fabrication substrate (typically a glass slide). Here, x is controlled by the photolithographic mask used during patterning, and is commonly 7, 10, or 15 μm . This profile view shows clearly delineated regions for illustrative simplicity, whereas the multilayering process produces highly interdigitated interfaces. 22
- Figure 1.3: Schematic of the multilayer film deposition process, for the specific case of a polyelectrolyte multilayer film. Adapted from Reference 55. 24
- Figure 1.4: Illustrations of two hydrogen-bonding systems, showing an individual hydrogen-bond crosslink between the two polymers. This illustration shows the hydrogen-bond between the hydrogen-bond acceptor and the labile, carboxylic acid proton serving as a hydrogen bond donor. At a sufficiently high pH, this proton will dissociate and compromise the crosslink. 25
- Figure 1.5: Schematics of the two methods developed to attach backpacks to a cell's surface. (a) shows the case in which backpacks are released from the fabrication substrate prior to cell exposure. The resulting colloidal backpacks are then free to attach to one or more cells, though only the one backpack per cell case is illustrated. (b) shows how cells were attached to backpacks, then released by dropping the temperature to 4°C. 27

Chapter 2

- Figure 2.1: (a) Ideal POPS result in which only the multilayer film on top of the PDMS posts is transferred onto the stamped substrate. These 5 μm backpacks are the following (starting from the stamped substrate, *not* the deposition order): (PAH4.0/SPS4.0)₅(PAAm3.0/PAA3.0)_{10.5}(FITC-PAH7.5/PAA3.5)₃. Scale bar = 20 μm . (b) The more common case found after POPS, in which the film does not effectively tear at each feature. The film is identical to (a). Scale bar = 100 μm 37
- Figure 2.2: Schematic of the photolithography technique used to fabricate multilayered, multi-region backpacks. 38
- Figure 2.3: Release behavior for the following heterostructure: (PAA3/20kMW-PEG3) _{x .5}(PAH3.0/SPS3.0)_{9.5}(HA3.0/FITC-CHI)_{3.5}. The thickness value (as determined by ellipsometry) as a function of x bilayers describes just the

PAA/PEG release region. The line connecting the thickness data is a liner regression; the line connecting lift-off data is a guide for the eye.	45
Figure 2.4: Timecourse of backpack liftoff as a function of salt concentration. PBS contains ~150mM NaCl. As the concentration of salt increases, the hydrogen-bonded system is stabilized, and requires more time to dissolve and release the backpack.	46
Figure 2.5: Release behavior for the following heterostructure: (PMAA3.0/100kDa-PEG3) _{x.5} (FITC-PAH3.0/SPS3.0) ₁₀ . The thickness value (as determined by ellipsometry) as a function of <i>x</i> bilayers describes just the PMAA/PEG release region. The line connecting the thickness data is a liner regression; the line connecting lift-off data is a guide for the eye.	47
Figure 2.6: Release behavior for the following heterostructure: (PMAA2/PVPON2) _{x.5} (FITC-PAH3.0/MNP4.0) ₁₀ with 100kDa PMAA and 1.3MDa PVPON. The thickness value as a function of <i>x</i> bilayers describes just the PMAA/PVPON release region. Due to film roughness, thickness values were determined by profilometry. The line connecting the thickness data is a liner regression; the line connecting lift-off data is a guide for the eye.	48
Figure 2.7: Time course of backpack liftoff for a (PMAA2/PVPON2) _{40.5} release region. Most backpacks are released in the first few minutes of neutral solution exposure, with nearly 100% detached from the substrate in 30 minutes.	49
Figure 2.8: Release behavior at room temperature for the following heterostructure: (PMAA3.0/PNIPAAm3.0) _{x.5} (FITC-PAH3.0/ Fe ₃ O ₄ NP4.0) ₁₀ . The thickness value as a function of <i>x</i> bilayers describes just the PMAA/PNIPAAm release region. The line connecting the thickness data is a liner regression; the line connecting lift-off data is a guide for the eye.	50
Figure 2.9: Temperature-induced release behavior for (PMAA3.0/PNIPAAm3.0) _{80.5} (FITC-PAH3.0/ Fe ₃ O ₄ NP4.0) ₁₀ . The onset of release is seen ~28°C, close to the LCST reported for homopolymer PNIPAAm in PBS (29.1°C) ^{16,22}	50
Figure 2.10: Schematic of the pH and temperature conditions require for film release. The assembly, attachment, and release conditions are shown.	51
Figure 2.11: Growth curves for (PMAA2/PVCL2) _{x.5} for 100kDa PMAA and 354kDa PVCL. No PVCL-based film was found to release a backpack from the surface in pH 7.4 conditions.	52
Figure 2.12: Schematic of the variable position Rhod-PMAA multilayers used to test if the release region is included in the final released backpack. The small number to the left of the diagram is the bilayer number.	54
Figure 2.13: CLSM images of released backpacks that contained Rhod-PMAA in the release region (see Figure 2.12). Both Rhod and FITC signals are seen,	

indicating that indeed the release region does remain attached to the released backpack. Scale bar is 10 μ m.....	54
Figure 2.14: XPS spectra and atomic percentages for a flipped (PAA3.0/PEG-SH3.0) _{20.5} (PAH3.0/MNP4.0) ₁₀ film. The peaks for C, N, O, and S are as indicated – all other peaks are due to residual salt from PBS. Inset shows the S peak at 168eV. Images courtesy Jonathan Gilbert.....	56
Figure 2.15: XPS spectra of an as-deposited (PAA3.0/PEG3.0) _{20.5} and flipped (PAA3.0/PEG3.0) _{20.5} (PAH3.0/MNP4.0) ₁₀ film. PAA’s carboxylic acid C peak in the flipped backpack film shifts to lower binding energy as would be expected when paired with an amine. PEG’s C peak also significantly shrinks in the flipped sample, suggesting the ejection of PEG upon PAH diffusing in and disrupting the former PAA-PEG hydrogen bonds. Data courtesy Jonathan Gilbert.	57
Figure 2.16: Growth profile of (PAH3.0/MNP4.0) _x , where x is the number of bilayers deposited on top of (PDAC4.0/SPS4.0) ₁₆	60
Figure 2.17: CLSM images of (PMAA3.0/PNIPAAm3.0) _{20.5} (AminoQD5.0/SPS5.0) ₃₀ (PAH4.0/MNP4.0) ₁₀ (CHI3.0/HA3.0) ₃ backpacks. These backpacks show fluorescence emission at 600nm, indicating that the quantum dots are incorporated and active. Scale bar is 50 μ m.	61
Figure 2.18: CLSM images of (PMAA3.0/PNIPAAm3.0) _{20.5} (AminoQD5.0/SPS5.0) ₃₀ (PAH4.0/MNP4.0) ₁₀ (CHI3.0/HA3.0) ₃ backpacks that have lifted off from the fabrication substrate. These backpacks were collected to one part of the dish with a rare earth magnet before imaging, indicating that the MNP region is also functional. Scale bar is 20 μ m.	62
Figure 2.19: CLSM images of (PMAA3.0/PNIPAAm3.0) _{20.5} (AminoQD5.0/SPS5.0) ₃₀ (PAH4.0/MNP4.0) ₁₀ (CHI3.0/HA3.0) ₃ backpacks on the surface of a CH27 B cell. Scale bar is 20 μ m.	63
Figure 2.20: Illustration of poly(lactic-co-glycolic acid) (PLGA).....	63
Figure 2.21: Growth profile of sprayed PLGA using the air brush method.....	65
Figure 2.22: Fluorescence image of DOX-containing PLGA backpacks. DOX fluoresces in the rhodamine channel. Scale bar is 20 μ m.	66
Figure 2.23: Summary of flow cytometry results of released backpacks of the following composition: (PMAA2.0/PVPON2.0) _{40.5} (PLGA-Rhod6G) ₁ (PAH3.0/MNP4.0) ₁₀ . Backpacks were incubated in pH 7.4 PBS at 37°C and tested at the time points indicated. After 7 days, up to 50% of the Rhod signal was lost (for the 3s spray sample).	67

Figure 2.24: Flow cytometry plot of CH27 B cells exposed to maleimide-tagged Alexa488 (Mal-Alexa). The green curve shows untreated cells, the red curve is untreated cells incubated in Mal-Alexa, and the blue curve is cells treated with TCEP and incubated in Mal-Alexa. 69

Figure 2.25: Illustration of the three heterobifunctional linker molecules used in this work. Each is reactive to both thiol and amine groups. R_1 is the spacer portion of the molecule, each of which is different. R_2 is a sequence of ethylene oxide groups for SM(PEG) and methylene groups for Sulfo-KMUS and SPDP..... 70

Figure 2.26: (a) Optical micrograph of a (HA3.0/PEI5) film exposed to SPDP and SAMSA. The right side of the image was not exposed to SPDP, but was exposed to SAMSA. The SPDP shows a much stronger fluorescence signal, and a clear border delineates the two regions. Scale bar is $200\mu\text{m}$. (b) UV-VIS spectroscopy of (HA3.0/PEI5)-terminated films after treatment with SM(PEG) or KMUS, followed by dyeing with SAMSA. The control was an identical film exposed to SAMSA but not exposed to SM(PEG) or KMUS... 71

Figure 2.27: Optical micrograph of B cells on a KMUS-terminated backpack system that has not yet been thermally released. The array occupancy is only slightly less than that seen in (HA3.0/CHI3.0) systems. Scale bar is $100\mu\text{m}$ 73

Figure 2.28: Illustration of the backpack liftoff efficiency measurement procedure. 78

Chapter 3

Figure 3.1: Schematics of the two methods developed to attach backpacks to a cell's surface. (a) shows the case in which backpacks are released from the fabrication substrate prior to cell exposure. The resulting colloidal backpacks are then free to attach to one or more cells, though only the one backpack per cell case is illustrated. (b) shows how cells were attached to backpacks, then released by dropping the temperature to 4°C 86

Figure 3.2: Viability of immobilized CH27 B cells over 72h following attachment to a backpack. 89

Figure 3.3: Viability of backpack-functionalized CH27 B cells that have been thermally released and cultured. Data courtesy Soong Ho Um. 90

Figure 3.4: Representative (a) brightfield and (b) fluorescence images of a CH27 B cell with fluorescein-labeled CD44. (c) is an overlaid composite of (a) and (b). Note that there does not seem to be any segregation of CD44 to the membrane region associated with the backpack. The scale bar is $10\mu\text{m}$ 91

Figure 3.5: A CLSM micrograph of a HuT78 T-cell with a fluorescent backpack attached. Notice that the backpack does not attach conformally, and seems to curl on the edges. The scale bar is $10\mu\text{m}$ 92

- Figure 3.6: Migration of a HuT 78 model T-cell on an ICAM1 coated cover slip. The cell was observed to travel at $\sim .5\mu\text{m}/\text{min}$ for at least 6 hours, at which point the backpack adsorbed to the cover slip preventing the cell from migrating further. The scale bar is $25\mu\text{m}$ 93
- Figure 3.7: A backpack functionalized B-cell responds to an applied magnetic field. The backpack system used was $(\text{PMAA}2.0/\text{PVPON}2.0)_{40.5}(\text{FITC-PAH}3.0/\text{MNP}4.0)_{10}(\text{CHI}3.0/\text{HA}3.0)_3$. The cell moved $\sim 200\mu\text{m}$ in 11s toward a rare earth magnet placed near the imaging chamber. Because the cell is free-floating in solution, it moves out of the field of focus during the course of imaging. Note that cells without backpacks do not respond to the applied field. 95
- Figure 3.8: AFM images of $(\text{FITC-PAH}3.0/\text{MNP}4.0)_{10}$ multilayers soaked in pH5.0 MES buffer with and without LPS. The LPS-containing buffer images show a much rougher morphology, likely due to adsorbed LPS on the backpack surface. Scale bar = $1\mu\text{m}$ 98
- Figure 3.9: Histograms of (a) CD54, (b) CD80, and (c) CD86 expression on DC2.4 cells following backpack exposure. The orange curve shows expression of each receptor for backpacks with adsorbed LPS. The green and blue curves are soluble LPS and antibody controls, respectively. The red curves show the background fluorescence for untreated cells..... 99

Chapter 4

- Figure 4.1: Schematic of a surface-bound backpack including the composition and deposition method. 109
- Figure 4.2: Confocal microscopy images of ways B cells attached to backpacks using the injectable backpack protocol. (a) shows how a $7\mu\text{m}$ backpack, may attach to several cells, and that (b) each cell may bind to more than one ($15\mu\text{m}$) backpack. Scale bars are $10\mu\text{m}$, and $R=10$ for both aliquots. 110
- Figure 4.3: Confocal microscopy images and flow cytometry plots (FITC vs. FSC) of aggregates formed under different cell to $7\mu\text{m}$ diameter backpack ratios ($R = 10$ to 0.1). A higher magnification view of a cell-backpack aggregate is provided for $R=0.2$. Scale bar is $100\mu\text{m}$ (inset scale bar for $R=0.2$ is $20\mu\text{m}$). 113
- Figure 4.4: Confocal microscopy images and flow cytometry plots (FITC vs. FSC) of aggregates formed under different cell to $15\mu\text{m}$ diameter backpack ratios ($R = 10$ to 0.1). A higher magnification view of a cell-backpack aggregate is provided for $R=3$. Scale bar is $100\mu\text{m}$ (inset scale bar for $R=3$ is $20\mu\text{m}$). 114
- Figure 4.5: Plots summarizing the flow cytometry results in Figure 4.3 and Figure 4.4. The total percentage of FITC^{high} events, which represents an attached backpack, are plotted versus R for (a) $d=7\mu\text{m}$ and (b) $d=15\mu\text{m}$ backpacks. As R increases, the number of cells associated with a backpack monotonically

decreases. The values here probably represent a lower bound of the actual value of cells with backpacks (see text for discussion).....	114
Figure 4.6: Examples of how some $d=15\mu\text{m}$ backpacks curl upon themselves. (a) shows a cylindrical folding, while (b) presents a “tricorne” like shape. Scale bar is $10\mu\text{m}$	115
Figure 4.7: Aggregate size distributions for (a) $d=7\mu\text{m}$ and (b) $d=15\mu\text{m}$ backpacks. These curves show two populations, one centered at $\sim 15\mu\text{m}$ (single CH27 cells) and the other at an increasingly greater diameter depending on R . For $d=7\mu\text{m}$ backpacks, a clear second peak appears at $R=1$; this second peak appears at $R=3$ for $d=15\mu\text{m}$ backpacks. Individual, non-backpacked CH27 cells are shown as the dashed line.....	117
Figure 4.8: Agitation-dependant laser diffraction distributions for $R=0.33$. The curve labeled “Immediately After” is $\sim 10\text{s}$ after agitation began, and “After” is for $>30\text{s}$	117
Figure 4.9: Confocal micrographs showing before and after photos of cellular aggregates for various values of R . Scale bar is $100\mu\text{m}$	118
Figure 4.10: Confocal microscopy images of aggregates seen after filtering an $R=.33$, $d=7\mu\text{m}$ aliquot through the indicated mesh pore sizes. As the mesh size decreases, so do the resulting aggregate size.	121

Chapter 5

Figure 5.1: The chemical structures of hyaluronic acid (HA), alginate (ALG, a random copolymer of guluronic and mannuronic acids), carboxymethylcellulose (CMC), and chitosan (CHI).....	128
Figure 5.2: B lymphocyte binding to (a) $(\text{HA}3.0/\text{CHI}3.0)_{3,x}$ and (b) $(\text{HA}5.0/\text{CHI}5.0)_{3,x}$ films, for $x=0$ or 5 . Error bars correspond to the standard error for 7 independent measurements.	132
Figure 5.3: Optical micrographs of B cells adhered to a (a) $(\text{HA}3.0/\text{CHI}3.0)_{3,5}$ film made with 100 mM NaCl (the best lymphocyte binding PEM), (b) $(\text{HA}3.0/\text{CHI}3.0)_{3,0}$ film made with no NaCl (the second best binding motif), and (c) $(\text{HA}3.0/\text{CHI}3.0)_{3,0}$ film made with 100 mM NaCl (least effective binding PEM). Scale bars = $50\mu\text{m}$	133
Figure 5.4: Fluorescent image of a $(\text{MNP}4.0/\text{FITC-PAH}3.0)_{9,5}(\text{CHI}3.0/\text{HA}3.0)_3 + 100\text{ mM NaCl}$ patterned slide. Scale bar = $50\mu\text{m}$	133
Figure 5.5: B lymphocytes arrays on (a) $(\text{CHI}3.0/\text{HA}3.0)_3$ ($\sim 57\%$ occupancy), (b) $(\text{CHI}3.0/\text{HA}3.0)_3 + 100\text{ mM NaCl}$ ($\sim 71\%$ occupancy), (c) $(\text{CHI}3.0/\text{HA}3.0)_{3,5}$ ($\sim 54\%$ occupancy), and (d) $(\text{CHI}3.0/\text{HA}3.0)_{3,5} + 100\text{ mM NaCl}$ ($\sim 56\%$ occupancy) after 1 hr of agitation and incubation. Scale bars = $50\mu\text{m}$	134
Figure 5.6: (a) B lymphocyte arrays on $(\text{CHI}3.0/\text{HA}3.0)_3 + 100\text{ mM NaCl}$ ($\sim 97\%$ occupancy) after 2 hrs of agitation and incubation. (b) B lymphocytes	

adhered non-specifically to a (PDAC4/SPS4) _{15.5} film, which is the background (i.e., interstitial) surface. Scale bars = 50 μm	135
Figure 5.7: Alcian blue absorbance for (a) (HA3.0/CHI3.0) and (b) (HA5.0/CHI5.0) films normalized by film thickness. The numbers 1 to 4 correspond to films with greatest to the least lymphocyte binding capability.	140
Figure 5.8: Rose bengal absorbance per film thickness for (a) (HA3.0/CHI3.0) and (b) (HA5.0/CHI5.0) films. The numbers 1 to 4 correspond to films with greatest to the least lymphocyte binding capability.	142
Figure 5.9: Raw QCM-D frequency shift and dissipation data for (HA3.0/CHI3.0) films deposited with (a) 0 mM NaCl and, (b) 100 mM NaCl in the polymer solutions.	143
Figure 5.10: (CMC4.0/CHI4.0) thickness vs. number of bilayers for as-deposited and EDC/NHS crosslinked films, as determined by ellipsometry ($n=1.46$).	151
Figure 5.11: Swelling ratio for (CMC4.0/CHI4.0) films as a function of number of bilayers, crosslinking status, and solvent. All films exhibit a monotonic increase in swelling with film thickness, followed by a plateau. Error bars reflect the standard deviation of at least three film measurements.	152
Figure 5.12: Advancing water contact angles for (a) the bare Equalens II material, $\sim 110^\circ$, and (b) (CMC4.0/CHI4.0) ₁₀ , $\sim 5^\circ$ in .5s.....	154
Figure 5.13: Optical transmission behavior of various CMC/CHI films assembled on glass. (a) shows the transmission in dry (CMC/CHI) films, while (b) shows films that had been soaked in distilled water immediately before measurement. Notice that the films show similar or greater transmission than through an uncoated glass slide.	155

Chapter 6

Figure 6.1: Confocal micrographs (with overlaid fluorescence signal from FITC-labeled PAH in the payload region) of backpacks attached to DC2.4 dendritic cells adhered to a polystyrene dish. (a) shows a backpack with an (CHI3.0/HA3.0) _{3.5} cell-adhesive region. (b) does not have an (HA/CHI) outer face and terminates with (PAH/MNP). Scale bars = 10 μm	172
Figure 6.2: Confocal micrographs (with overlaid fluorescence signal from FITC-labeled PAH in the payload region) of backpacks attached to DC2.4 dendritic cells above a PDAC-terminated glass slide. (a) shows backpacks with an (CHI3.0/HA3.0) _{3.5} cell-adhesive region. (b) does not have an (HA/CHI) outer face and terminates with (PAH/MNP). Scale bars = 10 μm	172
Figure 6.3: Select images of a time course; the time from the beginning of imaging is shown in the upper left. These backpacks do not have an (CHI/HA) outer	

face. While the dendritic cell interacts with the backpack, and at times seems to attempt phagocytosis (18 min), the backpack is never internalized. In fact, a backpack (indicated by the arrow) attached to the bottom of the cell (and outside of the confocal image plane), is released at 41 min and picked up again at 57 min. At 83 min, both backpacks are clearly seen on the cell surface. Scale bar = 20 μm 173

Figure 6.4: Scanning-electron micrographs of macrophages exposed to (CHI3.0/HA3.0)₃ coated (a) and (b) 7 μm backpacks and (c) 6 μm PS spheres. These backpacks and spheres were exposed to cells for 3 hours. 174

Figure 6.5: Optical microscopy images showing backpacks exposed to macrophages without being internalized. The arrow at 50min shows the only internalized backpack in the field of view. 175

Figure 6.6: Measurement of how many 7 μm diameter HA-coated backpacks, 6 μm diameter HA-coated spheres, and 6 μm diameter amine-functionalized spheres were internalized by macrophages. 176

Appendix A

Figure A.1: "Swiston Mask 1" design. 189

Figure A.2: "Swiston Mask 2" design. 190

Figure A.3: "Swiston Mask 3" design. 191

Figure A.4: "Swiston Mask 4" design. 191

Figure A.5: "Swiston Mask 5" design. 191

Figure A.6: "Swiston Mask 6" design. 191

List of Tables

Chapter 1

Table 1.1: Possible payloads in polymer multilayers, and the corresponding market or application area.....	28
------------------------------------------------------------------------------------------------------------	----

Chapter 2

Table 2.1: Critical pH values of select hydrogen-bonded polymer multilayer systems. All values from Ref ⁷ unless noted otherwise.	40
Table 2.2: Fluorescent images of backpacks before and after exposure to neutral solution conditions as a function of possessing a (PAH/SPS) diffusion barrier. Images are taken from the same position on the substrate.....	58
Table 2.3: Details on polymer and nanoparticle solutions used.	76

Chapter 5

Table 5.1: Thickness and roughness values of 3-3.5 bilayer HA/CHI films. Each value is the average of 7 independent measurements.....	131
Table 5.2: Quantification of the different cell-attachment scenarios as a function of film deposition conditions and seeding time. Total array occupancy increases with seeding time, but the number of cells off array sites is constant, indicating that off-array attachment is non-specific.	136
Table 5.3: Micrographs of B cells attached to (CHI3.0/HA3.0) ₃ film arrays and the percentage of array occupancy. B cells were found to attach very effectively after 4, 15min incubation/agitation cycles. (The before exposure, soluble HA image is lower than expected because of more vigorous washing than other slides. The identical film washed less vigorously is shown in Figure 5.2). Soluble HA was found to remove cells from the array, while soluble ALG did not: HA reduced array occupancy by 12%, while ALG did not seem to change the occupancy rate.	138
Table 5.4: Micrographs of B cells attached to (CHI3.0/HA3.0) _{3.5} film arrays and the percentage of array occupancy. B cells were found to attach very effectively after 4, 15min incubation/agitation cycles. Soluble HA was found to remove cells from the array, while soluble ALG did not: HA reduced array occupancy by 60%, while ALG did not seem to change the occupancy rate.....	139
Table 5.5: Values for the total thickness contributed by each polymer (t_{HA} or t_{CHI}) and their ratio. Since the density of HA and CHI are nearly equal, t_{HA} or t_{CHI} represent the total amount of each polymer in the final film.....	144

Table 5.6: AFM images of (CHI/ ALG) films assembled under the various conditions indicated. Notice the significant coarsening of the film morphology with exposure to CaCl₂ rinse solutions..... 159

Appendix B

Table B.1: List of Batch IDs and the corresponding multilayer film system built.
..... 195

Chapter 1: Introduction and Background

Motivation

The precise mechanical, spatial, and chemical control of polyelectrolyte multilayer thin films has encouraged their application in a wide variety of fields ranging from optics to biology. In particular, polyelectrolyte multilayers have been heavily used to precisely functionalize surfaces to control adherent cellular growth. However, very little has been done to explore how the enormous tunability of these nanoscale multilayer films could be used to modify cellular functionality by depositing such films *directly on the cellular surface* without occluding the entire cell surface and preventing or inhibiting native cellular behavior. This thesis seeks to demonstrate that synthetic materials, integrated into polymer multilayer assemblies, may be attached to living immune cells without interfering with normal cellular behavior, thus leveraging a biological system's native functions with the therapeutic or diagnostic abilities of synthetic materials.

Cellular Surface Modification and Bio-hybrid Materials

Modifying the cellular membrane has been the object of increasingly intense research efforts¹. The cellular surface is easily accessible for chemical modification, and is an important biological interface that determines how a cell

will interact with its immediate environment. Specifically, the cell surface governs critical events such as cell differentiation, attachment to the extracellular matrix, trafficking to tissues, and communication between cells. Perhaps the first example of directly modifying the surface of living cells is cellular encapsulation, introduced by Chang in 1964². Briefly, one or more cells are coated in a protective polymeric shell that allows for small diffusive stimuli to interact with the cell(s) and therapeutic agents to be released and enter the surrounding environment (see Figure 1.1). However, larger molecules (such as antibodies) and other cells (such as macrophages) are blocked and prevented from deactivating the cellular cargo³. This approach is commonly used to mitigate or eliminate the concomitant immune response after the transplant of xenogeneic cells, such as has been proposed in diabetes therapy^{4,5}. While this approach works well for small, diffusible stimuli and response molecules, this approach necessarily occludes the cell from coming into direct contact with its surroundings, limiting the approach to a small class of therapeutic cell systems.

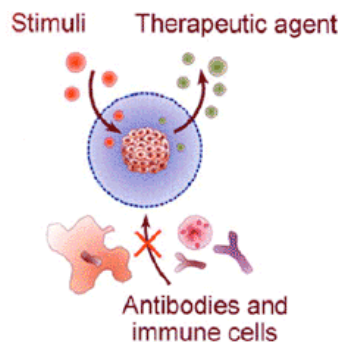


Figure 1.1: Prior surface modification techniques – primarily encapsulation – focused on coating the entire surface of one or more cells with a protective coating, allowing nutrients and stimuli across the barrier while precluding immune system components from de-activating the cells. From Reference 3.

Since the original Cheng concept, several strategies have been developed to attach synthetic materials or non-native moieties to the surface of living cells

without toxicity. These methods include direct reaction of N-hydroxysuccinimide-esters with surface amines⁶⁻⁹, antibody-conjugated nanoparticles^{10,11}, proteins via glycosylphosphatidylinositol (GPI) anchors¹², non-cytotoxic carbon nanotubes¹³, synthetic bioactive polymers^{14,15}, non-native oligosaccharide derivatives¹⁶⁻¹⁸, “click” chemistry¹⁹, and natural protein-based nanocapsules²⁰. All of these applications have biomedical applications in mind, including the earlier, higher-specificity, and more sensitive detection of disease, or the more efficient and lower side effect therapies to address them. The fundamental basis for all of these techniques is the marriage of biological systems synergistically with synthetic (i.e., non-native) materials *without deleteriously influencing the performance of either one*. Even further, some of the above mentioned examples seek to affect desirable cellular responses that would support a therapeutic or diagnostic goal, such as choosing antibodies that activate the immune system¹¹.

In addition to the modification systems mentioned above, polymer multilayer systems (described later) themselves have been used to uniformly coat and functionalize robust uni-cellular species such as bacteria and yeast. Living²¹⁻²⁴ and dead, fixed^{25,26} cells have been investigated, but few studies have sought to combine the multilayering technique with the native behaviors of coated cells.

All of these reports point to the emergence of a new, burgeoning field of “bio-hybrid” materials, in which synthetic materials are functionally integrated with cellular species while leveraging both biological and material properties and behaviors. Synthetic materials systems such as anisotropic microparticles²⁷, muscular thin films²⁸, thermally-responsive films with integrin ligands²⁹, films

capable of sensing and selectively releasing dead cells³⁰, magnetic micromanipulators³¹, and nanoparticulate cellular patches³², have recently been reported offering exciting possibilities for a new class of biomaterials based on the symbiosis between synthetic building blocks and native biological behavior. Motivated by the combination of innate cell functionality with payloads of non-native materials, we pioneered the concept of a cellular “backpack” comprised primarily of polymer multilayer assemblies.

Patterned Polymer Multilayers as Cellular “Backpacks”

Cellular backpacks are nanoscale thickness, micron-sized, photolithographically patterned heterostructured multilayer systems capable of non-cytotoxically attaching to the membrane of a living cell³³. The parallels with spherical microparticles are obvious, but the backpack’s materials, processing, and geometry offer advantages over microparticles. For instance, the precise nanoscale control of thickness³⁴ and mechanical properties³⁵, breadth of materials that may be integrated (including peptides³⁶⁻³⁸, drugs³⁹, and nanoparticles^{33,40}), and ease of processing⁴¹ make multilayer films excellent candidates for a platform synthetic material system for cellular functionalization.

The backpack geometry offers distinct advantages over microparticles. The backpack necessarily has two distinct faces that can contain entirely different functionalities. The burgeoning field of asymmetrically-functionalized (“Janus”) microparticles^{27,42} has begun to enterprise on this “patchiness” for assembly^{43,44} of

colloidal bodies, but only very recently have there been reports of asymmetrically-functionalized cells⁴⁵.

Furthermore, Mitragotri *et al* has shown that the backpack's geometry and aspect ratio itself provides resistance to phagocytic cell internalization⁴⁶⁻⁴⁹. Combining the options for functional materials that can be integrated into a backpack with phagocytosis resistance opens entirely new application possibilities in the fields of sustained drug delivery⁵⁰, chronic therapeutic agent release, and targeted biomedical imaging.

Backpacks are fabricated using an adaptation of the photolithography methods of McShane *et al*^{51,52}, and are covered in much greater detail in Chapter 2 (see page 38). A model backpack system, still attached to the fabrication substrate, is illustrated in Figure 1.2. Three distinct regions comprise the backpack system: a release region, one or more payload regions, and a cell-adhesive face. The release region consists of a hydrogen-bonded multilayer that dissolves above a critical pH (see page 41). Possible payload regions include magnetic nanoparticles, fluorescent polymers, bioresorbable polymers (PLGA), and dyes, and may be incorporated into the backpack by either layer-by-layer deposition or spraying from an organic solvent. The final region anchors the backpack to the surface of the cell, and must be chosen with a specific binding mechanism in mind. Except where noted otherwise, this region always consists of a biopolymer multilayer of chitosan and hyaluronic acid, the latter chosen for being the ligand of the cell surface receptor CD44⁵³. How backpacks are fabricated and detail on possible multilayer systems will be addressed in subsequent chapters.

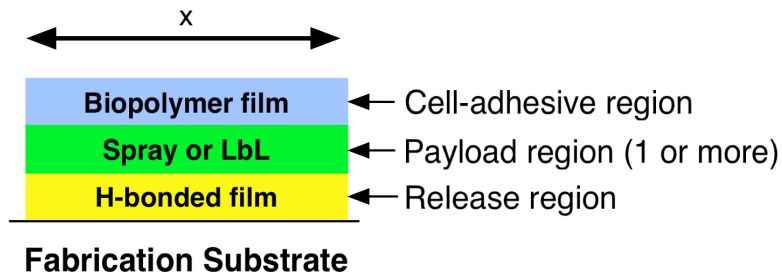


Figure 1.2: Schematic of a model backpack system still attached to the fabrication substrate (typically a glass slide). Here, x is controlled by the photolithographic mask used during patterning, and is commonly 7, 10, or 15 μm . This profile view shows clearly delineated regions for illustrative simplicity, whereas the multilayering process produces highly interdigitated interfaces.

Introduction to Polymer Multilayer Assemblies

Introduced by Decher⁵⁴ in the 1990s, polymer multilayers based on specific interactions offer a simple, aqueous-based deposition method that allows for precise mechanical³⁵, spatial³⁴, and chemical control^{38,55}. The ease of processing, environmentally-friendly aqueous solvent, breadth of materials that may be integrated into the film, and the conformal nature of these coatings make multilayer system ideal candidates for many biological, cell culturing, optical, and thin film applications. The general scheme for multilayer deposition is shown in Figure 1.3. A substrate, commonly glass or silicon, is consecutively submerged in solutions of polymers or nanoparticles with alternating specific interactions. These interactions may include electrostatic, in which case such multilayers are termed polyelectrolyte multilayers (PEMs), hydrogen-bonding⁵⁶, covalent⁵⁷, or hydrophobic interactions⁵⁸. In the case of PEMs, the substrate alternates between solutions of polyanions and polycations (solutions A and B in

Figure 1.3); for hydrogen-bonded multilayers, the substrate alternates between solutions of hydrogen bond donors and acceptors (solutions A and B in Figure 1.3). Between polymer solutions, rinse steps are used to remove loosely adhered polymer chains (i.e., chains that have been phys-adsorbed, rather than electrostatically crosslinked to the previous layer), which affords greater uniformity and mechanical integrity. With each submersion, the adsorbed species overcompensates the surface charge⁵⁹ (in the case of polyelectrolytes) or hydrogen bonding character (donor or acceptor, in the case of hydrogen bonded multilayers), thus providing the ability to adsorb the next species. Each pair of polycation-polyanion or polymeric hydrogen bond donor-acceptor deposited is referred to as a bilayer, and is commonly represented by the following equation:

$$(\textit{Species}_1\textit{X}/\textit{Species}_2\textit{Y})_n$$

where *Species*₁ and *Species*₂ are abbreviations for the polymer, nanoparticle, or small molecule used to build the multilayer, X and Y are the pH of the respective *Species*₁ and *Species*₂ solutions, and *n* is the total number of bilayers in the film. (For *n*=*x*.5, where *x* is any positive integer, this represents a “half” bilayer, where the *Species*₁ solution was the final deposition step.)

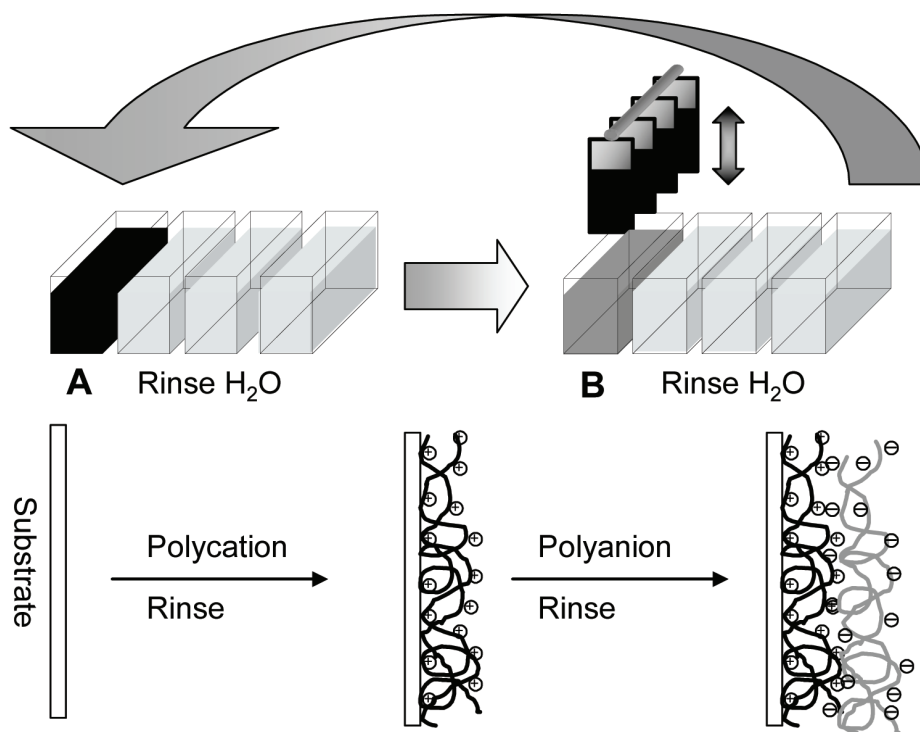


Figure 1.3: Schematic of the multilayer film deposition process, for the specific case of a polyelectrolyte multilayer film. Adapted from Reference 55.

The sequential dip-coating discussed above is a specific example of how multilayer films may be built on a substrate. Spin-coating⁶⁰⁻⁶³ and sequential centrifugation-resuspension^{64,65} techniques have been used to coat flat and colloidal substrates, respectively. While these methods offer some processing advantages to dip-coating, disadvantages include non-conformality (for spin-coating) and manually time-intensive steps (for centrifugation-resuspension).

As mentioned above, there are several different types of specific interactions that may be used to construct a multilayered film. This thesis work makes extensive use of hydrogen-bonded and electrostatically-bonded films. Since the hydrogen-

bonding interaction relies upon the hydrogen bond donating, labile proton in the carboxylic acid group, these films must be assembled at low pH. If an assembled film is exposed to a sufficiently high pH (the “critical pH”), the labile proton will dissociate and compromise the integrity of the film. The film will dissociate and release the constituent polymers into solution. Examples of hydrogen bonds between poly(ethylene oxide) (PEO) and poly(acrylic acid) (PAA), and between poly(N-isopropyl acrylamide) (PNIPAAm) and poly(methacrylic acid) (PMAA), are shown in Figure 1.4. More details on hydrogen-bonded systems may be found in Chapter 2, page 41.

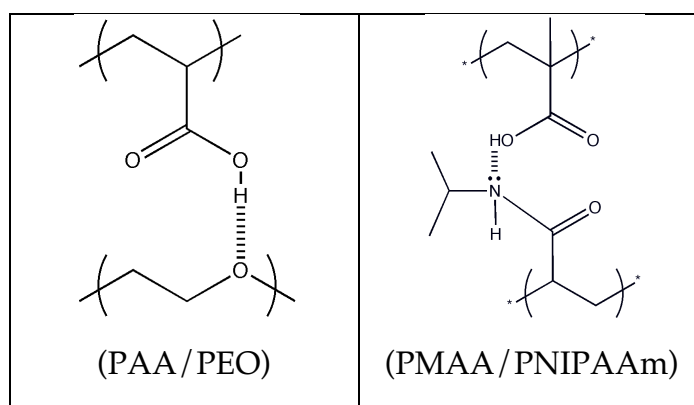


Figure 1.4: Illustrations of two hydrogen-bonding systems, showing an individual hydrogen-bond crosslink between the two polymers. This illustration shows the hydrogen-bond between the hydrogen-bond acceptor and the labile, carboxylic acid proton serving as a hydrogen bond donor. At a sufficiently high pH, this proton will dissociate and compromise the crosslink.

Attaching Backpacks to Cellular Surfaces

Two methods for attaching functional backpacks to cell surfaces were developed (see Figure 1.5) and are summarized here (detailed explanations may be found in Chapter 3, page 85). The fundamental difference between the two methods lies in whether the backpack is released from the fabrication substrate before or after

cell attachment; two different hydrogen-bonded release regions were developed to allow for control over release. Figure 1.5a shows the method where the release region dissolution is based solely on pH, i.e., the release region film is constructed at low pH and deconstructs when exposed to neutral pH conditions. Figure 1.5b shows the method where cells are attached at neutral pH and 37°C, and only upon lowering the temperature (while maintaining pH 7.4) does the release region dissolve. This method requires both pH and temperature triggers for release. Two techniques were developed because of clinical relevance considerations - a backpack system that may be injected into a patient directly (method shown in Figure 1.5a) is much more clinically useful than a system that requires collecting, purifying, and seeding cells, followed by thermal cycling and re-injection (Figure 1.5b).

Cellular Backpack Applications

Cellular backpacks seek to leverage the native functions of cellular systems for new diagnostic or therapeutic treatments. A unique characteristic of the backpack system is that it does not occlude or affect the entire cell surface; therefore, native functions requiring intimate interaction with the environment are possible. An example is attaching backpacks to tumor-infiltrating lymphocytes⁶⁶ that would traffic to cancerous tissue and deliver a diagnostic and/or cytolytic payload. Other immune cells, such as dendritic cells, will traffic to lymph nodes to present antigens to lymphocytes – dendritic cells could carry adjuvants (species that amplify an immune response) in their backpack to create

more effective vaccines at lower antigen doses. Both of these examples require that the cell surface remain accessible to interact with surrounding tissue. The backpack contains a synthetic payload, towed along by the attached cell, thus using normal homing and trafficking behavior to more efficiently place an imaging agent, drug, or adjuvant.

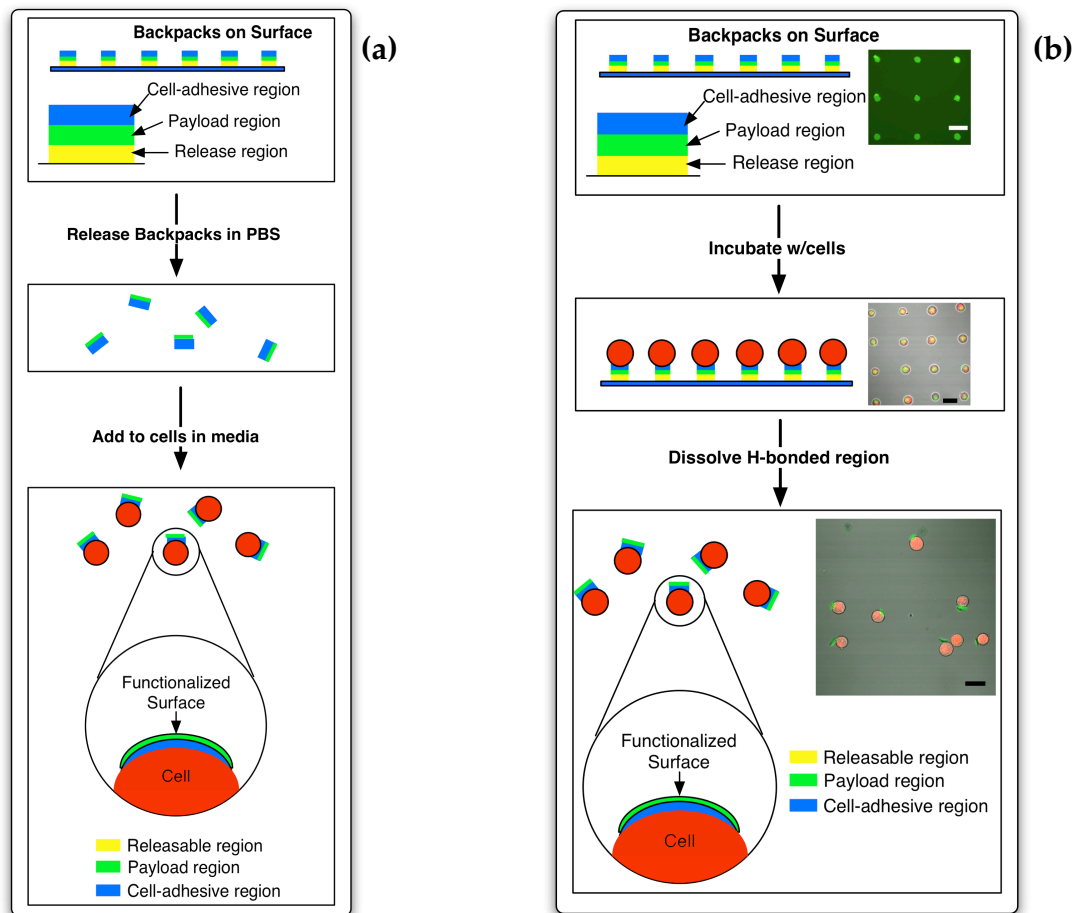


Figure 1.5: Schematics of the two methods developed to attach backpacks to a cell's surface. (a) shows the case in which backpacks are released from the fabrication substrate prior to cell exposure. The resulting colloidal backpacks are then free to attach to one or more cells, though only the one backpack per cell case is illustrated. **(b)** shows how cells were attached to backpacks, then released by dropping the temperature to 4°C.

The backpacks themselves, because of their shape and aspect ratio, seem to be resistant to internalization by phagocytic cells. This ability to bypass a normal

cellular function may itself provide applications for backpacks. Injectable backpacks containing elutable cytotoxic drugs could be introduced into tumors, and sustainably deliver these drugs while eluding clearance by phagocytes. The cell surface receptor CD44 is expressed as very high levels on many types of cancer cells⁶⁷, and the current hyaluronic acid-based cell-adhesion system could be used to attach backpacks to cancerous cells *in vivo*, a method currently being used to attach hydrogel nanoparticles⁶⁸ and prodrugs^{69,70} to CD44⁺ cancerous cells.

Aside from these specific applications, a look at the possible payloads that have been incorporated into polymer multilayers shows the breadth of applications possible for the backpack system (see Table 1.1).

Table 1.1: Possible payloads in polymer multilayers, and the corresponding market or application area.

	<i>Payload</i>	<i>Market</i>
Systems built	Nanoparticles (magnetic, gold, silver)	Bioimaging (MRI), targeting, RF heating, biocidal
	Fluorescent dyes, quantum dots, other contrast agents	Bioimaging by PET, X-ray, luminescence
	Biodegradable polymers (PLGA, PA) with drugs	Drug release: chemotherapy, antibacterial, etc.
Concepts	Chemokines, cytokines, and other immune components	Adoptive immunotherapy
	Antigens and adjuvants	Advanced vaccine therapy

Thesis Scope

This thesis introduces the concept of cellular backpacks, focusing on a particular photolithographic fabrication method of polymer multilayer assemblies. In particular, this work innovated several multilayer systems used to create a backpack. A non-toxic cell attachment method was developed, as well as pH and temperature-responsive films capable of releasing the backpack from the fabrication substrate. Cellular behavior following backpack attachment was investigated, and for the cell lines examined, backpacks were found to be non-toxic and did not interfere with natural cell behaviors. Finally, two specific backpack applications were explored, namely the ability of freely suspended backpacks to encourage reversible cell aggregation, and the unique backpack design which prevents internalization by phagocytes. In total, this thesis work introduces and lays the foundation for a new cell surface modification technique that does not entirely decorate the cell surface, thus allowing the cell to perform native functions requiring intimate environmental contact. A summary of results for each chapter is presented below.

Chapter 2 details the backpack fabrication approach and the new polymer systems developed to produce ultra-thin films with particular functional characteristics. Synthetic therapeutic and diagnostic payloads such as quantum dots, fluorescent and bioresorbable polymers, and nanoparticles were successfully integrated into backpacks that were attached to cells.

Chapter 3 presents how cells respond to attached backpacks. Cytotoxicity is of paramount concern since the backpack system cannot leverage the native

behaviors of the tethered cell if attachment is acutely cytotoxic. Other native behaviors such as migration were investigated, as well as ways to create backpacks that affect desirable phenotypical behaviors.

Chapter 4 presents how cell backpacks, with spatially controlled cellular affinity, can be used to create cellular aggregates of controllable size. The cell/backpack ratio and backpack diameter were found to be dominant variables in determining aggregate size. Applications in lymphoid tissue engineering are discussed.

Chapter 5 examines the all-biopolymer multilayer films built as candidates for backpacks. An obvious requirement for any backpack system is biocompatibility, and biopolymers are a natural material choice. The adhesion between hyaluronic acid-containing PEMs and cell surface CD44 is characterized and systematically optimized in terms of PEM deposition conditions.

Fundamental properties of carboxymethylcellulose/chitosan and alginate/chitosan films were also investigated as potential backpack regions.

Chapter 6 presents preliminary work on backpacks as functional phagocytosis-resistant materials. Collaboration with the Mitragotri group at the University of California at Santa Barbara has led to promising results showing that functional backpacks are resistant to internalization by macrophages. Previous work has provided the design rules for phagocytosis-resistant materials, and cell backpacks are an ideal candidate for functional microparticles that could be used to increase in vivo circulation time or functionalize the surface of phagocytic cell types.

Chapter 7 will summarize and conclude this work, as well as provide suggestions for future research efforts.

References

- (1) Zhao, W.; Teo, G. S. L.; *et al.* Chemistry and material science at the cell surface *Materials Today* **2010**, *13*, 14.
- (2) Chang, T. M. S. Semipermeable Microcapsules *Science* **1964**, *146*, 524.
- (3) Orive, G.; Hernandez, R. M.; *et al.* Cell encapsulation: Promise and progress *Nature Medicine* **2003**, *9*, 104.
- (4) Dove, A. Cell-based therapies go live *Nature Biotechnology* **2002**, *20*, 339.
- (5) Schneider, S.; Feilen, P. J.; *et al.* Multilayer capsules: a promising microencapsulation system for transplantation of pancreatic islets *Biomaterials* **2001**, *22*, 1961.
- (6) Singh, N. P.; Yolcu, E. S.; *et al.* A Novel Approach to Cancer Immunotherapy: Tumor Cells Decorated with CD80 Generate Effective Antitumor Immunity *Cancer Research* **2003**, *63*, 4067.
- (7) Singh, N. P.; Yolcu, E. S.; *et al.* ProtEx: A Novel Technology to Display Exogenous Proteins on the Cell Surface for Immunomodulation *Annals of the New York Academy of Sciences* **2005**, *1056*, 344.
- (8) Kim, H.; Cohen, R. E.; *et al.* Live Lymphocyte Arrays for Biosensing *Advanced Functional Materials* **2006**, *16*, 1313.
- (9) Kim, H.; Doh, J.; *et al.* Large Area Two-Dimensional B Cell Arrays for Sensing and Cell-Sorting Applications *Biomacromolecules* **2004**, *5*, 822.
- (10) Gruttner, C.; Muller, K.; *et al.* Synthesis and antibody conjugation of magnetic nanoparticles with improved specific power absorption rates for alternating magnetic field cancer therapy *Journal of Magnetism and Magnetic Materials* **2007**, *311*, 181.
- (11) Arruebo, M.; Valladares, M.; *et al.* Antibody-Conjugated Nanoparticles for Biomedical Applications *Journal of Nanomaterials* **2009**, *2009*, 24.
- (12) Paulick, M. G.; Bertozzi, C. R. The Glycosylphosphatidylinositol Anchor: A Complex Membrane-Anchoring Structure for Proteins *Biochemistry* **2008**, *47*, 6991.
- (13) Chen, X.; Tam, U. C.; *et al.* Interfacing Carbon Nanotubes with Living Cells *Journal of the American Chemical Society* **2006**, *128*, 6292.
- (14) Rabuka, D.; Forstner, M. B.; *et al.* Noncovalent Cell Surface Engineering: Incorporation of Bioactive Synthetic Glycopolymers into Cellular Membranes *Journal of the American Chemical Society* **2008**, *130*, 5947.
- (15) Wilson, J. T.; Cui, W.; *et al.* Layer-by-Layer Assembly of a Conformal Nanothin PEG Coating for Intraportal Islet Transplantation *Nano Letters* **2008**, *8*, 1940.
- (16) Mahal, L. K.; Yarema, K. J.; *et al.* Engineering Chemical Reactivity on Cell Surfaces Through Oligosaccharide Biosynthesis *Science* **1997**, *276*, 1125.
- (17) Sampathkumar, S.; Li, A. V.; *et al.* Metabolic installation of thiols into sialic acid modulates adhesion and stem cell biology *Nature Chemical Biology* **2006**, *2*, 149.
- (18) Campbell, C. T.; Sampathkumar, S.-G.; *et al.* Metabolic oligosaccharide engineering: perspectives, applications, and future directions *Molecular BioSystems* **2007**, *3*, 187.

- (19) Link, A. J.; Tirrell, D. A. Cell Surface Labeling of Escherichia coli via Copper(I)-Catalyzed [3+2] Cycloaddition *Journal of the American Chemical Society* **2003**, *125*, 11164.
- (20) Kickhoefer, V. A.; Han, M.; *et al.* Targeting Vault Nanoparticles to Specific Cell Surface Receptors *ACS Nano* **2008**, *3*, 27.
- (21) Diaspro, A.; Silvano, D.; *et al.* Single Living Cell Encapsulation in Nano-organized Polyelectrolyte Shells *Langmuir* **2002**, *18*, 5047.
- (22) Germain, M.; Balaguer, P.; *et al.* Protection of mammalian cell used in biosensors by coating with a polyelectrolyte shell *Biosensors and Bioelectronics* **2006**, *21*, 1566.
- (23) Hillberg, A. L.; Tabrizian, M. Biorecognition through Layer-by-Layer Polyelectrolyte Assembly: In-Situ Hybridization on Living Cells *Biomacromolecules* **2006**, *7*, 2742.
- (24) Krol, S.; Nolte, M.; *et al.* Encapsulated Living Cells on Microstructured Surfaces *Langmuir* **2005**, *21*, 705.
- (25) Georgieva, R.; Moya, S.; *et al.* Permeability and Conductivity of Red Blood Cell Templated Polyelectrolyte Capsules Coated with Supplementary Layers *Langmuir* **2004**, *20*, 1895.
- (26) Moya, S.; Dahne, L.; *et al.* Polyelectrolyte multilayer capsules templated on biological cells: core oxidation influences layer chemistry *Colloids and Surfaces A: Physicochemical and Engineering Aspects* **2001**, *183-185*, 27.
- (27) Yoshida, M.; Roh, K. H.; *et al.* Structurally Controlled Bio-hybrid Materials Based on Unidirectional Association of Anisotropic Microparticles with Human Endothelial Cells *Advanced Materials* **2009**, *21*, 4920.
- (28) Feinberg, A. W.; Feigel, A.; *et al.* Muscular Thin Films for Building Actuators and Powering Devices *Science* **2007**, *317*, 1366.
- (29) Ebara, M.; Yamato, M.; *et al.* Temperature-Responsive Cell Culture Surfaces Enable "On-Off" Affinity Control between Cell Integrins and RGDS Ligands *Biomacromolecules* **2004**, *5*, 505.
- (30) Okajima, S.; Sakai, Y.; *et al.* Development of a Regenerable Cell Culture System That Senses and Releases Dead Cells *Langmuir* **2005**, *21*, 4043.
- (31) Kriha, O.; Becker, M.; *et al.* Connection of Hippocampal Neurons by Magnetically Controlled Movement of Short Electrospun Polymer Fibers- A Route to Magnetic Micromanipulators *Advanced Materials* **2007**, *19*, 2483.
- (32) Cheng, H.; Kastrup, C. J.; *et al.* Nanoparticulate Cellular Patches for Cell-Mediated Tumorotropic Delivery *ACS Nano* **2010**, *4*, 625.
- (33) Swiston, A. J.; Cheng, C.; *et al.* Surface Functionalization of Living Cells with Multilayer Patches *Nano Letters* **2008**, *8*, 4446.
- (34) Shiratori, S. S.; Rubner, M. F. pH-Dependent Thickness Behavior of Sequentially Adsorbed Layers of Weak Polyelectrolytes *Macromolecules* **2000**, *33*, 4213.
- (35) Thompson, M. T.; Berg, M. C.; *et al.* Tuning compliance of nanoscale polyelectrolyte multilayers to modulate cell adhesion *Biomaterials* **2005**, *26*, 6836.
- (36) Lvov, Y.; Ariga, K.; *et al.* Molecular film assembly via layer-by-layer adsorption of oppositely charged macromolecules (linear polymer, protein and clay) and concanavalin A and glycogen *Thin Solid Films* **1996**, *285*, 797.
- (37) Lvov, Y.; Ariga, K.; *et al.* Layer-by-Layer Assembly of Alternate Protein Polyion Ultrathin Films *Chemistry Letters* **1994**, 2323.

- (38) Berg, M. C.; Yang, S. Y.; *et al.* Controlling Mammalian Cell Interactions on Patterned Polyelectrolyte Multilayer Surfaces *Langmuir* **2004**, *20*, 1362.
- (39) Berg, M. C.; Zhai, L.; *et al.* Controlled drug release from porous polyelectrolyte multilayers *Biomacromolecules* **2006**, *7*, 357.
- (40) Wu, Z.; Walish, J.; *et al.* Deformable Antireflection Coatings from Polymer and Nanoparticle Multilayers *Advanced Materials* **2006**, *18*, 2699.
- (41) Choi, J.; Rubner, M. F. Influence of the Degree of Ionization on Weak Polyelectrolyte Multilayer Assembly *Macromolecules* **2005**, *38*, 116.
- (42) Li, Z.; Lee, D.; *et al.* Layer-by-Layer Assembled Janus Microcapsules *Macromolecules* **2005**, *38*, 7876.
- (43) Zhang, Z. L.; Glotzer, S. C. Self-Assembly of Patchy Particles *Nano Letters* **2004**, *4*, 1407.
- (44) Glotzer, S. C. Some Assembly Required *Science* **2004**, *306*, 419.
- (45) Koyfman, A. Y.; Braun, G. B.; *et al.* Cell-Targeted Self-Assembled DNA Nanostructures *Journal of the American Chemical Society* **2009**, *131*, 14237.
- (46) Champion, J. A.; Mitragotri, S. Role of target geometry in phagocytosis *Proceedings of the National Academy of Sciences of the United States of America* **2006**, *103*, 4930.
- (47) Champion, J. A.; Katare, Y. K.; *et al.* Particle shape: A new design parameter for micro- and nanoscale drug delivery carriers *Journal of Controlled Release* **2007**, *121*, 3.
- (48) Champion, J. A.; Walker, A.; *et al.* Role of Particle Size in Phagocytosis of Polymeric Microspheres *Pharmaceutical Research* **2008**, *25*, 1815.
- (49) Champion, J. A.; Mitragotri, S. Shape Induced Inhibition of Phagocytosis of Polymer Particles *Pharmaceutical Research* **2009**, *26*, 244.
- (50) Mitragotri, S. In Drug Delivery, Shape Does Matter *Pharmaceutical Research* **2009**, *26*, 232.
- (51) ShaikhMohammed, J.; DeCoster, M. A.; *et al.* Micropatterning of Nanoengineered Surfaces to Study Neuronal Cell Attachment in Vitro *Biomacromolecules* **2004**, *5*, 1745.
- (52) ShaikhMohammed, J.; DeCoster, M. A.; *et al.* Fabrication of Interdigitated Micropatterns of Self-Assembled Polymer Nanofilms Containing Cell-Adhesive Materials *Langmuir* **2006**, *22*, 2738.
- (53) Underhill, C. CD44: the hyaluronan receptor *Journal of Cell Science* **1992**, *103*, 293.
- (54) Decher, G. Fuzzy Nanoassemblies: Toward Layered Polymeric Multicomposites *Science* **1997**, *277*, 1232.
- (55) Berg, M. C., Ph.D. Thesis, Massachusetts Institute of Technology, 2005.
- (56) Sukhishvili, S. A.; Granick, S. Layered, Erasable Polymer Multilayers Formed by Hydrogen-Bonded Sequential Self-Assembly *Macromolecules* **2002**, *35*, 301.
- (57) Zhang, Y.; Yang, S.; *et al.* Fabrication of Stable Hollow Capsules by Covalent Layer-by-Layer Self-Assembly *Macromolecules* **2003**, *36*, 4238.
- (58) Kotov, N. A. Layer-by-layer self-assembly: The contribution of hydrophobic interactions *Nanostructured Materials* **1999**, *12*, 789.
- (59) Schlenoff, J. B.; Dubas, S. T. Mechanism of Polyelectrolyte Multilayer Growth: Charge Overcompensation and Distribution *Macromolecules* **2001**, *34*, 592.

- (60) Cho, J.; Char, K.; *et al.* Fabrication of Highly Ordered Multilayer Films Using a Spin Self-Assembly Method *Advanced Materials* **2001**, *13*, 1076.
- (61) Chiarelli, P. A.; Johal, M. S.; *et al.* Controlled Fabrication of Polyelectrolyte Multilayer Thin Films Using Spin-Assembly *Advanced Materials* **2001**, *13*, 1167.
- (62) Chiarelli, P. A.; Johal, M. S.; *et al.* Polyelectrolyte Spin-Assembly *Langmuir* **2001**, *18*, 168.
- (63) Lee, H.-C.; Lee, T.-W.; *et al.* Fabrication and characterization of polymer/nanoclay hybrid ultrathin multilayer film by spin self-assembly method *Thin Solid Films* **2004**, *458*, 9.
- (64) Yang, S. Y.; Lee, D.; *et al.* Bioinert Solution-Cross-Linked Hydrogen-Bonded Multilayers on Colloidal Particles *Langmuir* **2004**, *20*, 5978.
- (65) Donath, E.; Sukhorukov, G. B.; *et al.* Novel Hollow Polymer Shells by Colloid-Templated Assembly of Polyelectrolytes *Angewandte Chemie International Edition* **1998**, *37*, 2201.
- (66) Yu, P.; Fu, Y.-X. Tumor-infiltrating T lymphocytes: friends or foes? *Laboratory Investigation* **2006**, *86*, 231.
- (67) Marhaba, R.; Zoller, M. CD44 in cancer progression: Adhesion, migration, and growth regulation *Journal of Molecular Histology* **2004**, *35*, 211.
- (68) Hyung, W.; Ko, H.; *et al.* Novel hyaluronic acid (HA) coated drug carriers (HCDCs) for human breast cancer treatment *Biotechnology and Bioengineering* **2008**, *99*, 442.
- (69) Platt, V. M.; Szoka, F. C. Anticancer Therapeutics: Targeting Macromolecules and Nanocarriers to Hyaluronan or CD44, a Hyaluronan Receptor *Molecular Pharmaceutics* **2008**, *5*, 474.
- (70) Leonelli, F.; La Bella, A.; *et al.* Design, Synthesis and Applications of Hyaluronic Acid-Paclitaxel Bioconjugates *Molecules* **2008**, *13*, 360.

Chapter 2: Backpack Fabrication and Multilayer Systems

Developed

Reproduced in part with permission from Swiston, A. J.; Cheng, C.; Um, S. H.; Irvine, D. J.; Cohen, R. E.; Rubner, M. F. *Nano Letters* **2008**, *8*, 4446. Copyright 2008 American Chemical Society.

Overview of Fabrication Methods

Cellular backpacks may be built and attached to cells using several methods, though some approaches offer clear advantages. One method initially investigated was to “stamp” backpack directly on cell surfaces. Functional PEMs were built atop flat poly(dimethylsiloxane) (PDMS) substrates. Cells were then seeded onto a surface, and the PDMS stamp was placed on top. Cells were then free to attach to the PEM, and if the adhesion between the PEM, PDMS, and cell was precisely balanced, the cell could remove a PEM “plug” from the film. Unfortunately, finding the exact correct balance in adhesive forces proved difficult, and this approach was unable to attach a backpack.

A second more promising approach was to stamp a full PEM backpack system as seen in Figure 1.2, page 22. This method is referred to as polymer-on-polymer stamping (POPS)¹⁻³. A multi-region backpack was built on PDMS patterned with a regular array of posts. When the PEM coated PDMS stamp is brought into contact with a surface, ideally only the film atop the posts will be transferred. This ideal case is shown in Figure 2.1a; the more commonly seen product is found in Figure 2.1b. A relationship exists between the thickness of the

multilayer film and the diameter and height of the PDMS posts. It seems that the diameter of relevantly sized backpacks (1-20 μ m diameter, just less than the diameter of most cells), and the thickness of a backpack make POPS a non-feasible technique for backpack fabrication.

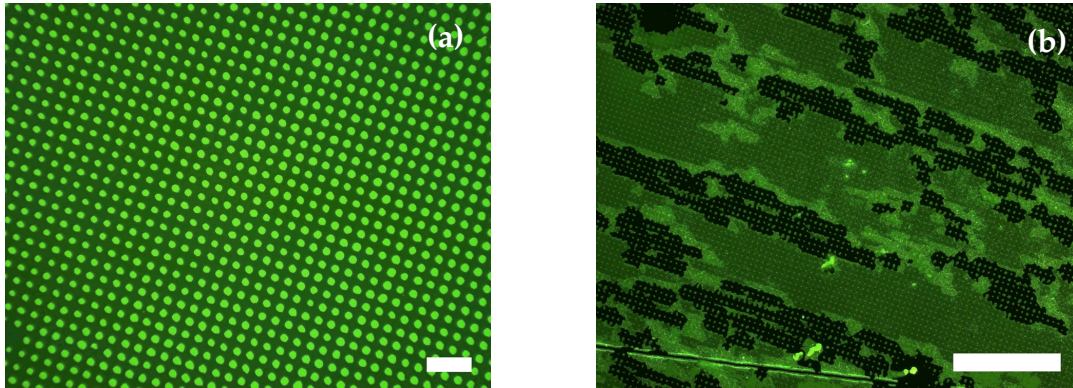


Figure 2.1: (a) Ideal POPS result in which only the multilayer film on top of the PDMS posts is transferred onto the stamped substrate. These 5 μ m backpacks are the following (starting from the stamped substrate, *not* the deposition order): (PAH4.0/SPS4.0)₅(PAAm3.0/PAA3.0)_{10.5}(FITC-PAH7.5/PAA3.5)₃. Scale bar = 20 μ m. (b) The more common case found after POPS, in which the film does not effectively tear at each feature. The film is identical to (a). Scale bar = 100 μ m.

The last fabrication method, and the method that will be used throughout the rest of this thesis, relies upon photolithographic patterning and liftoff. This method has the major advantage of being very well understood and characterized, as photolithography forms the basis for semiconductor manufacturing. Details of this method are the focus of the following section.

Photolithographic Fabrication

Backpacks are fabricated using a method adapted from McShane *et al*^{4,5}, extended to multi-region films built using hydrogen-bond multilayers, electrostatic multilayers, and copolymers. Briefly, a photoresist resin is spin-coated onto a

substrate, photolithographically patterned (using the masks whose design are found in Appendix A), and the backpack heterostructure is deposited conformally on the resist. In the final step, the resist is dissolved in acetone and the directly attached film is removed, leaving only film attached directly to the substrate (see Figure 2.2 and Figure 1.2, page 22).

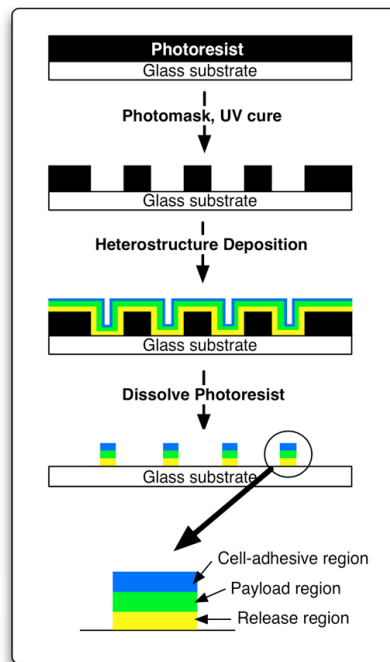


Figure 2.2: Schematic of the photolithography technique used to fabricate multilayered, multi-region backpacks.

Each backpack is a heterostructure consisting of three or more identifiable lamellar regions or strata, each of which consists of several bilayers of electrostatically complexed, hydrogen-bonded materials, or a polymer sprayed onto the surface from an organic solvent. The order of deposition to the surface is as follows: (1) a releasable region that deconstructs in noncytotoxic conditions, (2) a payload region that holds the functional cargo that will be exposed to the

cell culture medium, and (3) a cell-adhesive region that anchors the payload to the cell membrane (see Figure 2.2).

The first region of the backpack heterostructure was designed to deconstruct readily upon exposure to specific noncytotoxic conditions. Although there are a number of different triggering mechanisms that can be used to deconstruct suitably designed polyelectrolyte multilayers⁶, we focused on the controlled dissolution of different hydrogen-bonding systems including those based on poly(methacrylic acid) (PMAA), poly(acrylic acid) (PAA), poly(vinylpyrrolidone) (PVPON), poly(*N*-isopropylacrylamide) (PNIPAAm), poly(ethylene glycol) (PEG), and poly(vinyl caprolactam) (PVCL). Specifically, the following systems were built and tested for use as a release region:

1. (PAA/PEG)
2. (PMAA/PEG)
3. (PMAA/PVPON)
4. (PMAA/PNIPAAm)
5. (PMAA/PVCL)

It has previously been shown that hydrogen-bonded multilayer systems containing carboxylic acid groups can be readily assembled at low pH but will dissolve quickly when exposed to a pH sufficiently high to ionize the hydrogen-bonded acid groups⁷. The critical dissolution pHs of the different films are below in Table 2.1.

<i>Polymer System</i>	<i>Critical Dissolution pH</i>
(PAA/PEG)	3.6 ⁸
(PMAA/PEG)	4.6
(PMAA/PVPON)	6.4, 6.9 ⁸
(PMAA/PNIPAAm)	6.2
(PMAA/PVCL)	6.95

Table 2.1: Critical pH values of select hydrogen-bonded polymer multilayer systems. All values from Ref ⁷ unless noted otherwise.

The second important stratum of the heterostructured backpack is the payload region. Upon dissolution of the release region, the payload region of the PEM backpack is presented to the extracellular environment and is anchored to the surface of the cell via the cell-adhesive region. Examples of possible cargoes that may be incorporated into this region include drugs⁹, proteins^{10,11}, or nanoparticles^{12,13}. The most frequent payload consisted of anionic, superparamagnetic iron oxide nanoparticles (Fe_3O_4 , MNP) alternately deposited with fluorescein-labeled poly(allyl amine hydrochloride) (FITC-PAH) to create a fluorescent labeled and magnetically responsive PEM backpack. Ten bilayers of magnetic nanoparticles and FITC-PAH yield a ~100 nm thick payload region (see Figure 2.16, page 60).

Hydrogen-bonded Polymer Multilayer Release Regions

The first region of the backpack heterostructure was designed to deconstruct readily. Numerous polymer systems exist which will deconstruct or dissolve upon a given stimulus, such a solubility in an organic solvent, but any such system used in a backpack must do so in an aqueous environment under non-cytotoxic conditions (pH, salt, temperature, etc.). Furthermore, these systems must be compatible with the rest of the photolithographic fabrication process, most notably the final acetone sonication step. For example, one attractive candidate might be homopolymer poly(N-isopropylacrylamide) (PNIPAAm), which dissolves readily upon *lowering* the temperature below 32°C (more details below). If a homopolymer layer of PNIPAAm was deposited as the release region, chilling the system could easily and readily trigger backpack release. However, when a thin homopolymer PNIPAAm film was cast on photoresist patterned substrates, this film was readily dissolved upon sonication in acetone. Given the harsh chemical and mechanical conditions that exist during this final fabrication step, polymer multilayer films are desirable for two reasons: they adhere strongly to the underlying substrate and do not dissolve in acetone (even if the constituent polymers are individually soluble). We thus chose to use a multilayer-based approach to building a controllable release region.

Although there are a number of different triggering mechanisms that can be used to deconstruct suitably designed polyelectrolyte multilayers⁶, we focused on the controlled dissolution of different hydrogen-bonding systems. It has previously

been shown that hydrogen-bonded multilayer systems containing carboxylic acid groups can be readily assembled at low pH but will dissolve quickly when exposed to a pH sufficiently high to ionize the hydrogen-bonded acid groups⁷. Additionally, since a PMAA/PNIPAAm multilayer system contains a thermally responsive polymer (PNIPAAm), release only occurs both above the critical solution pH (6.2) and below a specific triggering temperature (32°C, to be discussed). All multilayer depositions during heterostructured backpack assembly must be carried out below the critical dissolution pH, and in the case of a PNIPAAm system, above the specific triggering temperature.

When utilizing hydrogen-bonded multilayers to release a heterostructured thin film, it is essential to determine how subsequently assembled layers influence the release behavior. Decher reported that an electrostatically bonded region built on top of a hydrogen-bonded region requires a critical thickness of the hydrogen-bonded region for successful dissolution and release¹⁴. Caruso also noted that deposition of polyelectrolytes onto hydrogen-bonded films seems to stabilize these films at high pH¹⁵. We observed similar behavior in a number of hydrogen-bonded polymer systems. In all cases, despite variations in polymer systems, molecular weights, and subsequent electrostatic layer depositions, a release region thickness of at least 200–300nm was required to achieve successful backpack lift-off. Initial x-ray photoelectron spectroscopy (XPS) results show that the polycationic species used in the payload region diffuses into and stabilizes the release region, thereby causing this critical thickness behavior. This phenomenon will be discussed in detail later.

When pH is used as the only release mechanism, the narrow pH range suitable for cell survivability coupled with the very rapid release (see Figure 2.4 and Figure 2.7) that occurs above the critical release pH resulted in a difficult to control release process (cell binding and backpack release are occurring simultaneously). To address the need for better control over backpack release, multilayers with increasing critical pH values were built and tested. We reasoned that as the critical pH increased, the liftoff kinetics at a given pH (7.4) would be slower. However, we observed that regardless of the critical pH release was extremely rapid and faster than the time needed for cells to contact and bind to the backpack.

We began researching an on-demand release mechanism, and decided to introduce thermal responsiveness into the release region as a non-cytotoxic method. Hydrogen-bonded multilayers can be built using polymers with known lower critical solution temperature (LCST) behavior, and we chose to focus on poly(N-isopropyl acrylamide) (PNIPAAm) and poly(vinyl caprolactam) (PVCL), which have LCSTs of 32°C and 31°C, respectively¹⁶. PMAA/PNIPAAm multilayers, when built into a patterned heterostructure, dissociate in water by a combined mechanism that is controlled by both pH and temperature. (We found that PMAA/PVCL films, regardless of thickness, temperature, or capping layers, were unable to dissociate and release a backpack.) The pH mechanism depends on the ionization level of PMAA's acid groups incorporated in the film. Below the critical pH, PMAA and PNIPAAm will form hydrogen-bonded multilayers that are stable at all biologically useful temperatures. The temperature mechanism relies on the interaction between water and PNIPAAm. Above the

LCST for PNIPAAm, polymer–polymer interactions are favored over polymer–water interactions, leading to insoluble PNIPAAm. Below the LCST, PNIPAAm prefers to hydrogen bond with water, leading to a homogeneous, single phase polymer–water solution. When PNIPAAm is incorporated into a patterned multilayer heterostructure, the solubility of PNIPAAm determines the dissolution behavior of the entire film. We find that PMAA/PNIPAAm films deconstruct in physiological pH conditions (~7.4, above the critical pH) at 4°C (below the LCST, PNIPAAm is soluble) but not at 37°C (above the LCST, PNIPAAm is insoluble). Thus, binding cells to the surface-confined backpacks can be carried out at 37°C for as long as needed, followed by controllable release by simply lowering the temperature to 4°C. We believe that this is the first demonstration of a thermally responsive thin film based on a hydrogen-bonded multilayer that can be controllably erased (rather than simply swollen^{17,18}) using a temperature trigger. It should be noted that non-patterned PMAA/PNIPAAm multilayers without the capping payload layers are not stable in pH 7.4 phosphate-buffered saline at 37 °C and that the thermal control described here is only observed in the patterned heterostructure. A schematic synopsis of the temperature and pH conditions required for liftoff may be found in Figure 2.10.

A review of relevant thickness, lift off data, and other release characteristics of each of the hydrogen-bonded multilayer systems investigated is presented and discussed below. Film dissolution was measured by counting the number of backpacks found to be off the array positions after gentle agitation in pH 7.4 PBS (see Figure 2.28). Film thickness was measured by profilometry or ellipsometry. More details on experimental methods may be found at the end of this chapter.

(PAA/PEG)

PAA and PEG were chosen as an ideal multilayer system for the extensive literature on the biocompatibility of poly(ethylene glycol) and its variants¹⁹.

PAA/PEG films were assembled, patterned, and tested for liftoff of a PAH/SPS electrostatic capping layer. As seen in Figure 2.3, at 19 bilayers (~220nm) the PAA/PEG film released nearly all backpacks from the array.

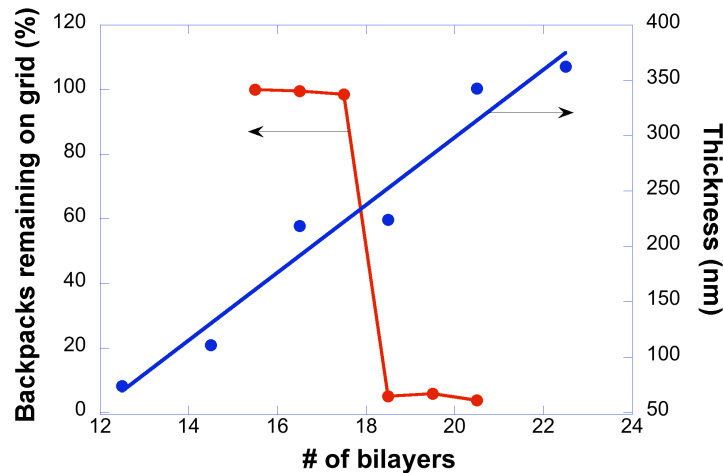


Figure 2.3: Release behavior for the following heterostructure: (PAA3/20kMW-PEG3)_{x,5}(PAH3.0/SPS3.0)_{9,5}(HA3.0/FITC-CHI)_{3,5}. The thickness value (as determined by ellipsometry) as a function of x bilayers describes just the PAA/PEG release region. The line connecting the thickness data is a liner regression; the line connecting lift-off data is a guide for the eye.

In a typical experiment, backpacks were released for 30min in PBS under gentle agitation; that nearly all backpacks lifted off called into question if cells could successfully dock with backpacks before release. Considering the small pH window for which cells are viable, dropping the pH to allow cells to dock while the film was stable would result in significant cytotoxicity. However, if at neutral pH the release kinetics were slower, cells could dock with the backpack

and then release from the substrate. Previous work has shown that salt can increase or decrease the stability of a hydrogen-bonded film^{8,20} depending on the nature of the salt ions and which polymers are used. Figure 2.4 shows that if the concentration of NaCl in the release solution doubles, the release kinetics are slower, suggesting NaCl stabilization of the PMAA/PEG film⁸. However, when this solution was used in a CH27 cell-attachment experiment, cells non-selectively attached to the substrate and aggregated, both perhaps due to a charge-screening effect between the anionic cell membrane and the cationic substrate (i.e., the PDAC-terminated pre-layer).

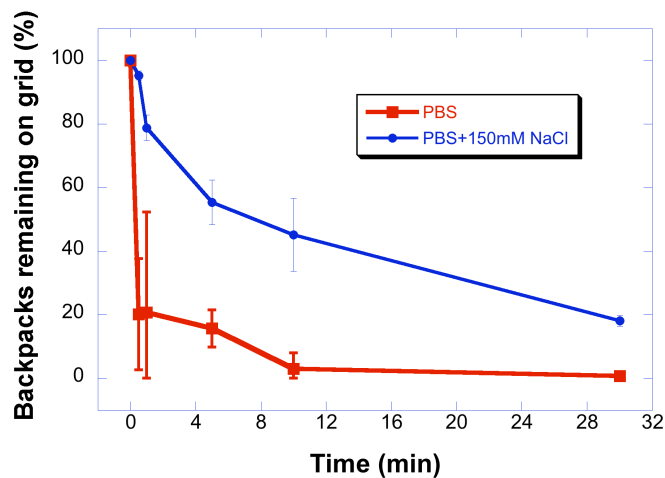


Figure 2.4: Timecourse of backpack liftoff as a function of salt concentration. PBS contains ~150mM NaCl. As the concentration of salt increases, the hydrogen-bonded system is stabilized, and requires more time to dissolve and release the backpack.

Even if B cells did not aggregate and attach non-selectively, the kinetics may still not yet be slow enough – as Figure 2.4 shows, ~50% of backpacks have already been released from the surface in 5 minutes, which may still be too fast to allow attachment before dissolution and release.

(PMAA/PEG)

In an effort to increase the critical dissolution pH and slow release kinetics without relying on salt stabilization, the more hydrophobic poly(methacrylic acid) and higher molecular PEG was used to construct (PMAA/PEG) release regions. Thickness and release behavior may be found in Figure 2.5. Again, release is observed at a critical thickness of $\sim 200\text{nm}$, which corresponds to 7.5 bilayers.

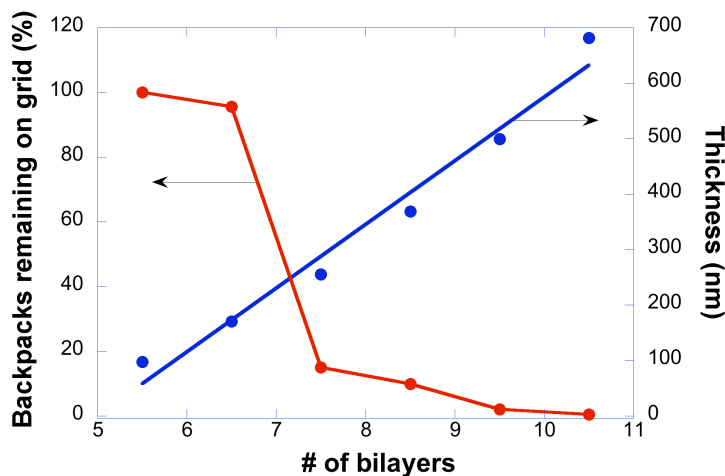


Figure 2.5: Release behavior for the following heterostructure: $(\text{PMAA}3.0/100\text{kDa-PEG}3)_{x.5}$ $(\text{FITC-PAH}3.0/\text{SPS}3.0)_{10}$. The thickness value (as determined by ellipsometry) as a function of x bilayers describes just the PMAA/PEG release region. The line connecting the thickness data is a liner regression; the line connecting lift-off data is a guide for the eye.

(PMAA/PVPON)

The final hydrogen-bonded system that relied solely upon a pH-triggered release was based on poly(vinylpyrrolidone) (PVPON), chosen for its high critical dissolution pH (~ 6.9) when complexed with PMAA. The critical thickness seen in this system is $\sim 300\text{nm}$, which corresponds to about 35 bilayers (see Figure 2.6).

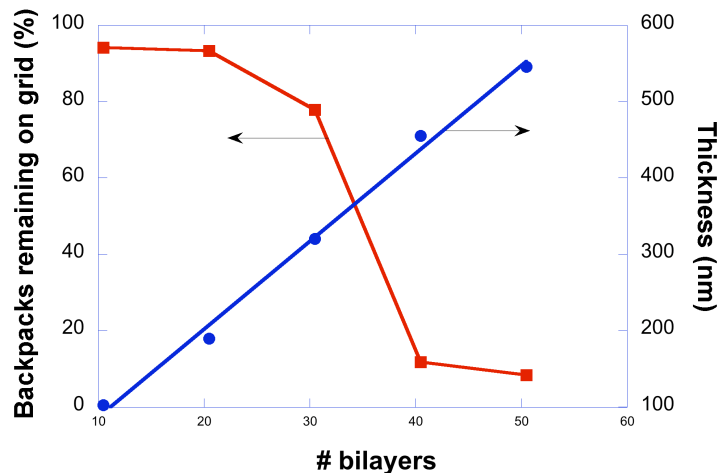


Figure 2.6: Release behavior for the following heterostructure: $(\text{PMAA2/PVPON2})_{x,5}$ (FITC-PAH3.0/MNP4.0)₁₀ with 100kDa PMAA and 1.3MDa PVPON. The thickness value as a function of x bilayers describes just the PMAA/PVPON release region. Due to film roughness, thickness values were determined by profilometry. The line connecting the thickness data is a liner regression; the line connecting lift-off data is a guide for the eye.

The critical dissolution pH of a (PMAA2/PVPON2) film is ~6.9, which is the closest to neutral among all the systems investigated. Since the pH difference between cell media (pH 7.4) and the critical pH is small, we reasoned that backpack release kinetics would be slow enough to allow cell docking and attachment prior to backpack liftoff. The time required for release of a (FITC-PAH3.0/MNP4.0) backpack in PBS was investigated and is shown in Figure 2.7.

The PMAA/PVPON system was used extensively when a rapidly-dissolving release region was required – for instance, for an “injectable” backpack formulation (see Chapter 4, page 105).

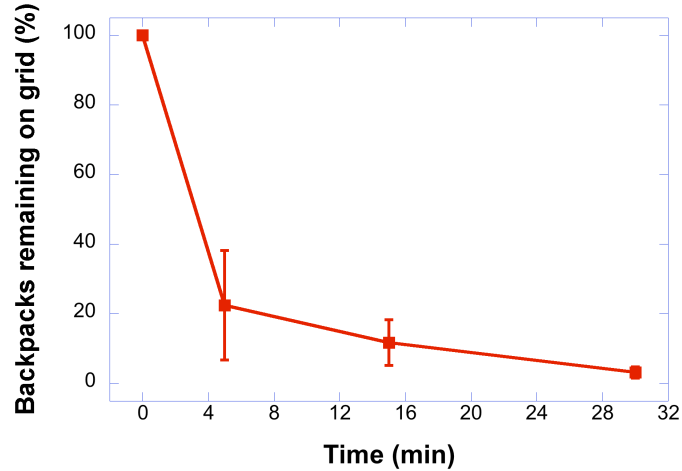


Figure 2.7: Time course of backpack liftoff for a (PMAA2/PVPON2)_{40.5} release region. Most backpacks are released in the first few minutes of neutral solution exposure, with nearly 100% detached from the substrate in 30 minutes.

(PMAA/PNIPAAm)*

To create a stimuli-responsive release region, hydrogen-bonded multilayers including PNIPAAm were built. Motivated by previous work that has shown grafted PNIPAAm can be used to release cell sheets²¹, PNIPAAm-containing multilayers were studied for their thermal liftoff behavior. Thickness and release behavior at pH 7.4 and room temperature conditions are found in Figure 2.8.

As seen in the previous hydrogen-bonded film examples, a critical film thickness (~250nm) is required before backpacks lift off the surface. Since the release results in Figure 2.8 are at room temperature (and sufficiently below PNIPAAm's LCST), the onset of thermally-induced release at neutral pH was measured and is

* I acknowledge the collaboration of Soong Ho Um in the results described in this section.

shown in Figure 2.9. Here we see the beginning of film dissolution and release at $\sim 29^\circ\text{C}$, which is nearly identical to the reported LCST value for homopolymer PNIPAAm^{16,22} in PBS.

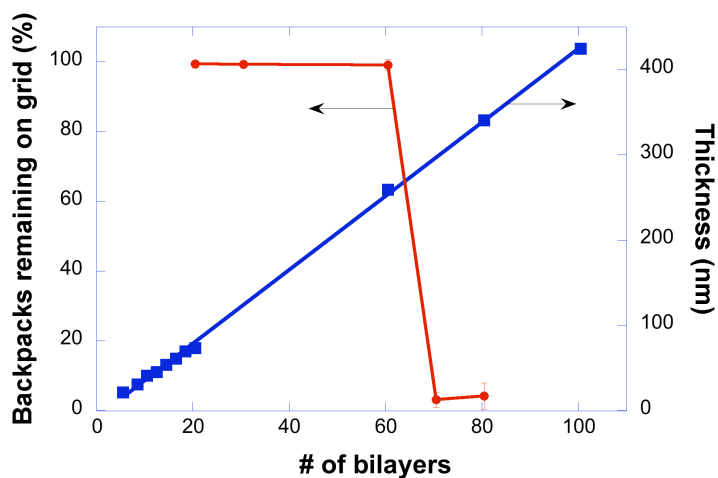


Figure 2.8: Release behavior at room temperature for the following heterostructure: $(\text{PMAA}3.0/\text{PNIPAAm}3.0)_{x,5}(\text{FITC-PAH}3.0/\text{Fe}_3\text{O}_4 \text{ NP}4.0)_{10}$. The thickness value as a function of x bilayers describes just the PMAA/PNIPAAm release region. The line connecting the thickness data is a liner regression; the line connecting lift-off data is a guide for the eye.

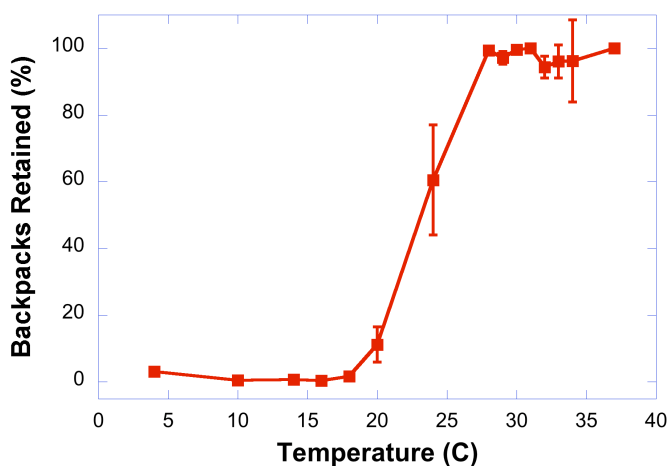


Figure 2.9: Temperature-induced release behavior for $(\text{PMAA}3.0/\text{PNIPAAm}3.0)_{80,5}(\text{FITC-PAH}3.0/\text{Fe}_3\text{O}_4 \text{ NP}4.0)_{10}$. The onset of release is seen $\sim 28^\circ\text{C}$, close to the LCST reported for homopolymer PNIPAAm in PBS (29.1°C)^{16,22}.

To summarize, release is seen only *below* the LCST of homopolymer PNIPAAm (thermal-responsive behavior) and *above* the critical dissolution pH. Since assembly can take place below the critical pH at any temperature, films were deposited at room temperature. The pH and thermal release conditions are schematically represented in Figure 2.10, which includes relevant pH and temperature conditions.

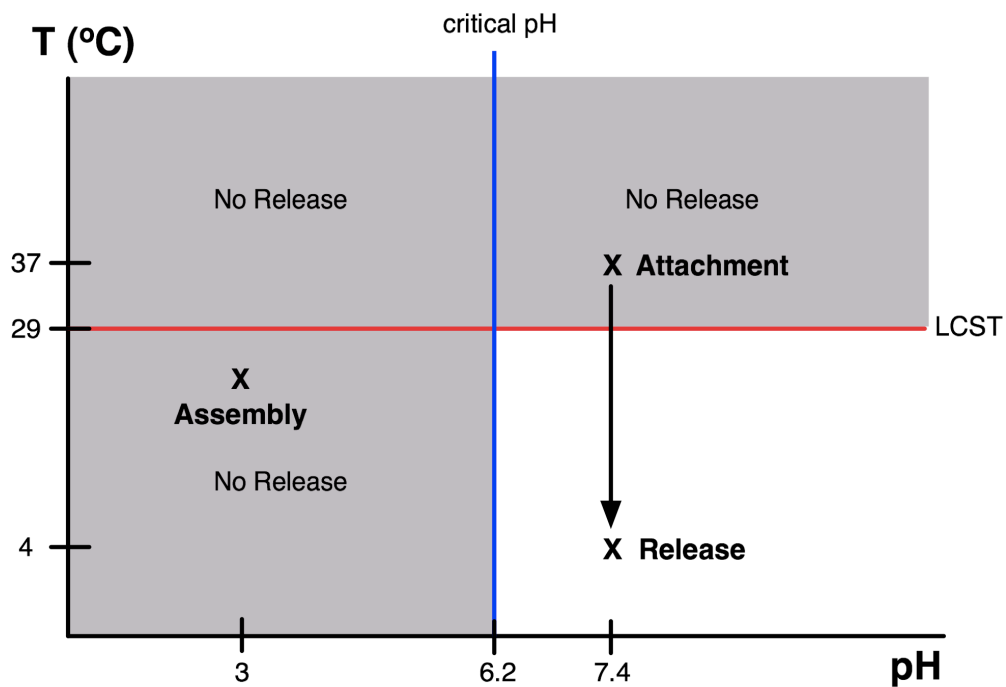


Figure 2.10: Schematic of the pH and temperature conditions require for film release. The assembly, attachment, and release conditions are shown.

(PMAA/PVCL)

A second LCST-polymer multilayer system based on poly(vinyl caprolactam) was built and tested. Despite the range of thicknesses tested, no backpack release was ever observed at neutral pH. Perhaps components from the payload

region diffused into and stabilized the PVCL-containing region, effectively moving the critical dissolution pH to above 7.4. Growth curves for PMAA/PVCL films prepared both in a Zeiss static dipper and a NanoStrata spinning dipper are shown in Figure 2.11.

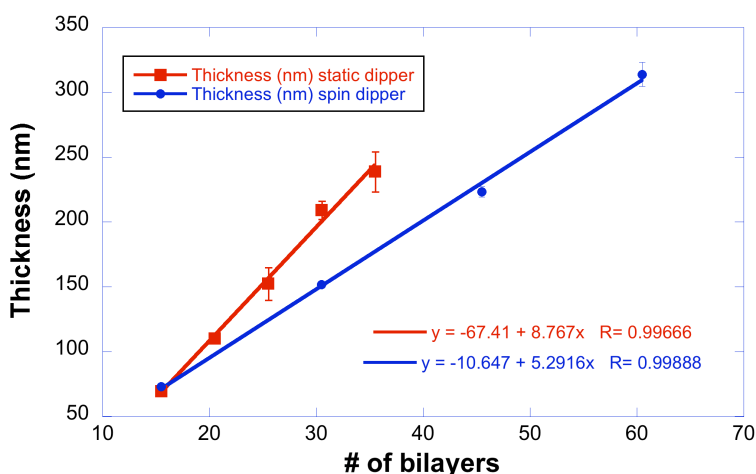


Figure 2.11: Growth curves for (PMAA₂/PVCL₂)_{x,5} for 100kDa PMAA and 354kDa PVCL. No PVCL-based film was found to release a backpack from the surface in pH 7.4 conditions.

Composition of a Released Backpack's Outer Face

All hydrogen-bonded release systems investigated (with the exception of PMAA/PVCL) required a critical thickness of ~200-300nm before the payload-containing backpack was released from the surface. After the backpack is released, however, the nature of the outer face (i.e., the side formerly directed toward the glass fabrication surface) is not well defined. The payload region may be directly exposed to the environment, or some of the release region could remain attached. This latter case is likely, since polycations are known to diffuse into polyelectrolyte multilayers^{23,24}, and similar behavior has been seen in

hydrogen-bonded multilayers¹⁵. Following deposition of the hydrogen-bonded release region, an electrostatically-complexed (PAH3.0/MNP4.0) film was deposited beginning with PAH. We hypothesize that these PAH molecules diffuse into and partially stabilize the release region. That the release region must be a certain thickness suggests that some or the entire release region is incorporated into the released backpack. We indirectly investigated if the outer backpack face included the release region using rhodamine-labeled polymers in the release region, and directly measured using XPS the presence of indicative functional groups on released films. Incorporating a “diffusion barrier” region in the backpack heterostructure, which was essential to hydrogen-bonded release region dissolution, further tested the polycation-diffusion theory. All results indicate that the release region is incorporated into the released backpack, and that polycation diffusion is responsible for this phenomenon.

Rhodamine-labeled PMAA Release Regions

To test if the release region was included in the final released backpack, release regions containing fluorescently labeled PMAA were built and the resulting released backpacks were examined using CLSM. These Rhod-PMAA containing release regions were constructed with 20 bilayers of (Rhod-PMAA/PNIPAAm) at variable positions within the release region. The case of particular interest is shown schematically in Figure 2.12. (Rhod-PMAA3.0/PNIPAAm3.0)₂₀ was deposited as the first 20 bilayers of an 80 total bilayer release region. All other layers were constructed with unlabeled PMAA under the same solution conditions.

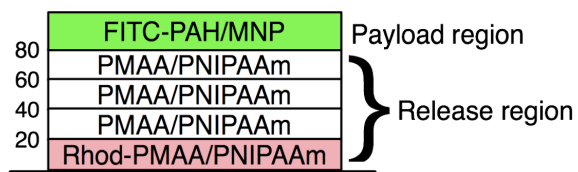


Figure 2.12: Schematic of the variable position Rhod-PMAA multilayers used to test if the release region is included in the final released backpack. The small number to the left of the diagram is the bilayer number.

Backpacks were released in pH 7.4 PBS and observed by CLSM (see Figure 2.13). Both rhodamine and fluorescein signals were detected in the released backpacks, indicating that backpacks included both FITC-labeled PAH from the payload and rhodamine-labeled PMAA from the release region. Controls for each signal (i.e., disabling the laser for Rhod and FITC) showed that there was a negligible amount of spectral overlap between the two dyes.

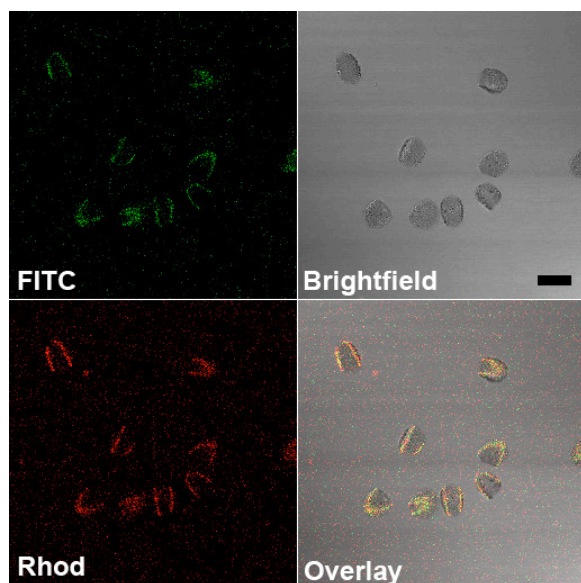


Figure 2.13: CLSM images of released backpacks that contained Rhod-PMAA in the release region (see Figure 2.12). Both Rhod and FITC signals are seen, indicating that indeed the release region does remain attached to the released backpack. Scale bar is 10 μ m.

XPS analysis of the Backpack's Outer Face*

To directly measure if the release region is attached to the released backpack, non-patterned hydrogen-bonded films were prepared as above with a 20kDa MW thiol-end group PEG (PEG-SH) and capped with (PAH3.0/MNP4.0)₁₀. Films were scored and released in pH 7.4 PBS, flipped over and placed on a glass slide so that the backpack's outer face (from an attached cell's perspective, i.e., the face exposed to the environment rather than attached to the cell membrane) was exposed. If the release region remains attached to the backpack after release, XPS results will show a S peak. If the polycation PAH from the payload region diffused into the release region, a N peak would also be found. (The (PAA/PEG) system was chosen over other amine-containing hydrogen-bonded systems so that any N peak must be due to PAH.) Further, if no Fe peak was seen, then the superparamagnetic Fe₂O₃ nanoparticles are not within ~10nm (the penetration depth of XPS) of the outer face. Figure 2.14 shows that both S and N peaks were found, but not Fe, proving that PEG from the release region and PAH from the payload were found on the outermost face of a released backpack, and that the Fe-containing payload region was >10nm beneath the surface.

* I acknowledge the collaboration of Jonathan Gilbert in performing the experiments described in this section.

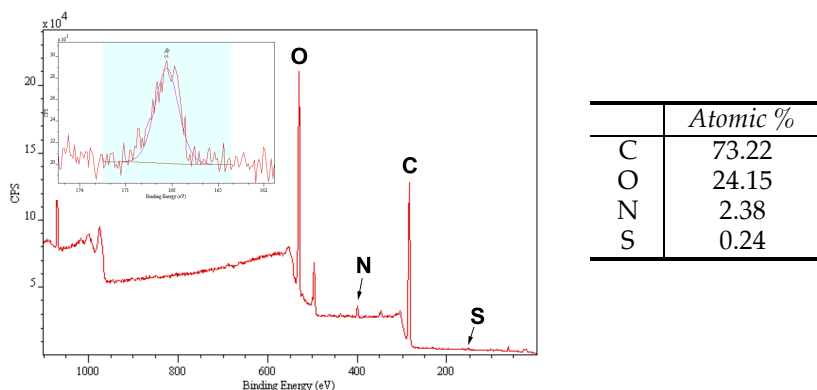


Figure 2.14: XPS spectra and atomic percentages for a flipped (PAA3.0/PEG-SH3.0)_{20.5} (PAH3.0/MNP4.0)₁₀ film. The peaks for C, N, O, and S are as indicated – all other peaks are due to residual salt from PBS. Inset shows the S peak at 168eV. Images courtesy Jonathan Gilbert.

Further XPS measurements were performed on films of the following compositions: (PAA3.0/PEG3.0)_{20.5} and (PAA3.0/PEG3.0)_{20.5} (PAH3.0/MNP4.0)₁₀, the second of which was flipped for analysis. When compared to as-deposited PAA/PEG hydrogen-bonded film, the functional groups presented on the outer face of the backpack indicate if PAH had diffused into the release region and if PEG is still present. Figure 2.15 shows two interesting behaviors. First, PAA's carboxylic acid C peak at ~290eV shifts to lower binding energies, as seen when a carboxylic acid is paired with a cation^{25,26}. This demonstrates that the previous PMAA-PEG hydrogen bonds are being disrupted and replaced with electrostatic PAA-PAH interactions. Second, the PEG C peak significantly shrinks in the flipped backpack film, suggesting the loss of PEG upon release. This is consistent with the previous finding – if PAH is disrupting PAA-PEG hydrogen bonds, PEG is free to leave the film.

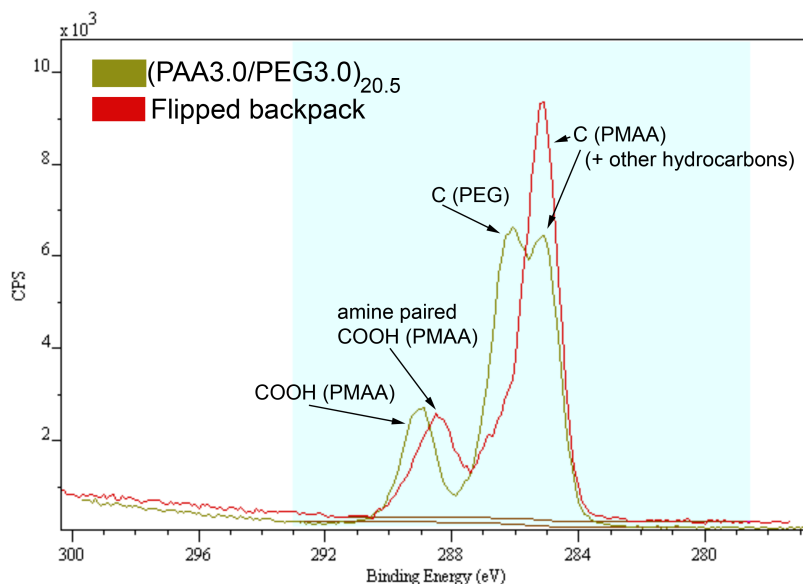


Figure 2.15: XPS spectra of an as-deposited $(\text{PAA3.0/PEG3.0})_{20.5}$ and flipped $(\text{PAA3.0/PEG3.0})_{20.5}$ $(\text{PAH3.0/MNP4.0})_{10}$ film. PAA's carboxylic acid C peak in the flipped backpack film shifts to lower binding energy as would be expected when paired with an amine. PEG's C peak also significantly shrinks in the flipped sample, suggesting the ejection of PEG upon PAH diffusing in and disrupting the former PAA-PEG hydrogen bonds. Data courtesy Jonathan Gilbert.

These results support our polycation diffusion hypothesis. First, we see that the release region is tethered to the outer face of the released backpack as shown by the S peak in Figure 2.14 and the C peak from PEG in Figure 2.15. Second, if PAH diffuses into the release region, driven by ionization of PAA carboxylic acids, then the XPS spectra should show both the presence of N (Figure 2.14) and a shift in the carboxylic acid peak from PAH pairing with PAA (Figure 2.15). Finally, expulsion of PEG from the film (decrease of C from PEG in Figure 2.15) confirms that an electrostatic PAA-PAH layer replaced the hydrogen-bonding PAA-PEG film. Though these XPS results strongly support our hypothesis, further work adjusting parameters of the diffusing polycation would lend a more complete mechanistic understanding of this behavior.

Barriers Against Polycation Diffusion

To further show that diffusion of subsequently deposited polycations is responsible for stabilizing the release region, identical films were built except for a “diffusion barrier” multilayer consisting of (PAH3.0/SPS3.0)_{9,5}. This film was previously reported to effectively block the diffusion of polyelectrolytes into existing PEM films²⁷. As Table 2.2 shows, the (PAH/SPS) barrier is required for the (PAA/PEG) release region to dissociate; here, FITC-CHI is the diffusing species, consistent with previous findings that CHI copiously interdiffuses in polymer multilayers²⁸.

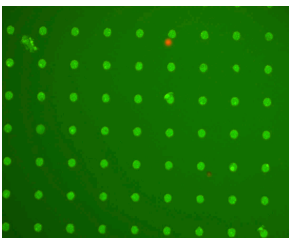
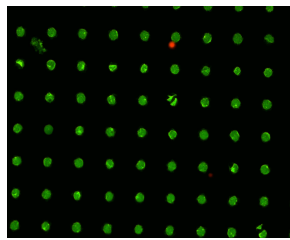
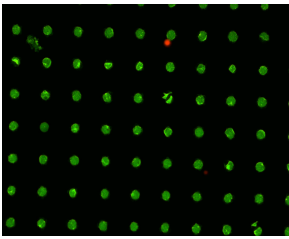
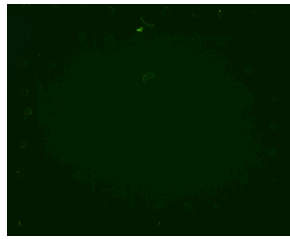
	Before PBS exposure	After 30min PBS
No Diffusion Barrier (PAA/PEG) _{25,5} (HA3.0/FITC-CHI) _{3,5}		
With Diffusion Barrier (PAA/PEG) _{25,5} (PAH3/SPS3) _{9,5} (HA3.0/FITC-CHI) _{3,5}		

Table 2.2: Fluorescent images of backpacks before and after exposure to neutral solution conditions as a function of possessing a (PAH/SPS) diffusion barrier. Images are taken from the same position on the substrate.

Conclusions on the Composition of the Backpack’s Outer Face

Some or the entire release region remains associated with the backpack following release. The polycation from the electrostatically assembled layers diffuses into

the hydrogen-bonded region driven by the ability to ionize some of the carboxylic groups^{23,24}. The resulting electrostatic crosslinks stabilize the release region against dissolution. This leads to the need for a critical release region thickness before successful backpack liftoff. If the hydrogen-bonded release region is thicker than the diffusion path length of the polycation, some non-crosslinked hydrogen-bonded chains remain to dissolve and release the backpack. The polycation crosslinked portion of the release region is electrostatically attached to the rest of the backpack and thus remains associated following release (as shown by Rhod-PMAA and XPS results). When a non-intercalating cationic species, such as amine-functionalized nanoparticle, is used to build the first layers of the payload region a critical thickness is not observed. In this case, liftoff in neutral pH conditions occurs with very thin release regions (see the “Quantum Dot Payloads” section below). The underlying physics of polycation diffusion are not yet understood, and this remains an area of open inquiry. For instance, how the molecular weight of the diffusing polycation may influence the critical thickness will provide fundamental mechanistic insights. Since it was proven that the release region remains attached to the backpack, reengineering this outer face is of great importance for any clinical application. Integrating particular functional abilities into the outer face could render the backpack more or less adhesive to certain tissues, affect immunogenicity, or provide an elution barrier to the payload region’s cargo. This remains a fertile area for ongoing investigation.

Payload Regions

Poly(allylamine hydrochloride) (PAH)/Magnetic Nanoparticle (MNP) Regions

Throughout this thesis, the most frequently used payload region was a multilayer comprised of (PAH3.0/MNP4.0)₁₀. Commercially available superparamagnetic nanoparticles (EMG 705, FerroTec) with an anionic surfactant stabilizer were layered with PAH. Fluorescein-tagged PAH was often used to aid in fluorescence imaging, and is designated FITC-PAH. Figure 2.16 shows a growth profile for unlabeled-PAH built on (PDAC4.0/SPS4.0)₁₆. This system grows linearly with a per bilayer thickness nearly identical to the diameter of the MNP used (reported to be 10-12nm by manufacturer), suggesting deposition of MNP monolayers during each bilayer cycle.

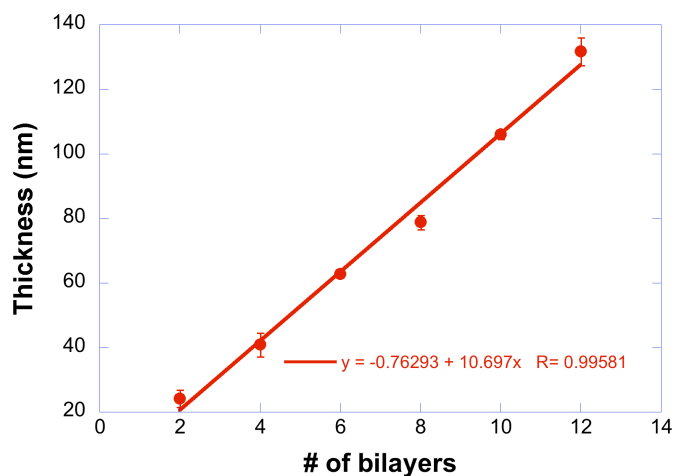


Figure 2.16: Growth profile of (PAH3.0/MNP4.0)_x, where x is the number of bilayers deposited on top of (PDAC4.0/SPS4.0)₁₆.

We tested the ability of the MNP region to respond to external magnetic fields – namely, we used the magnetic backpack to manipulate B cells in solution.

Details may be found in Chapter 3, page 94.

Quantum Dot Payloads

Commercially available amine-functionalized quantum dots (AminoQD) from Evident Technologies were incorporated into the payload region and successfully attached to the surface of CH27 B cells. These 600nm emission quantum dots are functionalized with a proprietary amine-containing coating, rendering them cationic over a broad pH range. Multilayers of AminoQDs and MNPs were built initially, but were found to completely dissociate during acetone sonication. During sonication, the film must tear and lift-off, and an all-nanoparticle film may be too rigid to remain associated under such harsh mechanical conditions. When AminoQDs were deposited with the strong polyanion SPS, acetone sonication yielded a high-fidelity array of backpacks as seen in Figure 2.17.

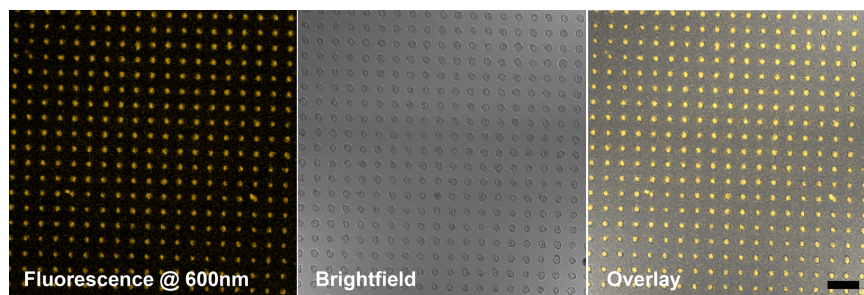


Figure 2.17: CLSM images of $(\text{PMAA}3.0/\text{PNIPAAm}3.0)_{20.5}(\text{AminoQD}5.0/\text{SPS}5.0)_{30}(\text{PAH}4.0/\text{MNP}4.0)_{10}(\text{CHI}3.0/\text{HA}3.0)_3$ backpacks. These backpacks show fluorescence emission at 600nm, indicating that the quantum dots are incorporated and active. Scale bar is $50\mu\text{m}$.

The composition of these backpacks is as follows:

$(\text{PMAA}3.0/\text{PNIPAAm}3.0)_{20.5}(\text{AminoQD}5.0/\text{SPS}5.0)_{30}(\text{PAH}4.0/\text{MNP}4.0)_{10}$

$(\text{CHI}3.0/\text{HA}3.0)_3$. It is important to note that the release region is only 20.5

bilayers, corresponding to a thickness of ~80nm (see Figure 2.8). These backpacks were agitated in 4°C pH 7.4 PBS for 20min, and then collected in one area of the Petri dish using a rare earth magnet. The resulting backpacks are shown in Figure 2.18.

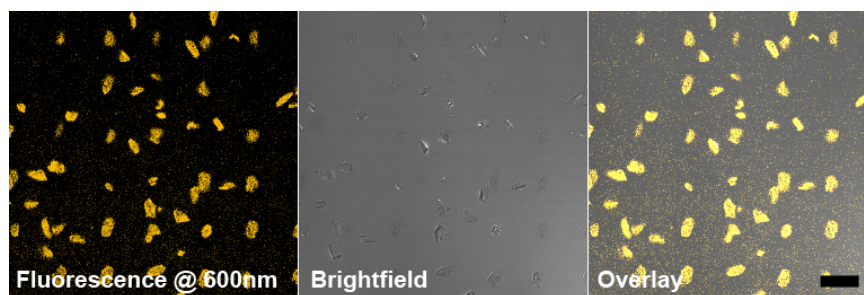


Figure 2.18: CLSM images of (PMAA3.0/PNIPAAm3.0)_{20.5}(AminoQD5.0/SPS5.0)₃₀(PAH4.0/MNP4.0)₁₀(CHI3.0/HA3.0)₃ backpacks that have lifted off from the fabrication substrate. These backpacks were collected to one part of the dish with a rare earth magnet before imaging, indicating that the MNP region is also functional. Scale bar is 20 μ m.

Successful liftoff with only 20.5 bilayers in the release region shows that when a non-intercalating species such as a nanoparticle is deposited directly on the release region, a critical thickness is *not* observed. This further supports the hypothesis that the diffusing polycation enters the release region and prevents dissolution even above the critical pH.

CH27 B cells were attached to an array of AminoQD payload backpack and thermally released. These cells attached to the backpacks, and upon lowering the temperature to 4°C, successfully released from the surface. One example of a AminoQD backpack on the surface of a B cell may be found in Figure 2.19.

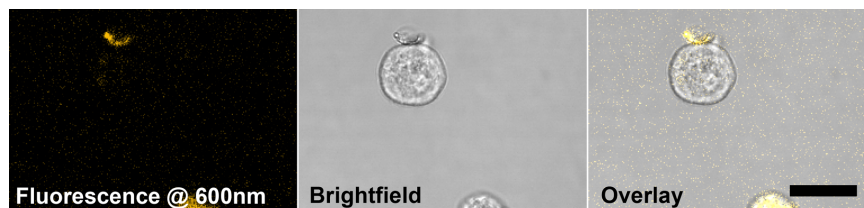


Figure 2.19: CLSM images of (PMAA3.0/PNIPAAm3.0)_{20.5}(AminoQD5.0/SPS5.0)₃₀(PAH4.0/MNP4.0)₁₀(CHI3.0/HA3.0)₃ backpacks on the surface of a CH27 B cell. Scale bar is 20 μ m.

Payloads containing Poly(lactic-co-glycolic acid) (PLGA)

PLGA is a poly(ortho ester) which hydrolyzes under physiological conditions (37°C, pH 7.4), releasing the bioresorbable products lactic and glycolic acid (see Figure 2.20). The rate of PLGA hydrolysis has been extensively studied, and is a function of lactic to glycolic acid ratios, molecular weight, crystallinity, and solution conditions²⁹⁻³¹. PLGA has been investigated for a number of biomaterial applications, the most common being drug delivery vehicles with well-defined release profiles.

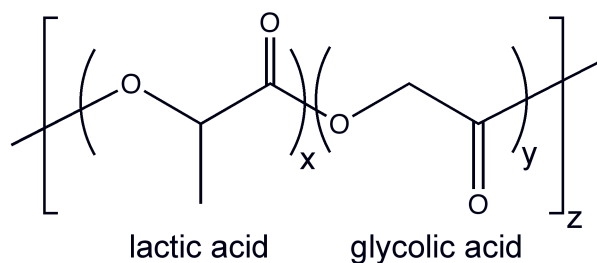


Figure 2.20: Illustration of poly(lactic-co-glycolic acid) (PLGA).

Because of these desirable biocompatibility characteristics, PLGA is a natural choice for a backpack payload. A PLGA backpack could be loaded with an elutable species (such as a drug or nanoparticle), shuttled to a site in the body by

an immune cell, then degrade and release the payload at a well-defined rate. The hydrolysis mechanism also allows backpacks to be cleared from the body, which may be critically important since backpacks seem to be resistant to the active clearance process of phagocytosis (see Chapter 6, page 169).

Attaching a PLGA copolymer layer to the rest of the backpack system posed several challenges. First, PLGA is water insoluble and lacks an electrostatic or hydrogen-bonding moiety: therefore, PLGA cannot be deposited using layer-by-layer techniques. PLGA can be sprayed onto to the backpack substrate, but the solvent used must:

1. not degrade or affect the dissolution of the hydrogen-bonded release region. Any water-containing solvent may destroy the hydrogen-bonding crosslinks.
2. not degrade the photoresist. If the photoresist is compromised, then the film cannot be patterned during the acetone lift-off step.
3. be a co-solvent for PLGA and the elutable species contained within it. For instance, the drug doxorubicin (DOX) is soluble in water, and a mutual solvent for hydrophobic PLGA and hydrophobic DOX must be used.
4. have a sufficiently high vapor pressure to successfully spray-deposit, i.e., the solvent evaporates immediately after contacting the substrate.

With all of these criteria in mind, two solvent systems were identified.

Chloroform worked well for spraying only PLGA onto a (PMAA2.0/PVPON2.0) release region. PLGA thickness was measured via ellipsometry by spraying PLGA onto Si wafers. Figure 2.21 shows the PLGA thickness profile as a

function of spraying time. Given the spraying distance and PLGA concentration (1mg/mL), nanometer-level resolution of PLGA thickness is possible.

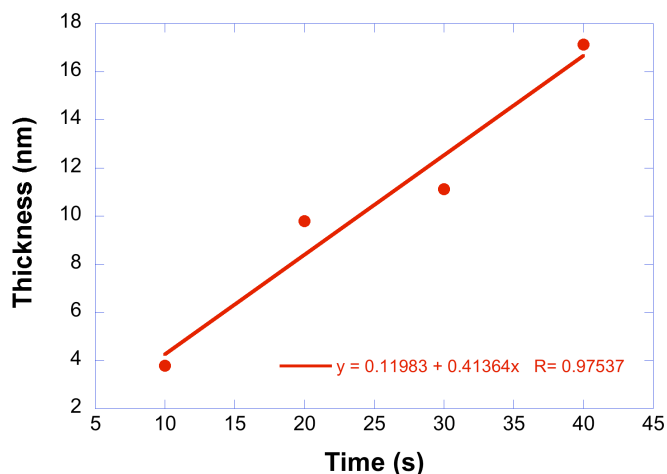


Figure 2.21: Growth profile of sprayed PLGA using the air brush method.

When PLGA is deposited along with a functional material, such as a drug or dye, a mutual solvent system must be chosen to create a homogenous solution. The chemotherapy drug doxorubicin (DOX) was chosen as a model drug system to incorporate within a PLGA matrix. Previous work has shown the cytotoxicity of encapsulated DOX in PLGA microparticle carriers³². A 3% dH₂O/THF binary solvent system was used to create a homogenous solution of the hydrophobic PLGA and hydrophilic DOX. This solution was sprayed onto a (PMAA2.0/PVPON2.0)_{20.5} release region, capped with PLGA sprayed from chloroform for 30s, then a (PAH3.0/MNP4.0)₁₀ payload was deposited last. This yielded a releasable, DOX-eluting backpack. Figure 2.22 shows the DOX signal of an array of backpacks prior to release.

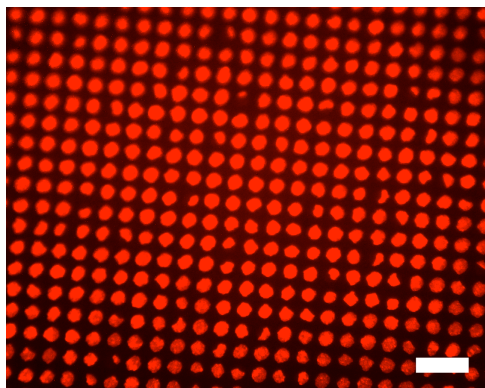


Figure 2.22: Fluorescence image of DOX-containing PLGA backpacks. DOX fluoresces in the rhodamine channel. Scale bar is 20 μ m.

Finally, to show the ability of PLGA backpacks to release a small molecule into the surrounding solution, flow cytometry was performed on released backpacks of the following composition: (PMAA2.0/PVPON2.0)_{40.5}(PLGA-Rhod6G)₁(PAH3.0/MNP4.0)₁₀. Rhodamine 6G was chosen as a DOX analog due to the high cost of DOX and thus could be used at significantly higher concentrations for imaging experiments. Three different spraying times (3s, 6s, and 10s) were tested to see if there was a significant difference in Rhod release with different PLGA region thicknesses. Backpacks were released from the surface, then incubated in pH 7.4 PBS at 37°C. Aliquots were removed and analyzed in the phycoerythrin (PE) channel of the cytometer. Figure 2.23 shows a steadily decreasing PE signal up to one week following backpack release.

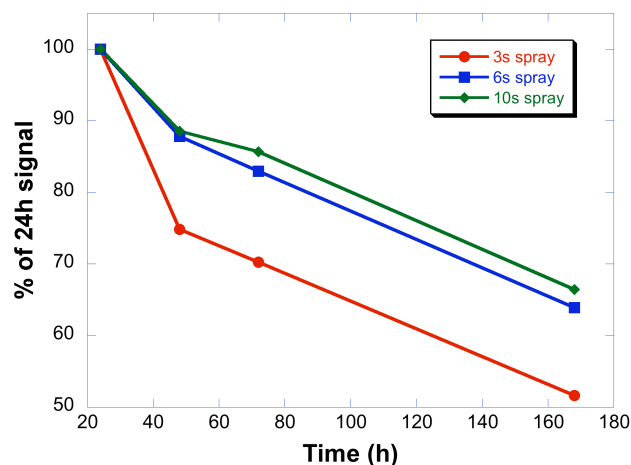


Figure 2.23: Summary of flow cytometry results of released backpacks of the following composition: (PMAA2.0/PVPON2.0)_{40.5}(PLGA-Rhod6G)₁(PAH3.0/MNP4.0)₁₀. Backpacks were incubated in pH 7.4 PBS at 37°C and tested at the time points indicated. After 7 days, up to 50% of the Rhod signal was lost (for the 3s spray sample).

Figure 2.23 shows that the fluorescence intensity of individual backpacks decreased with time – this may be due to either diffusion of the rhodamine dye out of the PLGA backpack or hydrolysis of the PLGA matrix and subsequent dye release. The latter scenario is obviously more desirable, since it affords greater control over release kinetics, but either scenario would effectively deliver a small molecule into the surrounding environment. More work is needed to more precisely quantify the rate and method of release.

Cell-Adhesive Regions

The final stratum of the assembled backpack heterostructure is cell-adhesive, anchoring the underlying payload region to the cell membrane. A cell-adhesive region may rely upon a binding mechanism specific to a particular cell type

(such as a binding receptor, integrin, etc.), or rely upon covalent chemistry that does not require any cell-dependant properties. For the majority of this work, we chose a hyaluronic acid/chitosan (HA/CHI) multilayer, since lymphocytes contain CD44 cell-surface receptors whose natural ligand is a three-structure unit repeat of the polysaccharide HA³³. HA forms the outermost layer of the cell-adhesive region in most backpacks. Chitosan was chosen as a complementary polycation for its biocompatibility when complexed with HA in multilayer films^{34,35}. The properties of HA/CHI multilayer films, including thickness, roughness, adsorption behavior, and most importantly, ability to bind to CD44⁺ lymphocytes are presented in much greater detail in Chapter 5.

For non-cell dependant attachment schemes, a most general method would chemically attach the backpack to a functional group found on all cell surfaces, such as a hydroxyl (-OH), amine (-NH₂), carbonyl (C=O), or thiol (-SH, also called sulfhydryl). Thiols in particular are an attractive candidate for covalent attachment schemes because of their high constitutive expression level on cell surfaces and are not found in any of the polymer multilayers used (see discussion below on homo- vs. heterobifunctional crosslinking molecules). To test the presence of thiols on a cell surface, B cells were incubated in tris(2-carboxyethyl)phosphine (TCEP), a reducing agent active at neutral pH. TCEP will reduce di-sulfide (S-S) bonds to thiols, which could then be used to attach a backpack. A fluorescent dye (Alexa488) with a thiol-reactive maleimide group (Mal-Alexa) was used to stain the cells. Flow cytometry shows (see Figure 2.24) that maleimide reacts with cell surface thiols, and that TCEP exposure effectively

doubles the number of thiol groups that may participate in covalent backpack attachment.

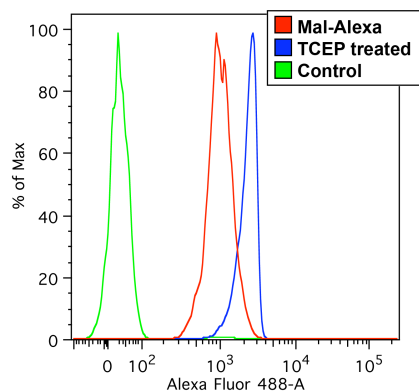


Figure 2.24: Flow cytometry plot of CH27 B cells exposed to maleimide-tagged Alexa488 (Mal-Alexa). The green curve shows untreated cells, the red curve is untreated cells incubated in Mal-Alexa, and the blue curve is cells treated with TCEP and incubated in Mal-Alexa.

A heterobifunctional crosslinking molecule with reactivity to both a surface thiol and a chosen functional group (such as an amine) on the top surface of the backpack may then be used to covalently attach the backpack. (Nothing precludes a *homobifunctional* crosslinker from being used, but the possibility of both linker ends reacting to the same surface makes this less attractive than a heterobifunctional molecule.) For example, PAH or branched PEI may be deposited as the outermost layer of the backpack, thereby presenting primary amines on the surface. *N*-hydroxysuccinimide (NHS) and isothiocyanate are two functional groups highly reactive to amines. Either of these groups could be one end of the heterobifunctional linker. The other end could then be chosen to be reactive to thiols, found on the surface of all cells from cell-surface cysteine residues. Figure 2.25 shows the three heterobifunctional linkers used in this work, each of which are reactive to both thiols and amines.

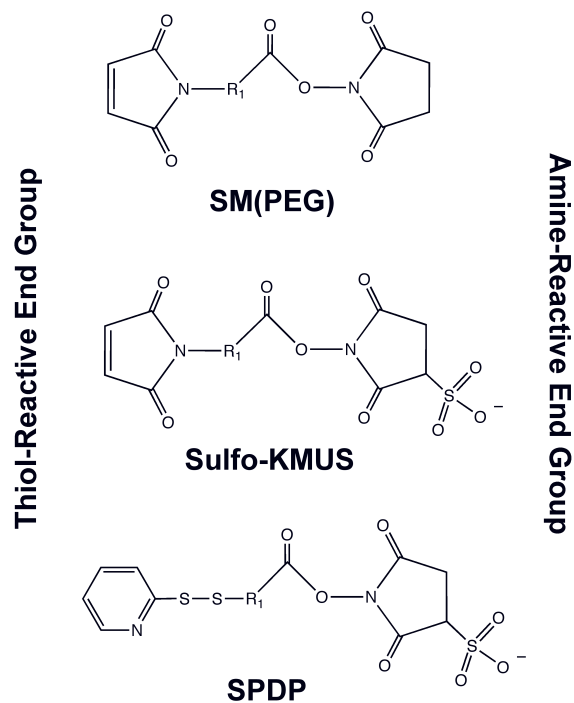


Figure 2.25: Illustration of the three heterobifunctional linker molecules used in this work. Each is reactive to both thiol and amine groups. R_1 is the spacer portion of the molecule, each of which is different. R_1 is a sequence of ethylene oxide groups for SM(PEG) and methylene groups for Sulfo-KMUS and SPDP.

To test that this heterobifunctional reaction occurs, (PEI5/HA3.0)_{5,5} films were built on glass without a release region. Thiol-reactive group presence (maleimide or 2-pyridyldithio) was tested using fluorescence microscopy (see Figure 2.26a) and UV-VIS spectroscopy (Figure 2.26b) of a thiol-containing fluorescein derivative (SAMSA) was exposed to the functionalized surface.

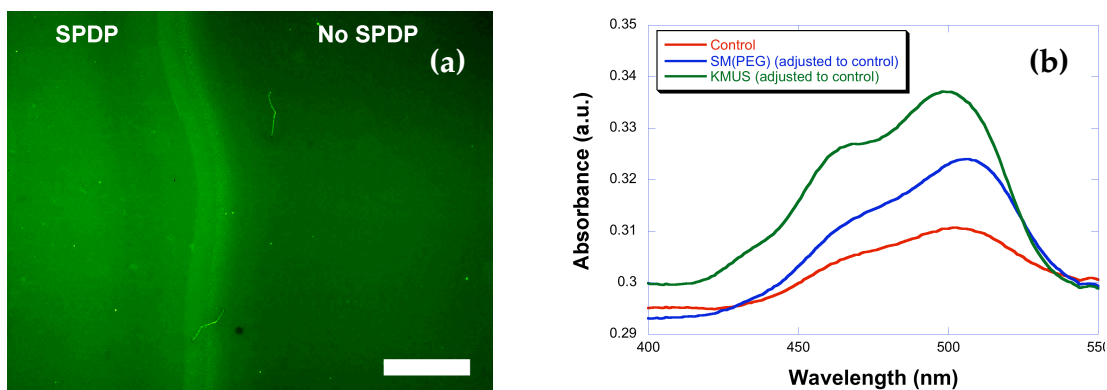


Figure 2.26: (a) Optical micrograph of a (HA3.0/PEI5) film exposed to SPDP and SAMSA. The right side of the image was not exposed to SPDP, but was exposed to SAMSA. The SPDP shows a much stronger fluorescence signal, and a clear border delineates the two regions. Scale bar is 200 μ m. (b) UV-VIS spectroscopy of (HA3.0/PEI5)-terminated films after treatment with SM(PEG) or KMUS, followed by dyeing with SAMSA. The control was an identical film exposed to SAMSA but not exposed to SM(PEG) or KMUS.

Figure 2.26a shows a slide that was partially exposed to SPDP but entirely exposed to SAMSA. The SPDP-treated side shows much greater fluorescence intensity, and a clear border delineates the two regions. UV-VIS spectroscopy indicates much greater SAMSA absorption in the blue region for KMUS and SM(PEG)-treated films compared to the (PEI5.0/HA3.0)_{5.5} control film exposed only to SAMSA. These results show that there is greater attachment of SAMSA to KMUS, SM(PEG), and SPDP-treated surfaces, and that maleimide and pyridyldithio moieties can be attached to the surface of PEMs and remain reactive to thiol groups.

Backpacks with a (PMAA3.0/PNIPAAm3.0)_{80.5} release region were built with an outermost (PEI5.0/HA3.0)_{5.5} region. Branched PEI contains primary, secondary, and tertiary amines: pendant primary amines decorate the polymer backbone where higher-order amines are found. These primary amines can react with the NHS end of the linker, while secondary and tertiary amines can participate in electrostatic crosslinks with HA. HA was chosen as the complementary

polyanion to bind to CD44 on the cell surface (see Chapter 5). While this is not intended to be the primary attachment mechanism, the CD44 interaction could initially dock the cells and bring the cell membrane into more intimate contact with the thiol-reactive moiety. Films were exposed to a 37°C pH 7.4 PBS linker solution (for Sulfo-KMUS and SPDP) or a 37°C DMSO/PBS solution (SM(PEG)). Elevated temperature is critical here, as the release region is unstable at neutral pH, a condition required for linker reactivity. Primary amines react with the NHS, leaving a backpack surface replete with thiol reactive maleimide or 2-pyridyldithio groups.

CH27 B cells were attached to the surface of KMUS-treated backpacks (see Figure 2.27) and showed only slightly lower array occupancy than (HA3.0/CHI3.0) systems (see Chapter 5). That the attachment was motivated by SPDP or HA was uncertain, and a method sensitive enough to detect if the thiol-KMUS reaction occurred was not found. This more general cell-attachment method offers the flexibility to indiscriminately attach to any cell surface, and is worthy of further investigation.

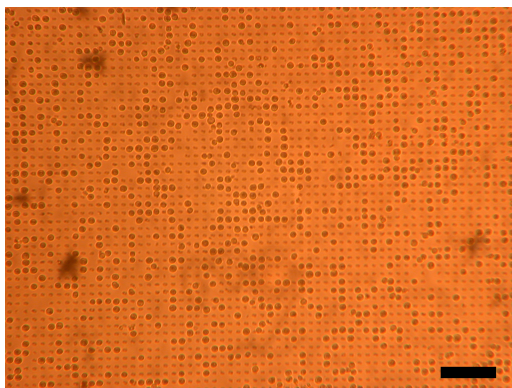


Figure 2.27: Optical micrograph of B cells on a KMUS-terminated backpack system that has not yet been thermally released. The array occupancy is only slightly less than that seen in (HA3.0/CHI3.0) systems. Scale bar is 100 μ m.

Conclusions

Cellular backpacks are fabricated using a photolithographic lift-off technique of polymer thin films built using a layer-by-layer deposition technique. Building backpacks *ex vivo* allows for a breadth of materials, solvents, and processing conditions (temperature, pH, salt concentration, etc.) that may be cytotoxic if used in the presence of cells. A three region backpack design was used throughout this work, including a release, payload, and cell-adhesive region. Several different multilayer systems were developed for use as a release region, and the exact choice for which to use depends on the desired cell attachment method. Materials incorporated into the payload region include quantum dots, magnetic nanoparticles, fluorescent polymers, the biodegradable polymer poly(lactic-co-glycolic acid), and doxorubicin, a model chemotherapy drug. The cell-adhesive region tethers the payload region to the cell surface and must be chosen with consideration to the type of cell. We developed a hyaluronic-acid

containing multilayer that efficiently binds to the cell-surface receptor CD44, commonly found on immune system cell membranes. (Details on this system may be found in Chapter 5.) We also developed a non-cell-specific binding strategy based upon small molecule heterobifunctional linkers capable of binding to functional groups on both the backpack and cell surface. These initial studies demonstrate the feasibility of creating functional backpacks capable of non-cytotoxically attaching to the surface of living immune system cells.

Experimental Details

Materials. Poly(methacrylic acid) (PMAA, PolySciences, M=100kDa), poly(acrylic acid) (PAA, Aldrich, M=450kDa), poly(allylamine hydrochloride) (PAH, Aldrich, MW=70kDa), poly(ethylene glycol) (20kMW-PEG, PolySciences, M=20kDa), poly(ethylene glycol) (100kMW-PEG, Aldrich), poly(N-isopropylacrylamide) (PNIPAAm, Polymer Source, M=258kDa), fluorescein-labeled poly(allylamine hydrochloride) (FITC-PAH, Aldrich, M=70kDa), poly(allylamine hydrochloride) (PAH, Aldrich, M=70kDa), poly(diallyldimethylammonium chloride) (PDAC, Aldrich, M=200-350kDa in 20% aqueous solution), branched poly(ethyleneimine) (PEI, Sigma, $M_n=10kDa$, $M_w=25kDa$), poly(styrene sulfonate) (SPS, Aldrich, M=70kDa), thiol-eng group poly(ethylene glycol) (PEG-SH, Creative PEGWorks, M=20kDa), hyaluronic acid (HA, from Streptococcus equi, Fluka, $M\sim 1.58 \times 10^6$ Da), and low MW chitosan (CHI, DS=.75-.85, $M\sim 5 \times 10^4$ Da) were used without purification. Fluorescein-labeled chitosan was prepared according to the method of Tikhonov and Monfort³⁶ and stored in a desiccator. Amine-functionalized quantum dots (600nm emission) were purchased from Evident Technologies. SM(PEG)₈, KMUS, and SPDP were purchased from Pierce Biotechnologies. SAMSA was purchased from Invitrogen.

Photolithographic Patterning. Typically, glass slides were coated with (PDAC4.0/SPS4.0)_{15.5} (each polymer solution containing 100mM NaCl) prior to any photolithographic processing. Dried, (PDAC/SPS)-coated slides were loaded into a spin-coating system, and ~1.5mL Rohm&Haas S1813 positive photoresist (MicroChem) was placed on top. The slides were spun at 4000rpm for 10s, removed, and immediately placed on a 120°C hotplate for 7 minutes to evaporate all solvents. Specially designed chromium on glass photomasks (Advance Reproductions) with several regions containing different diameter holes (3, 4, 5, 8, 10, 15 and 20 microns) were used for photoresist exposure. A custom-made vacuum apparatus was used to bring the photoresist-coated slide into direct contact with the photomask. Exposure at 365nm was done for 4

minutes at an intensity of $\sim 7\text{mW}/\text{cm}^2$. Slides were gently agitated in MF319 developer solution for 40s, rinsed with Milli-Q water, and gently dried with nitrogen.

<i>Region</i>	<i>Polymer or Nanoparticle</i>	<i>Concentration (molarity based on monomer)</i>	<i>pH</i>
Release	PMAA	.01M	2 or 3
	PAA	.01M	3
	PNIPAAm	.01M	3
	PVPON	.01M	2
	PVCL	.1% (1g/L)	2
	20kMW-PEG	.1% (1g/L)	3
	100kMW-PEG	.1% (1g/L)	3
Payload	fluorescein-labeled PAH	.1% w/v (1g/L)	3
	Fe ₃ O ₄ superparamagnetic nanoparticles	.005% (.5mL of a 3.2% w/v solution in 400mL water)	4
	SPS	.01M	3 or 5
	Amine-functionalized quantum dots	$2.4 \times 10^{-14}\text{M}$ (300 μl of the as-received 6nmol solution in 150mL dH ₂ O)	5
Cell Adhesive	Hyaluronic Acid (HA)	.1% (1g/L)	3
	Chitosan (CHI)	.1% (1g/L) in .1M acetic acid (6mL/L dH ₂ O)	3
	FITC-CHI	.1% (1g/L) in .1M acetic acid (6mL/L dH ₂ O)	3
	PEI	.01M	5

Table 2.3: Details on polymer and nanoparticle solutions used.

Deposition of Heterostructured Multilayered Films. Photolithographically patterned (PDAC4.0/SPS4.0)_{15.5} coated glass substrates were sequentially dipped in dilute polymer or nanoparticle solution using an automated Zeiss

programmable slide stainer or nanoStrata dipping unit (details below). The fully-charged polyelectrolyte, hydrogen-bonded release, and most functional material regions were built in the Zeiss dipper; the cell adhesive region was built in the nanoStrata unit. The dipping time in the Zeus dipper for polymers or nanoparticles was 10 minutes, followed by two Milli-Q water rinses (pH3, adjusted with 1M Hal) for 2 and 1 minutes with mild agitation. In the nanoStrata unit, biopolymer depositions for the cell-adhesive region were done for 10 minutes, followed by three (pH3) Milli-Q water rinses: one for 2 minutes and two for 1 minute, each while the substrate was rotating within the rinse bath.

Quantum dot films were deposited using a StratoSequence VI spinning dipper running StratoSmart v6.2 software from nanoStrata Inc. (USA). AminoQD and SPS deposition steps were performed without stirring for 2 minutes. The three consecutive rinse steps (1min, 30s, and 30s) with pH3 Milli-Q water were performed while spinning the substrate within the solutions at a frequency of approximately 100 rpm.

The polymers, nanoparticles, and solution concentrations (in terms of molarity of monomer repeat unit, unless otherwise specified) used in each region may be found in Table 2.3.

Spraying PLGA. The PLGA payload region was assembled using an airbrush spray technique. Either PLGA (1mg/mL) and DiO (1mg/mL) in chloroform or PLGA (1mg/mL) and DOX (500ug/mL) in 3% dH₂O/THF was sprayed (10mL/min for 30s, substrate 15cm from Badger Model 150 air brush) onto the surface of a (PMAA₂/PVPON₂)_{20.5} multilayer atop a patterned photoresist layer. PLGA in chloroform (without DiO) was sprayed onto Si wafers and thickness was determined using spectroscopic ellipsometry.

Measurement of Backpack Release Efficiency. Coordinate axes were drawn on substrates containing surface-bound backpack arrays, which were photographed using a Zeiss AxioPlan 2 microscope before exposure to neutral pH conditions. The substrates were submerged in 37°C PBS and gently agitated on an orbital shaker at 100s⁻¹ for 30min. If the release region contained PNIPAAm, slides were then immediately transferred to 4°C PBS for an additional 30min. Using the

coordinate axes, the exact same regions could be photographed before and after PBS exposure. These before and after micrographs were compared, and each backpack was determined to have either not released (still on original lattice site) or released and re-adsorbed onto the glass substrate. The ratio of the number of non-released backpacks to the total number of backpacks counted before exposure is reported. Each value is the average of at least three micrographs representing separate regions on the substrate, which typically included ~300 backpacks. An illustration of the process can be found in Figure 2.28.

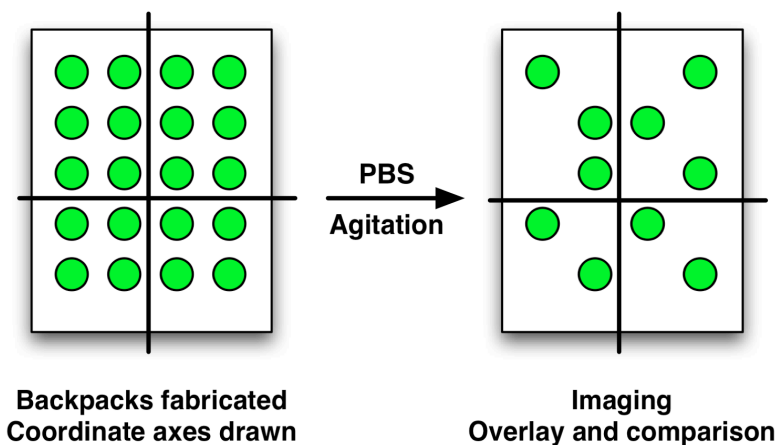


Figure 2.28: Illustration of the backpack liftoff efficiency measurement procedure.

Film Thickness. Non-patterned films were assembled on silicon substrates and unless explicitly noted otherwise, the thickness measured using variable-angle spectroscopic ellipsometry. Ellipsometry measurements were made using a Woolham Co. ellipsometer operating at a 70° angle of incidence. Measurements from 300 to 1000nm were used, and all data analysis was done using the WVASE32 software. A P-10+ stylus profilometer (KLA Tenor Corporation, USA) was used for measurements noted as observed by profilometry.

Synthesis of rhodamine-labeled PMAA. Rhodamine-labeled PMAA (Rhoda-PMAA) was prepared by adapting a protocol by deBelder and Wik³⁷. First, 1g PMAA was completely dissolved (stirred overnight) in 40mL water in a Teflon reaction vessel. The following was added simultaneously: 50mL dimethyl sulfoxide (Sigma), .1 sodium bicarbonate (Sigma), .1mL dibutyltin dilaureate

(Sigma), and .05g rhodamine isothiocyanate (Fluke). The vessel was sealed and the reaction was allowed to proceed while stirred in an 80°C oil bath for 1.5h. The product was precipitated in isopropyl alcohol, collected, dried under vacuum at 50°C, redissolved in 30mL water, and dialyzed against 2L water (pH~3) for 72h. The aqueous solvent was evaporated at 50°C under vacuum for 48h. The final product was then dissolved in water at .435g/500mL (.01M per the non-functionalized PMAA monomer concentration). Since the molar ratio of acrylic acid species on PMAA to rhodamine isothiocyanate was 120:1, even 100% reaction yield would not significantly interfere with hydrogen-bonding during film deposition.

X-ray photoelectron spectroscopy. Chemical composition of was determined by X-ray photoelectron microscopy (XPS) using a Kratos AXIS Ultra spectrometer with a monochromatized Al K_α source. Survey spectra were taken with a pass energy of 160 eV and a step size 1 eV. High resolution data were taken with a pass energy 20 eV and a step size 0.1 eV with a minimum of three scans of a region. Three films were studied: as-deposited (PAA3.0/PEG3.0)_{20.5} and flipped (PAA3.0/PEG3.0)_{20.5}(PAH3.0/MNP4.0)₁₀ and (PAA3.0/PEG-SH3.0)_{20.5}(PAH3.0/MNP4.0)₁₀. A flipped film was deposited on a glass slide, scored into a ~10mm x 10mm area, lifted off with PBS, gently rinsed with water and then placed face down on another glass slide. XPS was then performed on this face previously directed toward the fabrication substrate. All data was analyzed using Casa XPS software.

Flow Cytometry. Backpack aliquots were analyzed on a BD FACS Canto II flow cytometer. The phycoerythrin (PE) channel of the cytometer was used since among the different detectors available, PE had the greatest amount of spectral overlap with rhodamine. Data sets were gated so that only sufficiently large objects were analyzed (i.e., above the FSC value for a backpack), and the mean PE value was recorded. All data was analyzed using FlowJo software, and normalized against the mean PE intensity at 24h.

KMUS, SM(PEG)₈, and SPDP reactions. (PEI5.0/HA3.0)_{5.5} films were deposited using a NanoStrata spin dipper. PEI was dipped at pH 5 to deprotonate primary

amines so that fewer are involved with electrostatic crosslinks with HA, but not at sufficiently high pH to destabilize the release region. Polymers were rinsed with distilled water at the same pH as the polymer solution. KMUS and SPDP are directly soluble in water, and were suspended in 37°C PBS at 1mg/mL. SM(PEG) was first dissolved in DMSO to form a 1mM stock solution, then diluted 20 μ l stock to 2mL 37°C PBS. The heterobifunctional linker solution was pipetted onto the surface of a film laying horizontally in a 37°C humidity chamber. The reaction was allowed to proceed overnight, after which the film was copiously washed in 37°C PBS and 37°C distilled water.

References

- (1) Berg, M. C.; Yang, S. Y.; *et al.* Controlling Mammalian Cell Interactions on Patterned Polyelectrolyte Multilayer Surfaces *Langmuir* **2004**, *20*, 1362.
- (2) J. Park, L. D. F. P. T. H. Multicomponent Patterning of Layer-by-Layer Assembled Polyelectrolyte/Nanoparticle Composite Thin Films with Controlled Alignment *Advanced Materials* **2005**, *17*, 2575.
- (3) J. Park, P. T. H. Multilayer Transfer Printing for Polyelectrolyte Multilayer Patterning: Direct Transfer of Layer-by-Layer Assembled Micropatterned Thin Films *Advanced Materials* **2004**, *16*, 520.
- (4) ShaikhMohammed, J.; DeCoster, M. A.; *et al.* Fabrication of Interdigitated Micropatterns of Self-Assembled Polymer Nanofilms Containing Cell-Adhesive Materials *Langmuir* **2006**, *22*, 2738.
- (5) ShaikhMohammed, J.; DeCoster, M. A.; *et al.* Micropatterning of Nanoengineered Surfaces to Study Neuronal Cell Attachment in Vitro *Biomacromolecules* **2004**, *5*, 1745.
- (6) Lynn, D. M. Peeling Back the Layers: Controlled Erosion and Triggered Disassembly of Multilayered Polyelectrolyte Thin Films *Advanced Materials* **2007**, *19*, 4118.
- (7) Kharlampieva, E.; Sukhishvili, S. A. Hydrogen-Bonded Layer-by-Layer Polymer Films *Polymer Reviews* **2006**, *46*, 377
- (8) Sukhishvili, S. A.; Granick, S. Layered, Erasable Polymer Multilayers Formed by Hydrogen-Bonded Sequential Self-Assembly *Macromolecules* **2002**, *35*, 301.
- (9) Berg, M. C.; Zhai, L.; *et al.* Controlled drug release from porous polyelectrolyte multilayers *Biomacromolecules* **2006**, *7*, 357.
- (10) Lvov, Y.; Ariga, K.; *et al.* Layer-by-Layer Assembly of Alternate Protein Polyion Ultrathin Films *Chemistry Letters* **1994**, 2323.
- (11) Lvov, Y.; Ariga, K.; *et al.* Molecular film assembly via layer-by-layer adsorption of oppositely charged macromolecules (linear polymer, protein and clay) and concanavalin A and glycogen *Thin Solid Films* **1996**, *285*, 797.
- (12) Wu, Z.; Walish, J.; *et al.* Deformable Antireflection Coatings from Polymer and Nanoparticle Multilayers *Advanced Materials* **2006**, *18*, 2699.
- (13) Li, Z.; Lee, D.; *et al.* Two-level antibacterial coating with both release-killing and contact-killing capabilities *Langmuir* **2006**, *22*, 9820.
- (14) Ono, S. S.; Decher, G. Preparation of Ultrathin Self-Standing Polyelectrolyte Multilayer Membranes at Physiological Conditions Using pH-Responsive Film Segments as Sacrificial Layers *Nano Letters* **2006**, *6*, 592.
- (15) Cho, J.; Caruso, F. Polymeric Multilayer Films Comprising Deconstructible Hydrogen-Bonded Stacks Confined between Electrostatically Assembled Layers *Macromolecules* **2003**, *36*, 2845.
- (16) Vihola, H.; Laukkanen, A.; *et al.* Cytotoxicity of thermosensitive polymers poly(N-isopropylacrylamide), poly(N-vinylcaprolactam) and amphiphilically modified poly(N-vinylcaprolactam) *Biomaterials* **2005**, *26*, 3055.

- (17) Serpe, M. J.; Jones, C. D.; *et al.* Layer-by-layer deposition of thermoresponsive microgel thin films *Langmuir* **2003**, *19*, 8759.
- (18) Jones, C. D.; Lyon, L. A. Synthesis and Characterization of Multiresponsive Core-Shell Microgels *Macromolecules* **2000**, *33*, 8301.
- (19) Harris, J. M. *Poly(ethylene glycol) chemistry : biotechnical and biomedical applications*; Plenum Press: New York, 1992, pages
- (20) Sukhishvili, S. A.; Granick, S. Layered, Erasable, Ultrathin Polymer Films *Journal of the American Chemical Society* **2000**, *122*, 9550.
- (21) Okano, T.; Yamada, N.; *et al.* A novel recovery system for cultured cells using plasma-treated polystyrene dishes grafted with poly(N-isopropylacrylamide) *Journal of Biomedical Materials Research* **1993**, *27*, 1243.
- (22) Schild, H. G.; Tirrell, D. A. Microcalorimetric detection of lower critical solution temperatures in aqueous polymer solutions *The Journal of Physical Chemistry* **2002**, *94*, 4352.
- (23) Zacharia, N. S.; DeLongchamp, D. M.; *et al.* Controlling Diffusion and Exchange in Layer-by-Layer Assemblies *Macromolecules* **2007**, *40*, 1598.
- (24) Zacharia, N. S.; Modestino, M.; *et al.* Factors Influencing the Interdiffusion of Weak Polycations in Multilayers *Macromolecules* **2007**, *40*, 9523.
- (25) Olivier, G. K.; Shin, D.; *et al.* Supramolecular Ion-Pair Interactions To Control Monolayer Assembly *Langmuir* **2009**, *25*, 2159.
- (26) Willey, T. M.; Vance, A. L.; *et al.* Chemically Transformable Configurations of Mercaptohexadecanoic Acid Self-Assembled Monolayers Adsorbed on Au(111) *Langmuir* **2004**, *20*, 2746.
- (27) Boulmedais, F.; Bozonnet, M.; *et al.* Multilayered Polypeptide Films: Secondary Structures and Effect of Various Stresses *Langmuir* **2003**, *19*, 9873.
- (28) Richert, L.; Lavallo, P.; *et al.* Layer by Layer Buildup of Polysaccharide Films: Physical Chemistry and Cellular Adhesion Aspects *Langmuir* **2004**, *20*, 448.
- (29) Li, S.; Vert, M. In *Encyclopaedia of Controlled Drug Delivery*; Mathowitz, E., Ed.; John Wiley and Sons: New York, 1999; Vol. 1, p 71.
- (30) Park, K.; Shalaby, W. S. W.; *et al.* *Biodegradable hydrogels for drug delivery*; Technomic Pub.: Lancaster, PA, 1993, pages
- (31) Anderson, J. M.; Shive, M. S. Biodegradation and biocompatibility of PLA and PLGA microspheres *Advanced Drug Delivery Reviews* **1997**, *28*, 5.
- (32) Hyung, W.; Ko, H.; *et al.* Novel hyaluronic acid (HA) coated drug carriers (HCDCs) for human breast cancer treatment *Biotechnology and Bioengineering* **2008**, *99*, 442.
- (33) Underhill, C. CD44: the hyaluronan receptor *Journal of Cell Science* **1992**, *103*, 293.
- (34) Hillberg, A. L.; Tabrizian, M. Biorecognition through Layer-by-Layer Polyelectrolyte Assembly: In-Situ Hybridization on Living Cells *Biomacromolecules* **2006**, *7*, 2742.
- (35) Serizawa, T.; Yamaguchi, M.; *et al.* Alternating Bioactivity of Polymeric Layer-by-Layer Assemblies: Anti- vs Procoagulation of Human Blood on Chitosan and Dextran Sulfate Layers *Biomacromolecules* **2000**, *1*, 306.
- (36) Tikhonov, V. E.; Lopez-Llorca, L. V.; *et al.* Endochitinase activity determination using N-fluorescein-labeled chitin *Journal of Biochemical and Biophysical Methods* **2004**, *60*, 29.

- (37) de Belder, A. N.; Wik, K. O. Preparation and properties of fluorescein-labelled hyaluronate *Carbohydrate Research* **1975**, *44*, 251.

Chapter 3: Cellular Behavior with Attached Backpacks

Reproduced in part with permission from Swiston, A. J.; Cheng, C.; Um, S. H.; Irvine, D. J.; Cohen, R. E.; Rubner, M. F. *Nano Letters* **2008**, *8*, 4446. Copyright 2008 American Chemical Society.

Introduction

To successfully leverage native cell behaviors with functional synthetic materials, native cell behaviors must be unimpinged. The design of the backpack allows for the majority of the cell surface to freely interact with its environment. Since only a small portion of the membrane is physically occluded, cell functions requiring intimate cell-environment interaction are possible, thus opening a range of cell behaviors that could not be leveraged in a traditional cell encapsulation paradigm.

How cells react to having a backpack tethered to their surface is the focus of this chapter. Different methods for attaching backpacks to cell surfaces are discussed first, along with considerations for which method to use. The most fundamental cell functions – viability and reproduction – were examined for CH27 B cells.

Backpacked T-cells were observed to continue migrating on ICAM-coated cover slips, showing that a native cell behavior of particular interest proceeded following backpack attachment. B cells with magnetic nanoparticle-containing backpacks were manipulated in a magnetic field, demonstrating the conferral of new properties to the cell via the attached backpack. Finally, backpacks were

used to affect a particular cellular response by activating dendritic cells, showing potential for backpacks to not just be “ghost”-like vessels, but also actively interact with the attached cell.

Backpack Attachment to Cell Surfaces

Two methods were developed to attach backpacks to the surface of living immune cells under non-cytotoxic salt concentration, temperature, and pH conditions. The fundamental difference between the two methods is when the backpack is released from the surface. The backpack may be released either prior to cell exposure, resulting in a random association of cells to backpacks, or following cell exposure, forcing single cell-single backpack associations. The polymers used in the release region give rise to these different methods.

The first method relies solely upon a pH-triggered release mechanism (for a detailed discussion, see page 41) of the hydrogen-bonded release region.

Poly(methacrylic acid) (PMAA) and poly(vinylpyrrolidone) (PVPON) were the two most commonly used hydrogen-bonding polymer system used for this method. Following fabrication, pH 7.4 PBS was pipetted on the surface, and backpacks were gently scraped (with a cell scraper) to encourage liftoff. An aliquot of backpacks was collected, centrifuged, and resuspended at a desired concentration (typically 10^7 backpacks/mL). Backpacks were not found to aggregate during this processing, and could be easily resuspended by pipetting. Backpacks were then added to cells in media, which attached randomly and

commonly led to cellular aggregates (see Chapter 4). This first method is schematically represented in Figure 3.1a.

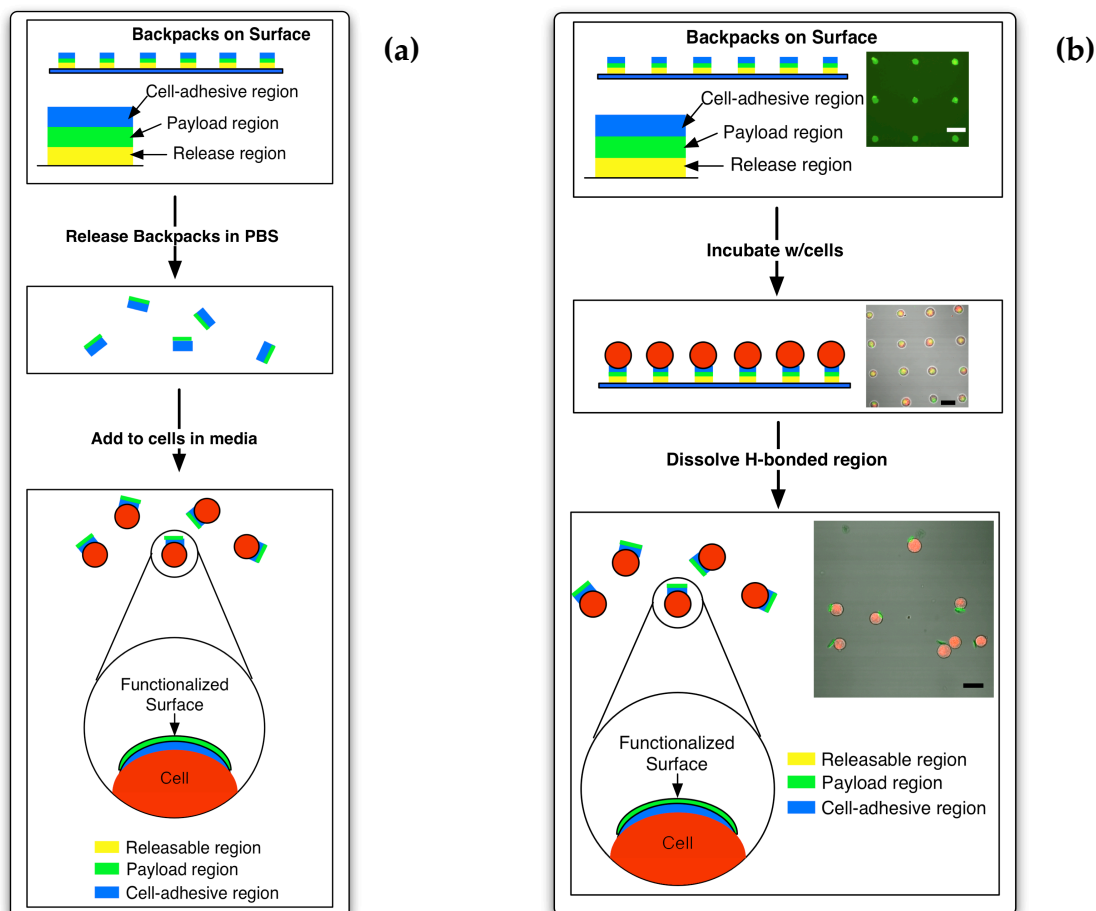


Figure 3.1: Schematics of the two methods developed to attach backpacks to a cell's surface. (a) shows the case in which backpacks are released from the fabrication substrate prior to cell exposure. The resulting colloidal backpacks are then free to attach to one or more cells, though only the one backpack per cell case is illustrated. (b) shows how cells were attached to backpacks, then released by dropping the temperature to 4°C.

The second attachment method affords greater control over cell-backpack association. Here, backpacks remain attached to the surface as cells bind to the cell-adhesive outer face (see Figure 3.1b). Poly(methacrylic acid) (PMAA) and poly(N-isopropyl acrylamide) (PNIPAAm) are used for the release region in this case. Backpacks are released from the surface only when the temperature is

lowered to below a critical value ($\sim 29^{\circ}\text{C}$) that corresponds very closely to the lower critical solution temperature (LCST) of homopolymer PNIPAAm. A detailed explanation for the concurrent pH and temperature dissolution mechanisms, see Chapter 2 and Figure 2.10.

The reason for developing two separate attachment methods was in consideration for clinical relevance. While the second method affords greater control over cell-backpack association, this protocol would require collecting and purifying a patient's cells, seeding them onto the surface, then followed by temperature-triggered release. The backpacked cells would finally be injected back into the patient. This time-intensive protocol, with very precise temperature and equipment needs, would probably prevent widespread clinical adoption. Thus, a more straightforward, "injectable" formulation was sought, and the first method (a pH-only trigger) was developed. Instead of isolated and seeding cells, backpacks with a cell-adhesive region specific to a particular cell type could be injected directly into a patient. These targeted cells would attach to a backpack and carry it along as they performed their native functions, achieving the same result as the temperature-triggered system.

CH27 B Lymphocyte Cytotoxicity and CD44 Migration

Biocompatibility is the primary requirement for any backpack system. If the backpack were to kill the cell to which it was attached, the cell's native functions could not be leveraged, rendering the synthetic materials within the backpack useless.

Two methods were used to determine cell-backpack interaction toxicity. Both methods used the following backpack composition:

$(\text{PMAA}3.0/\text{PNIPAAm}3.0)_{80.5}(\text{FITC-PAH}3.0/\text{Fe}_3\text{O}_4 \text{ NP}4.0)_{10}(\text{CHI}3.0/\text{HA}3.0)_3$.

The first method relied upon monitoring cells attached to backpacks on a surface. CH27 B cells were attached to backpacks (as seen in Figure 3.1b) but *without* initiating thermal backpack release. These anchored cells were incubated at 37°C and examined in duplicate at 1, 24, 48, and 72 hours using trypan blue staining. The slide containing the attached cell-backpack array was removed from media, washed 3x in 37°C PBS, incubated in 1:10 trypan blue:PBS for 2min, and the number of dead cells in a .25mm x .25mm area were counted. Approximately 250 cells were examined at each time point, and the percentage of viable cells reported is defined as follows:

$$\text{Viable Cells (\%)} = \frac{\% \text{ live cells at 1h}}{\% \text{ live cells counted}}$$

Figure 3.2 shows that for 48h, the cells are nearly 100% viable. At 72 hours, however, there seems to be a precipitous drop in the number of live cells, likely due to the cell cycle of the immobilized cells. We observe that the doubling time for CH27 cells is ~12h, meaning that an individual cell will have split 6 or more times during observation.

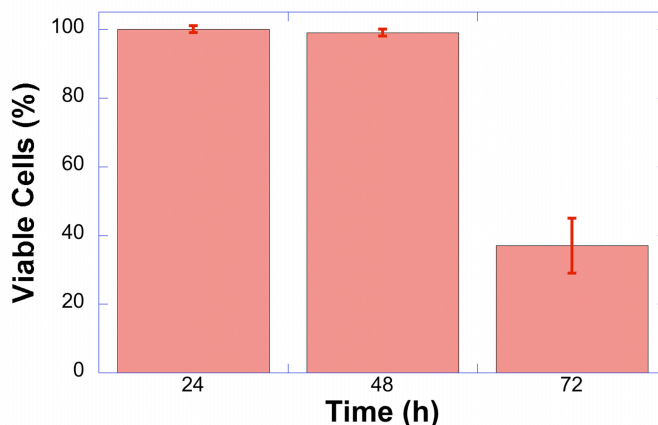


Figure 3.2: Viability of immobilized CH27 B cells over 72h following attachment to a backpack.

The second method measured the viability of backpacked cells after thermal release. Cells were attached to backpacks (Figure 3.1b), and after lift-off at 4°C, backpacked-cell containing media was centrifuged at 2,000 rpm for 5 min, resuspended, and washed twice with PBS (pH 7.4) and once with fresh RPMI media. The concentration of backpack-functionalized CH27 cells was measured to be 25,000 cells/mL (average of 9 samples); an aliquot of CH27 cells (at 25,000 cells/mL) without a polymer backpack was prepared as a control. Three six well plates were used, one for each time point tested (24, 48, and 72h). Each plate contained three different samples and three controls. In addition, fresh RPMI was incubated and measured as a blank solution on another six well plate. After incubation at 37°C and 5% CO₂ for 24, 48, and 72 hours, cell viability was tested using Promega’s CellTiter-Glo Luminescent cell viability assay following the manufacturer's protocol.

Figure 3.3 shows that there does not seem to be any acute toxicity from backpack attachment, and that following thermal release backpacked cells are able to reproduce.

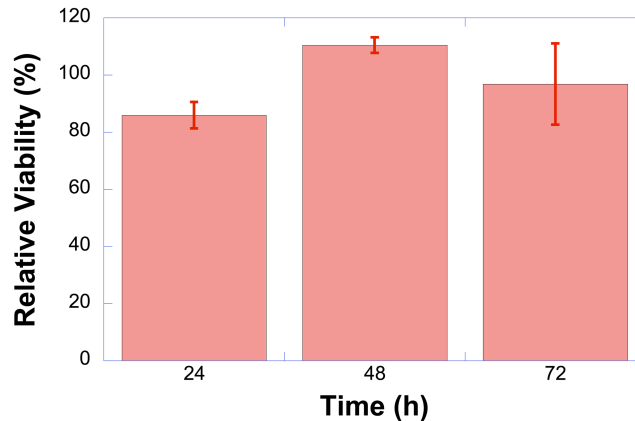


Figure 3.3: Viability of backpack-functionalized CH27 B cells that have been thermally released and cultured. Data courtesy Soong Ho Um.

As a final test to determine if the backpack negatively impacts normal B cell behavior, we examined how CD44 migrated on the cell membrane following backpack attachment. Since the backpack attaches via a CD44-HA mediated mechanism (see Chapter 5), surface CD44 may selectively migrate to the backpack, thereby reducing or eliminating native behaviors requiring accessible CD44. Cells were exposed in the normal way to backpacks of the following composition: $(\text{PMAA}3.0/\text{PNIPAAm}3.0)_{80.5}(\text{PAH}3.0/\text{MNP}4.0)_{10}(\text{CHI}3.0/\text{HA}3.0)_3$ (note that these patches do not contain FITC labeled PAH). Before 4°C thermal lift-off, a fluorescein-labeled anti-CD44 antibody was added to the media at a final concentration of 5µg/mL. The samples were agitated at 4°C for 1h and cells were imaged in the antibody/media mixture.

Figure 3.4 presents optical and fluorescence micrographs of a CD44 stained cell that is representative of over 20 cells examined. There seems to be no significant amount of CD44 clustering in the membrane region attached to the backpack. These results suggest that CD44 is still accessible on the membrane, and the cell will be able to perform any other CD44-dependant function.

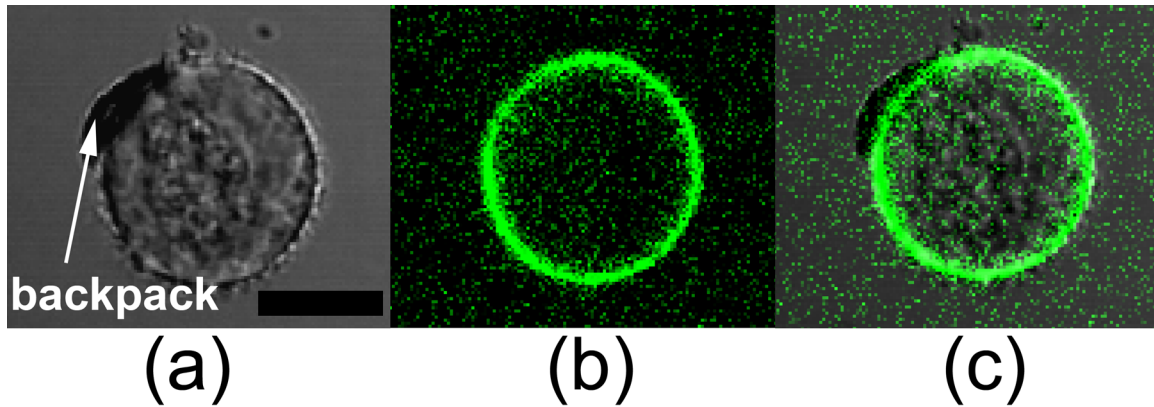


Figure 3.4: Representative (a) brightfield and (b) fluorescence images of a CH27 B cell with fluorescein-labeled CD44. (c) is an overlaid composite of (a) and (b). Note that there does not seem to be any segregation of CD44 to the membrane region associated with the backpack. The scale bar is 10 μ m.

HuT78 T Lymphocyte Migration

As a test of whether backpack attachment would negatively affect intrinsic cell functions, we assessed the ability of backpack-modified T-cells to migrate. Hut 78 T-cells spontaneously migrate on substrates coated with intercellular adhesion molecule-1 (ICAM-1), an adhesion ligand present in tissue and on endothelial cells that binds to the T-cell integrin lymphocyte function-associated molecule-1. We attached fluorescent, superparamagnetic nanoparticle-containing backpacks to the surfaces of T-cells, and tracked their migration over time by

videomicroscopy. We found that this type of T-cell attached to backpacks with less efficiency than CH27 B cells, likely due to their lower expression of CD44 cell surface receptors. An LSM image of a backpack attached to a T-cell is shown in Figure 3.5.

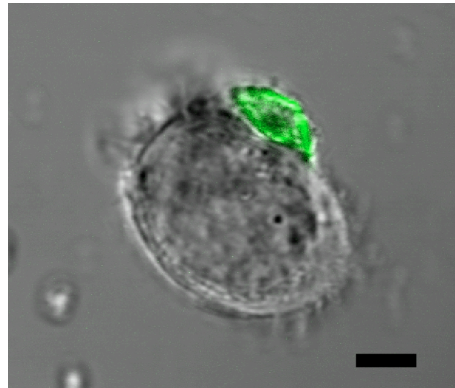


Figure 3.5: A CLSM micrograph of a HuT78 T-cell with a fluorescent backpack attached. Notice that the backpack does not attach conformally, and seems to curl on the edges. The scale bar is 10 μ m.

While several T-cells decorated with backpacks were found to migrate on ICAM-1-coated surfaces, we chose to closely monitor one, and this cell is shown in the time-lapse sequence in Figure 3.6 at 3 different time points for the same field of view. This cell polarized, developed a characteristic lamellipodium-extending leading edge and trailing uropod, and migrated continuously for over 6h. The backpack was not conformally attached to the cell membrane, which seems to suggest that the cell has chosen to locally cluster some of the available surface receptors responsible for cell-backpack binding. Interestingly, while the cell changes its migration direction several times, including reversing the leading and trailing ends by changing the migration direction nearly 180°, the cell-backpack attachment point is always found at the trailing end of the cell. This

may reflect the fact that CD44, like a number of other adhesion molecules on T-cells, preferentially accumulates in the uropod at the rear of the cell during migration¹. After 6h, the backpack stuck to the cover slip surface, but the cell continued polarizing. However, the cell-backpack association was strong enough to frustrate actual migration, indicating that the strength of binding between the backpack and cell surface was greater than the traction force exerted by the cell migrating on ICAM-1. The preliminary, proof-of-concept results presented here suggest that T-cells have the capability to migrate normally while bearing a backpack.

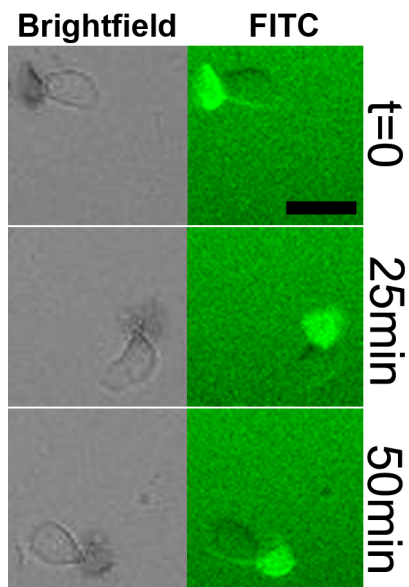


Figure 3.6: Migration of a HuT 78 model T-cell on an ICAM1 coated cover slip. The cell was observed to travel at $\sim .5\mu\text{m}/\text{min}$ for at least 6 hours, at which point the backpack adsorbed to the cover slip preventing the cell from migrating further. The scale bar is $25\mu\text{m}$.

Magnetic Manipulation of B cells

To test that we conferred magnetic properties to the cell via the attached backpack, B lymphocytes were exposed to superparamagnetic backpacks containing a PMAA/PVPON-release region. The free-floating lymphocytes were washed off the previously backpack-laden surface into a LabTek chambered cover slip and imaged using an inverted microscope. After cells were allowed to settle, a rare earth magnet was placed close to the imaged region but outside of the chamber. Figure 3.7 shows how a single B-cell–single backpack complex responds to the applied magnetic field. This cell moved $\sim 200\mu\text{m}$ in 11s, much faster than a freely suspended cell would normally move. Further, cells without backpacks, as seen in Figure 3.7, do not respond to the applied magnetic field. Since the PMAA/PVPON system was used, large cell–backpack aggregates (see Chapter 4) also move in the direction of the magnet. The adhesion between the backpack and cell is strong enough that the cell is pulled along with, rather than releasing, the backpack. A first-order analysis of the drag force exerted on the cell in Figure 3.7 is $\sim 3\text{ pN}^{\text{a}}$. In general, cells do not adhere to the entire surface area of the backpack (see Figure 4.2, page 110), which means that the cell–backpack adhesion is quite high (see “Nylon Mesh Filtering: A Model for Extravasation,” page 119).

^a The Stokes equation for drag ($F = 6\pi\eta vr$) was used for this calculation. Values used were as follows: $\eta = 10^{-3}\text{ Pa}\cdot\text{s}$, $v = 20\ \mu\text{m}/\text{s}$, and $r = 8\mu\text{m}$.

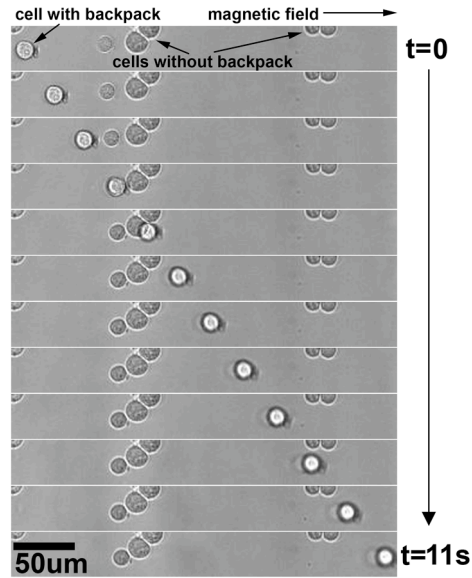


Figure 3.7: A backpack functionalized B-cell responds to an applied magnetic field. The backpack system used was $(\text{PMAA}2.0/\text{PVPON}2.0)_{40.5}(\text{FITC-PAH}3.0/\text{MNP}4.0)_{10}(\text{CHI}3.0/\text{HA}3.0)_3$. The cell moved $\sim 200\mu\text{m}$ in 11s toward a rare earth magnet placed near the imaging chamber. Because the cell is free-floating in solution, it moves out of the field of focus during the course of imaging. Note that cells without backpacks do not respond to the applied field.

DC2.4 Dendritic Cell Activation

In the above two examples, backpacks were passive bodies attached to cellular surfaces. That the backpack did not kill the cell, or impair an important native behavior is encouraging. In these cases, the backpack is a “ghost”-like particle, interacting only enough with the cell to remain attached, but not fundamentally change how the cell behaves.

However, if the backpack could actively interact with the attached cell, a synergistic synthetic-biological device could be created. Perhaps the backpack could contain a cue to affect a desired behavior, moving beyond a “ghost”-like particle to a more active therapeutic tool.

We chose to study how a specific type of antigen-presenting cell (APC) would react to backpack attachment. APCs are a class of immune cells that play a critical role in the T-cell mediated immune response, and serve as the link between the innate and adaptive immune systems. APCs actively seek non-native objects (antigens) in the body, ingest them, migrate to the lymph nodes, and present fragments of these antigens to naïve lymphocytes. APCs are commonly found in mucus membrane and directly beneath the skin – areas where pathogens are most likely to enter the body. When an APC encounters and ingests an antigen, it becomes “activated” and upregulates certain cell-surface markers (CD54, CD80, CD83, and CD86^{2,3}) while homing to the lymph nodes. Dendritic cells are the most potent APCs, and have become the focus of new adjuvant and antigen delivery systems.

A number of molecules, including lipopolysaccharides (LPS), monophosphoryl lipid A (MPLA, the hydrophobic anchor of LPS which activates toll-like receptor 4 (TLR4)⁴), and CpG ODN (cytosine-phosphate-guanine oligodeoxynucleotides⁵), are exogenous mediators for DC activation². In the soluble form, LPS is an extremely strong activator, and is commonly used to produce the reference activation state. Exposing dendritic cells to microparticles with attached activating species (LPS³ or CpG⁶) caused dendritic cells to express characteristic activation markers at levels higher than upon exposure to soluble activators. This finding shows that adjuvant therapy may be more efficient when used in conjunction with microparticles, and that backpacks may provide a unique system to selectively deliver large antigen payloads to the lymph.

For instance, if a backpack could be loaded with an adjuvant (such as aluminum, LPS, or CpG) and/or an antigen and attached to an activated DC, this could greatly enhance antigen immunogenicity while being trafficked to the lymph system. Even better, if a loaded backpack itself activated the DC, a new type of “all-included” vaccine system could be possible. Given that DCs are phagocytes, a backpack’s phagocytosis-resistance may also offer unique benefits for this application.

To create an activating backpack, MPLA or LPS were adsorbed onto the outer surface of the backpack following photolithographic patterning. The outermost (FITC-PAH3.0/MNP4.0)₁₀ multilayer has a contact angle of ~120°; such a hydrophobic surface should be able to adsorb the amphiphilic MPLA or LPS molecule. Figure 3.8 shows AFM images of (FITC-PAH3.0/MNP4.0)₁₀ films exposed to pH5.0 MES buffer overnight. The images labeled “LPS” included soluble LPS (1 μg/mL). The surface morphology significantly changed with LPS exposure, indicating adsorption of the LPS on the surface. Follow-up ellipsometry to determine the exact thickness of this LPS layer was inconclusive due to how thin the LPS layer seems to be.

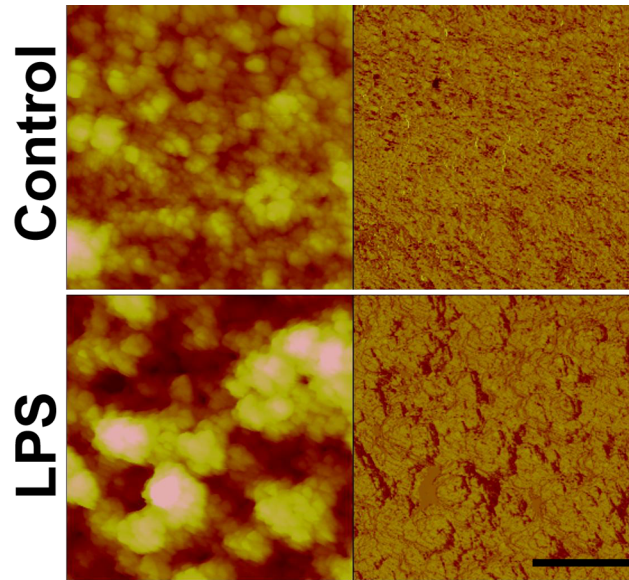


Figure 3.8: AFM images of (FITC-PAH3.0/MNP4.0)₁₀ multilayers soaked in pH5.0 MES buffer with and without LPS. The LPS-containing buffer images show a much rougher morphology, likely due to adsorbed LPS on the backpack surface. Scale bar = 1 μ m.

Backpacks with adsorbed LPS or MPLA were attached to DC2.4 cells using the first attachment method above (see Figure 3.1a) and allowed to incubate overnight. These cells were stained for certain cell-surface receptors indicative of activation (CD54, CD80, CD86), and receptor expression was measured using flow cytometry. After gating data based on size (FSC) and viability (PI signal), LPS, MPLA, and “plain” (no LPS or MPLA) backpacks affect greater receptor expression. As seen in the histograms in Figure 3.9, CD54, CD80, and CD86 each show higher expression levels for the LPS-adsorbed backpacks than even the soluble LPS control. We found that phagocytes were unable to internalize backpacks (see Chapter 6, page 169), which may allow for a more chronic exposure to LPS or MPLA, thus leading to higher surface CD molecule expression.

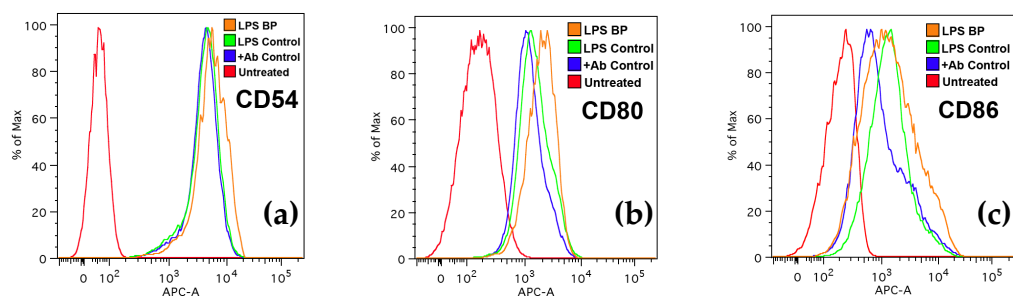


Figure 3.9: Histograms of (a) CD54, (b) CD80, and (c) CD86 expression on DC2.4 cells following backpack exposure. The orange curve shows expression of each receptor for backpacks with adsorbed LPS. The green and blue curves are soluble LPS and antibody controls, respectively. The red curves show the background fluorescence for untreated cells.

Conclusions

Backpack attachment does not seem to negatively impact native cellular behaviors, and if certain backpack surface chemistries are chosen, backpack attachment can affect desirable cell behaviors. The first and most important native function following backpack attachment is viability and reproduction; if contact with a backpack is acutely toxic, the cell's native functions cannot be used to deliver a backpack's payload. B cells were attached to (CHI3.0/HA3.0)₃-terminated backpacks and monitored both on the surface (i.e., backpacks were not thermally released) and in solution (i.e., backpacks were released). In both cases, no significant cytotoxicity was observed. A more active cell behavior, and one very pertinent to adoptive immunotherapy applications, is lymphocyte migration. Backpacks were attached to T cells known to migrate on ICAM-coated surfaces. Even with a backpack attached, these T cells were found to migrate for several hours, showing that the backpack did not interfere with this native function. Finally, backpacks were built with a cell-adhesive region based on lipopolysaccharides (LPS) which is known to activate naïve dendritic cells

(DCs). Upon activation, these cells will migrate to draining lymph nodes, a desirable behavior for precisely delivering materials to the immune system. After exposure to LPS-coated backpacks, we observed the up-regulation of cell surface markers characteristic of activation. This demonstrates that backpacks need not be passive bodies attached to cell surfaces, but rather could actively engage with the cell. This opens exciting possibilities not only for more accurate delivery of payloads via cell couriers, but creating synergistic bio-synthetic hybrid systems for therapy and diagnostics.

Experimental Details

Antibodies and Reagents. AlexaFluor 647-conjugated anti-CD54, anti-CD86, and anti-CD80 (and each Ab's respective isotype control) were purchased from BioLegend and used at 1 $\mu\text{g}/\text{mL}$. Propidium iodide (PI, Calbiochem) was purchased from VWR and used at $40\mu\text{l}/10^6$ cells.

Cell Culture and Staining. CH27 B lymphocytes and DC2.4 dendritic cells were maintained and passaged in RPMI 1640 cell culture media (Mediatech) supplemented with 10% FCS, penicillin/streptomycin, 25mM HEPES, and 36mM NaHCO_3 . DC2.4 cells were gently removed from the TCPS dish using a cell scraper. HuT 78 cells (ATCC, Manassas, VA) were maintained and passaged in IMDM cell culture media (Gibco) supplemented with 10% FCS, 10mL/L P/S solution, and 36mM NaHCO_3 (as suggested by manufacturer).

When needed, cell visualization was aided by non-selectively staining the cell interior with a red fluorophore. CellTracker Red CMPTX (Molecular Probes) was added at a 1 μM concentration (from 10mM stock solution in DMSO) to a cell aliquot (concentration $\sim 10^6$ cells/mL), incubated for 30min, washed 2x with cold complete media, and incubated overnight in complete media before backpack attachment and imaging.

Cell Functionalization. For backpacks made with a (PMAA/PNIPAAm) release region, a backpack-laden glass slide was cut and placed in the bottom of a well in a 6-well plate or a small Petri dish. 2mL of B lymphocytes suspended in 37°C RPMI media ($\sim 10^6$ cells/mL) were pipetted onto the surface. The entire plate was agitated for 15 minutes at 37°C, followed by 37°C incubation for 15 minutes, and this cycle was repeated identically once more. Once on the surface of a backpack, CD44 cell surface receptors anchor onto the HA within the cell-adhesive region. The glass slide, now containing lymphocytes attached to surface-bound backpacks (Figure 1b), was removed and gently shaken for $\sim 15\text{s}$ upside down in 37°C PBS to remove all cells not attached to a backpack. The

glass slide was returned to a new well containing 4°C media, and the entire plate or dish was chilled to 4°C for 30 minutes, manually agitated periodically.

An alternative method of backpack attachment was employed for backpacks containing the (PMAA2.0/PVPON2.0) release region. In this case, $\sim 3 \times 10^5$ cells in 300 μ L media were pipetted onto a backpack-laden surface. A 22x30mm glass cover slip was placed on top of the media, and the surface and cover slip were agitated at 50rpm for 15min. The media containing cell-backpack complexes could be washed via pipette into a LabTek chamber (for imaging using an inverted microscope) or imaged directly through the cover slip (for upright microscope imaging).

Videomicroscopy of functionalized lymphocytes. Confocal laser scanning microscopy (CLSM), fluorescence microscopy and epifluorescence microscopy were used to image cells decorated with a fluorescent polymer backpack. High resolution images of live cell-backpack complexes were imaged using either CLSM at ambient conditions on a Zeiss 510 upright microscope (40x or 63x water immersion objective) or fluorescence microscopy on a Zeiss Axioplan 2 upright microscope (20x and 50x air objectives). T-cell migration and magnetic field behavior was imaged using inverted epifluorescence microscopy on a Zeiss Axiovert 200 microscope (20x air objective) equipped with an environmental chamber (37°C, 5% CO₂). Brightfield time course images on the inverted epifluorescent microscope were acquired with the aid of MetaMorph software (Universal Imaging).

T-cell migration. Eight-welled chambered cover slips (Lab-Tek II, Nalge Nunc) were incubated with 10 μ g/mL recombinant intercellular adhesion molecule-1 (ICAM1/Fc fusion protein, R&D Systems) in PBS at 4°C overnight to provide adhesion ligands promoting cell attachment and migration. HuT 78 T-cells ($\sim 5 \times 10^5$ cells/mL) were exposed to backpacks containing a PMAA/PNIPAAm release region on a ~ 0.8 cm² piece of slide. A chamber was filled with 300 μ L 4°C complete IMDM media, and the slide was inverted in the chamber. The entire cover slip was chilled to 4°C for 30 minutes, manually agitated periodically. As backpacks released from the surface, cell-backpack complexes sedimented onto

the ICAM-coated cover slip. The cover slip was then loaded into the epifluorescence microscope's environmental chamber thermostated at 37°C under a 5% CO₂ atmosphere and imaged at 1 frame per minute for several hours.

Flow Cytometry. Aliquots of cell-backpack complexes were analyzed on a BD FACS Canto II flow cytometer. PI was added during backpack attachment at 40µL/10⁶ cells. Data was gated so that only sufficiently large objects were analyzed (i.e., above the FSC value for a cell), and further gated on a low PI signal (i.e., only live cells).

For DC2.4 flow cytometry, aliquots were made either from the supernatant or from cells removed by exposing the surface to a .5mM EDTA (versene) solution in PBS. The versened aliquots were centrifuged and resuspended in cold complete RPMI 1640.

References

- (1) Gomez-Mouton, C.; Abad, J. L.; *et al.* Segregation of leading-edge and uropod components into specific lipid rafts during T cell polarization *Proceedings of the National Academy of Sciences of the United States of America* **2001**, *98*, 9642.
- (2) Okada, N.; Saito, T.; *et al.* Efficient Antigen Gene Transduction Using Arg-Gly-Asp Fiber-Mutant Adenovirus Vectors Can Potentiate Antitumor Vaccine Efficacy and Maturation of Murine Dendritic Cells *Cancer Research* **2001**, *61*, 7913.
- (3) Kempf, M.; Mandal, B.; *et al.* Improved Stimulation of Human Dendritic Cells by Receptor Engagement with Surface-modified Microparticles *Journal of Drug Targeting* **2003**, *11*, 11
- (4) Raetz, C. R. H.; Whitfield, C. Lipopolysaccharide Endotoxins *Annual Review of Biochemistry* **2002**, *71*, 635.
- (5) Weiner, G. J.; Liu, H.-M.; *et al.* Immunostimulatory oligodeoxynucleotides containing the CpG motif are effective as immune adjuvants in tumor antigen immunization *Proceedings of the National Academy of Sciences of the United States of America* **1997**, *94*, 10833.
- (6) Zhang, X.-Q.; Dahle, C. E.; *et al.* Potent Antigen-specific Immune Responses Stimulated by Codelivery of CpG ODN and Antigens in Degradable Microparticles *Journal of Immunotherapy* **2007**, *30*, 469.

Chapter 4: Cellular Aggregation Behavior Led by Freely Suspended Backpacks

Introduction

There exists a new, burgeoning field of bio-hybrid materials, in which synthetic materials are functionally integrated with cellular species while leveraging both biological and material properties and behaviors. Synthetic materials systems such as anisotropic microparticles¹, muscular thin films², thermally-responsive films with integrin ligands³, films capable of sensing and selectively releasing dead cells⁴, magnetic micromanipulators⁵, nanoparticulate cellular patches⁶, and functional cell “backpacks”⁷ have recently been reported offering exciting possibilities for a new class of biomaterials based on the symbiosis between synthetic building blocks and native biological behavior.

Cellular backpacks are nanoscale thickness, micron-sized, photolithographically patterned heterostructured multilayer systems capable of non-cytotoxically attaching to the membrane of a living cell⁷. Cellular backpacks have been attached to the surface of two types of living immune cells without impairing their native behaviors⁷. If a functional backpack is attached to a cell that normally performs a useful function – such as homing to solid tumors or areas of trauma – then these native functions can be leveraged to deliver functional materials.

Diagnostic (such as imaging) or therapeutic (such as delivery) payloads are possible, as well as combining several modalities in a single platform.

Each backpack contains a functional payload which may be any material that can be integrated in multilayer or homopolymer thin films, including drugs, imaging contrast agents, and nanoparticles. The attachment mechanism between the backpack and the cell surface must be chosen based on the cell type of interest.

In this work, we used a B cell line that expresses an abundance of the cell surface receptor CD44, for which the natural ligand is hyaluronic acid (HA). One face of the backpack consists of a HA-containing multilayer that attaches to the membrane of one or more cells.

In previous work⁷, backpacks were fabricated on a glass slide and tethered to the substrate via a pH- and temperature-labile region. Cells were attached to backpacks at a controlled ratio ($R = \# \text{ of cells} / \# \text{ of backpacks}$) via the CD44-HA interaction and released upon lowering the temperature. This yielded cell-backpack complexes with a well-defined number of cells and backpacks. While this technique afforded great control over cell-backpack association, the effort-intensive process of seeding and releasing on a 2D surface may limit its clinical relevancy. An alternative method is one where the backpacks are released and collected from the fabrication substrate *ex vivo* and exposed to cell suspensions. We refer to this approach as an injectable formulation since backpack solutions could easily be loaded into a syringe and injected into a patient. Since injectable backpacks are free to attach to cells in many different configurations, including multiple cells per backpack and vice versa, cell-backpack aggregates form.

Suematsu *et al*⁸ recently reported forming immune cell aggregates for tissue engineering applications. A collagen scaffold seeded with stromal cells was transplanted into mice. This traditional tissue engineering approach produced artificial lymphoid-like organoids that functioned much like secondary lymphoid organs, recruiting B and T cells and forming follicular dendritic cell networks. This work offers exciting possibilities in engineering hybrid synthetic-biological devices for treating immunodeficiency diseases.

Cellular backpacks may offer an alternative strategy to create injectable synthetic lymphoid organoids that achieve the extremely high cell density typical of lymphoid tissues. Cells could be mixed with backpacks to form aggregates that may be passed through small pores (for example, a needle tip), disaggregate and dynamically re-form. Since the backpacks do not occlude the entire cell surface, cells are free to interact with the environment, an essential requirement for immune system components. Motivated by the work of Suematsu *et al* and our original observation that cells would aggregate upon freely-suspended backpack exposure, we sought to create cellular aggregates that are reversibly associated, but with enough cell-backpack association strength to withstand mechanical challenges.

In this paper, we present fundamental studies on forming cellular aggregates using injectable cellular backpacks, how to control aggregate size, and observations on cell-backpack association strength. We found that two parameters strongly determined the size and character of aggregates: the ratio of cells to backpacks in a culture and the diameter of the backpack. Using confocal microscopy, flow cytometry, and laser diffraction, we observed that while very

large (>1mm) aggregates can form, they may also dissociate and re-form. Aggregates were forced through a nylon mesh filter and observed afterwards – as the filter size decreased, the final aggregates were smaller. For a pore size less than the diameter of the cell, backpacks were still attached, indicating a strong cell-backpack association that may predict a backpack's behavior on lymphocytes undergoing extravasation *in vivo*. We feel that an injectable backpack system could have applications in lymphoid tissue engineering as described by Suematsu⁸, as well as more general cellular engineering applications requiring close cell association.

Flow Cytometry and Confocal Microscopy Studies

Backpacks were assembled on a glass substrate using a photolithographic lift-off technique^{9,10}. Photoresist was deposited and patterned on a (PDAC4/SPS4)_{15,5} coated glass slide, which was then coated using a combination of two different methods. A number of sequential, layer-by-layer (LbL) deposition techniques are possible, including spin assembly¹¹, spraying¹²⁻¹⁴, and dip-coating deposition¹⁵⁻¹⁷. We used traditional dipping LbL deposition for most regions of the backpack system and an airbrush spraying method to create the backpack's biodegradable PLGA payload region. PLGA is known as an ideal delivery system as it degrades at physiological conditions into bioresorbable products¹⁸. We added DiO, a hydrophobic fluorescent dye, to the payload region for visualization. Chloroform was chosen as the mutual PLGA/DiO solvent since it did not dissolve the release region (described below) or the patterned

photoresist. We are able to build a functional backpack that contains a PLGA payload, along with any functional component that may be integrated into a PLGA homopolymer film. Traditional LbL dipping was used to build the rest of the backpack. An overview of the backpack fabrication process, including which assembly technique was used for each region, is shown in Figure 4.1.

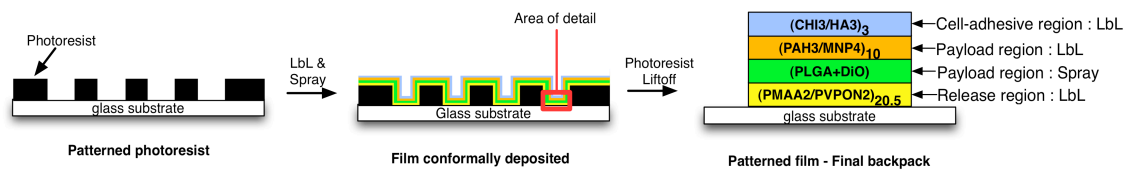


Figure 4.1: Schematic of a surface-bound backpack including the composition and deposition method.

The backpack's release region attaches the functional payload to the glass substrate and is labile under certain conditions. Previously⁷, this region was based on a hydrogen-bonded poly(N-isopropylacrylamide) (PNIPAAm) system found to be labile only below PNIPAAm's lower critical solution temperature (LCST, $\sim 32^{\circ}\text{C}$ ¹⁹) and above a critical pH (~ 6.2 ¹⁶). Cells were seeded onto the surface-bound backpacks at a ratio of 1:1 (depending on the backpack diameter), which minimized cell-backpack aggregation upon release. While imposing a one-backpack-per-cell association condition is useful, there is much greater clinical ease in a system where the backpack is released prior to cell exposure. In this work, we used a backpack release region based on poly(methacrylic acid) (PMAA) and poly(vinylpyrrolidone) (PVPON) which dissolves and releases the backpack above pH ~ 6.4 ¹⁶. As shown previously¹⁶, this critical dissolution pH is due to the de-protonation of PMAA carboxylic acids which are participating in

hydrogen-bonds, thus compromising the film. Using this mechanism, backpacks can be released from the fabrication substrate and collected, then attached to cells in an *ex vivo* cell culture or injected directly into the body where cells of interest may bind to specific ligands on the backpack surface.

An “injectable” backpack formulation, however, leads to cell-backpack aggregates. These aggregates contain any number of cells and backpacks, and the factors influencing the order of these aggregates include the number of cells per backpack and the number of backpacks attached to each cell. Non-conformal attachment can occur due to curvature of the flexible backpack; an overhanging portion of the backpack may then bind to one or more cells. An example is shown in Figure 4.2a, where three cells attached to a single backpack. When a single cell is associated with more than one backpack, and each backpack may attach multiple cells, aggregates form. Figure 4.2b shows one of the lowest order aggregates that may form, where one cell has two backpacks and each backpack has three cells attached.

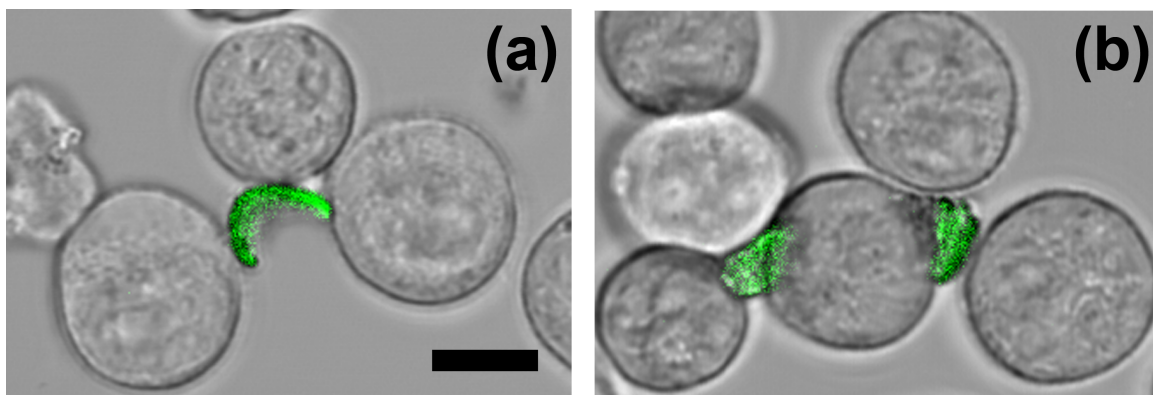


Figure 4.2: Confocal microscopy images of ways B cells attached to backpacks using the injectable backpack protocol. (a) shows how a $7\mu\text{m}$ backpack, may attach to several cells, and that (b) each cell may bind to more than one ($15\mu\text{m}$) backpack. Scale bars are $10\mu\text{m}$, and $R=10$ for both aliquots.

Aggregate size depends both on the number of cells associated per backpack and the number of backpacks per cell. Backpack size, controllable during fabrication, will strongly influence the number of cells associated per backpack⁷ (see Figure 4.2a-b). We fabricated backpacks of two different diameters ($d=7\mu\text{m}$ and $15\mu\text{m}$) and controlled the number of backpacks associated per cell by changing the ratio of cells to backpacks ($R = \# \text{ of cells} / \# \text{ of backpacks}$). We find that aggregate size monotonically decreases with R and increases with d (for a given R).

Figure 4.3 shows flow cytometry plots and confocal micrographs of cell-backpack ($d = 7\mu\text{m}$) aliquots for $R=10$ to 0.1 . Shown are FITC signal vs. forward scatter (FSC) data from flow cytometry: cell aggregates are detected at higher FSC, and aggregates associated with one or more backpacks are detected at higher FITC values (since each backpack contains DiO in the PLGA region, which fluoresces almost identically to FITC). Thus, aggregates with backpacks are found in the upper right quadrant, and single cells with one or more backpacks are found in the upper left quadrant. We used confocal microscopy to directly observe aggregate size, which dramatically increases with decreasing R . For $R>1$, we see very small aggregates (less than 3 cells), with primarily only one backpack associated per cell. At $R=1$, larger aggregates begin to form, and by $R=0.2$, large complexes are found. At $R=0.1$, a single aggregate formed in the dish; the micrograph in Figure 4.3 shows only the edge of this aggregate. To further quantify these aggregate structures, flow cytometry analysis of backpack fluorescence vs. FSC on cell-backpack aliquots show that as R decreases, the number of cells associated with a backpack increases. Since the flow cytometer passes the cell suspension through a small quartz capillary, aggregates break up

before passing through the laser path for analysis. This limits analysis to small aggregates, single cells, and single backpacks (which are excluded from this analysis based on PI signal and FSC value) though the starting aliquot included large aggregates. As laser diffraction data indicates, the large aggregates seen in the optical images below are associated via both strong, specific CD44-HA interactions and weak, non-specific cell-backpack binding. Small clusters, as seen in Figure 4.2, associate only via the strong CD44-HA interactions, and these are the FSC^{high} events shown in Figure 4.3 and Figure 4.4. A detailed discussion of how different association strengths lead to large aggregates versus small cell clusters is presented along with the laser diffraction data below.

The backpack diameter d also strongly influences the size of aggregates. Figure 4.4 shows confocal images and flow cytometry plots of cell-backpack aggregates formed with $d=15\mu\text{m}$ backpacks. Aggregate size trends are similar to the $d=7\mu\text{m}$ case, but the onset R value at which aggregation begins increases to greater than $R=10$. Indeed, the aggregates seen for $d=7\mu\text{m}$ and $R=0.33$ are roughly the same size as those seen for $d=15\mu\text{m}$ and $R=10$. This suggests a superposition of the d (backpack diameter) and R (number of backpacks per cell) variables.

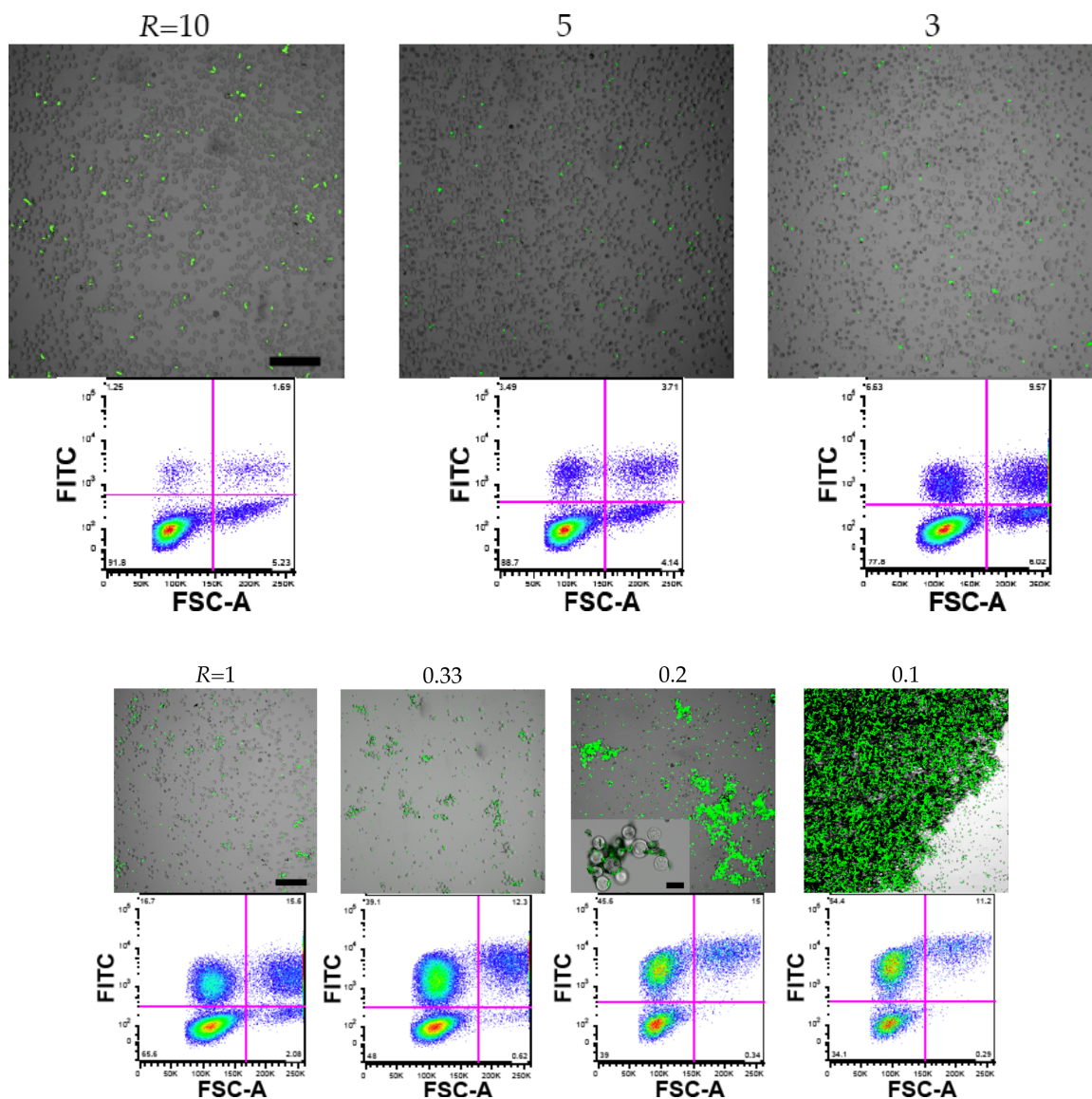


Figure 4.3: Confocal microscopy images and flow cytometry plots (FITC vs. FSC) of aggregates formed under different cell to $7\mu\text{m}$ diameter backpack ratios ($R = 10$ to 0.1). A higher magnification view of a cell-backpack aggregate is provided for $R=0.2$. Scale bar is $100\mu\text{m}$ (inset scale bar for $R=0.2$ is $20\mu\text{m}$).

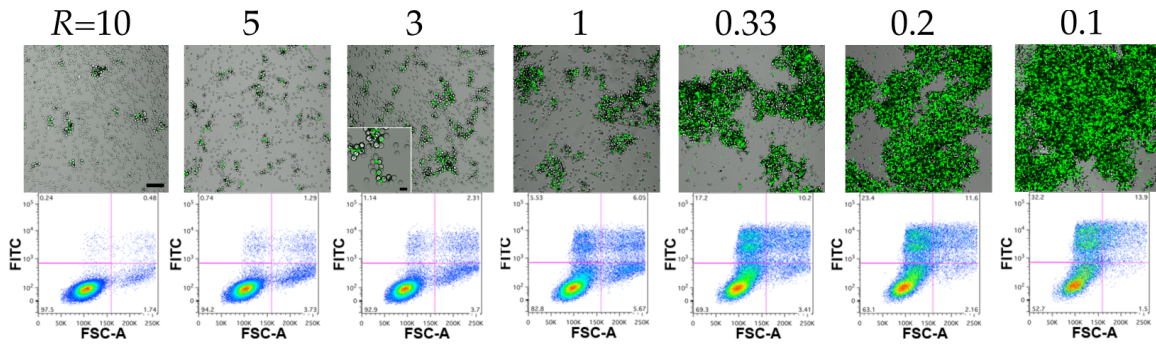


Figure 4.4: Confocal microscopy images and flow cytometry plots (FITC vs. FSC) of aggregates formed under different cell to $15\mu\text{m}$ diameter backpack ratios ($R = 10$ to 0.1). A higher magnification view of a cell-backpack aggregate is provided for $R=3$. Scale bar is $100\mu\text{m}$ (inset scale bar for $R=3$ is $20\mu\text{m}$).

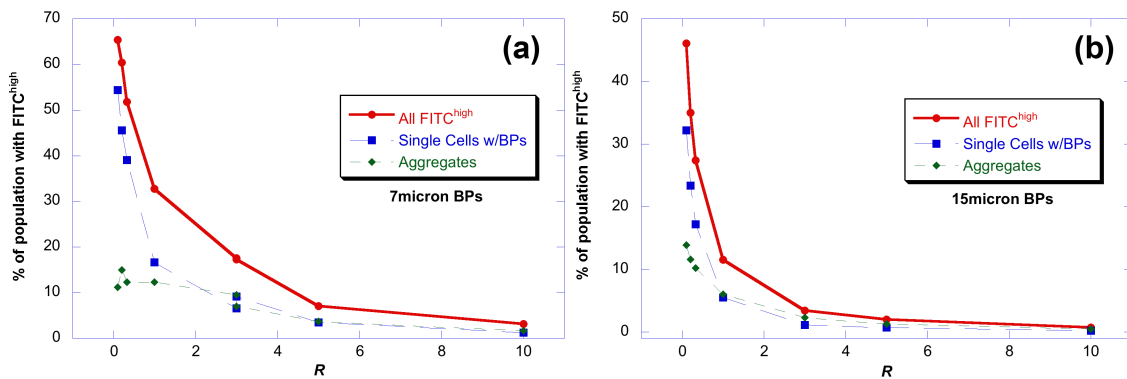


Figure 4.5: Plots summarizing the flow cytometry results in Figure 4.3 and Figure 4.4. The total percentage of $\text{FITC}^{\text{high}}$ events, which represents an attached backpack, are plotted versus R for (a) $d=7\mu\text{m}$ and (b) $d=15\mu\text{m}$ backpacks. As R increases, the number of cells associated with a backpack monotonically decreases. The values here probably represent a lower bound of the actual value of cells with backpacks (see text for discussion).

As can be seen in Figure 4.3, $\text{FITC}^{\text{high}}$ events have two distinct FSC populations differing by a factor of two. This reflects single cells with a backpack or small aggregates with one or more backpacks associated. Figure 4.5 shows the percentage of $\text{FITC}^{\text{high}}\text{FSC}^{\text{low}}$ (single cells with a backpack) and $\text{FITC}^{\text{high}}\text{FSC}^{\text{high}}$ (small clusters) events, as well as the sum, for both $d=7\mu\text{m}$ and $15\mu\text{m}$. For $d=7\mu\text{m}$, at $R=10$, 3% of cells are associated with a backpack; at $R = 0.1$, 65% of events include a backpack. When the diameter increases to $15\mu\text{m}$, the highest

number of cells with an attached backpack decreases to 46%. While this might reflect slight differences in sample handling, it is more likely that this decrease is due to curling of some backpacks upon themselves, thus reducing the total surface area available to strongly bind. Examples of how $d = 15\mu\text{m}$ backpacks fold are seen in Figure 4.6. This curling behavior was not observed for $d = 7\mu\text{m}$ backpacks, suggesting some critical size required for folding.

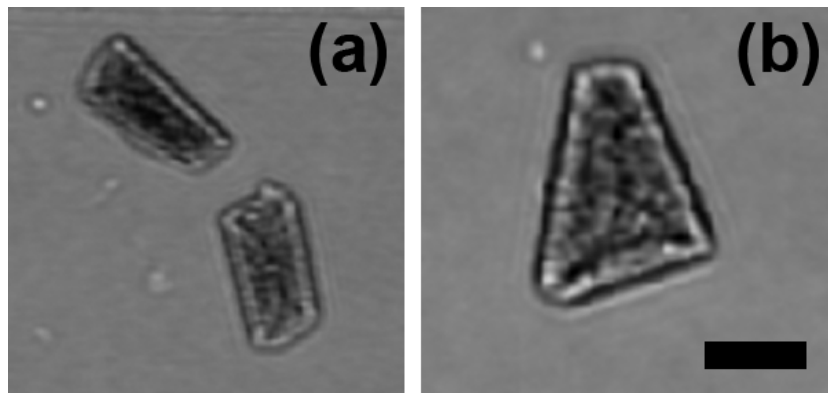


Figure 4.6: Examples of how some $d=15\mu\text{m}$ backpacks curl upon themselves. (a) shows a cylindrical folding, while (b) presents a “tricorne” like shape. Scale bar is $10\mu\text{m}$.

As cells pass through the cytometer’s fluidics system, the solution is forced through a small capillary. The values reported in Figure 4.5 are lower bound estimates for the true number of cells associated with backpacks, since some backpacks will be sheared off the surface of cells during flow through the instrument.

Laser Diffraction Studies*

We used laser diffraction to further quantify the nature of these aggregates and investigate their association strength. Aliquots of cell-backpack complexes mixed at the same ratios as above show increasingly large aggregates with decreasing R , which agrees with the confocal microscopy results presented above. Unlike the confocal results, all diffraction samples were mildly agitated (using a built-in stir bar) before analysis. Prior to agitation, most samples show an extremely large aggregate distribution curve (mean $>1\text{mm}$) that is not constant with time – very large fluctuations led to inconsistent data. Upon agitation, this distribution falls to the curves shown in Figure 4.7, which are consistent and reproducible. Furthermore, if agitation was stopped, the large aggregate distribution appeared again, showing that aggregate dissociation is reversible. An agitation-dependant distribution for $R=0.33$ is provided in Figure 4.8; confocal microscopy images of before- and after-agitation aliquots are found in Figure 4.9.

* I acknowledge the collaboration of Jonathan Gilbert in the results described in this section.

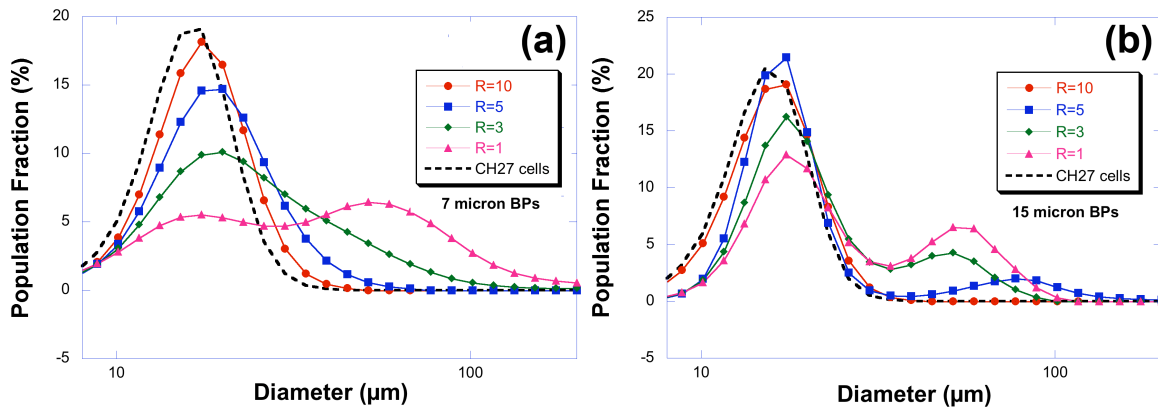


Figure 4.7: Aggregate size distributions for (a) $d=7\mu\text{m}$ and (b) $d=15\mu\text{m}$ backpacks. These curves show two populations, one centered at $\sim 15\mu\text{m}$ (single CH27 cells) and the other at an increasingly greater diameter depending on R . For $d=7\mu\text{m}$ backpacks, a clear second peak appears at $R=1$; this second peak appears at $R=3$ for $d=15\mu\text{m}$ backpacks. Individual, non-backpacked CH27 cells are shown as the dashed line.

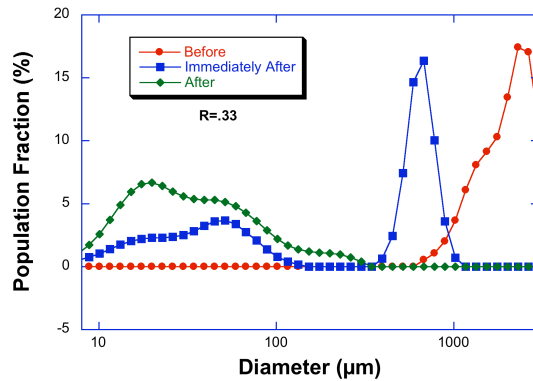


Figure 4.8: Agitation-dependant laser diffraction distributions for $R=0.33$. The curve labeled "Immediately After" is $\sim 10\text{s}$ after agitation began, and "After" is for $>30\text{s}$.

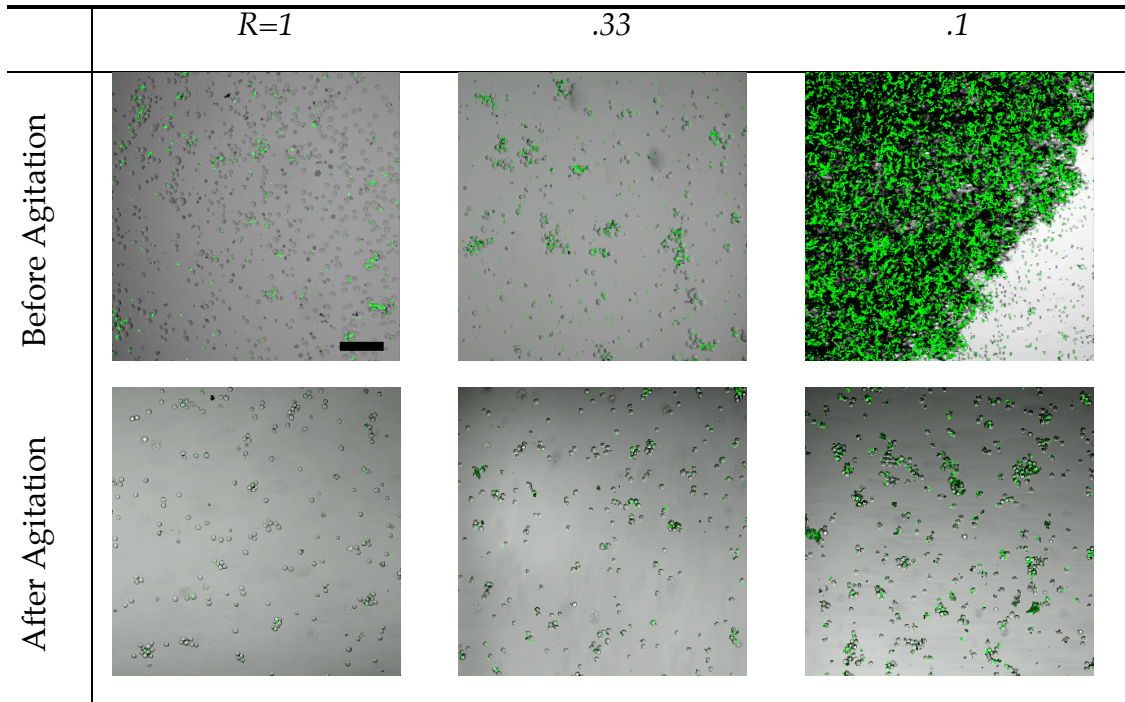


Figure 4.9: Confocal micrographs showing before and after photos of cellular aggregates for various values of R . Scale bar is $100\mu\text{m}$.

In Figure 4.7, B cells are shown as the dashed line, which has a distribution mean of $\sim 15\mu\text{m}$, slightly smaller than the $17\mu\text{m}$ cell diameter observed by microscopy. At $R=10$, we see a similarly shaped curve shifted to the right, suggesting one-backpack-to-cell complexes. As R decreases, multi-cell, multi-backpack aggregates begin to form, both shifting the mean value higher and changing the shape of the curve to include a broad shoulder. At $R=1$ for $d=7\mu\text{m}$ and $R=3$ for $d=15\mu\text{m}$, a second peak emerges, indicating a distinct aggregate population. Consistent with the confocal results above, as d increases the aggregation-onset R value increases as well.

From the flow cytometry and laser diffraction data, we find that aggregates are able to dissociate into smaller cell-backpack clusters. The number of cells in each cluster depends on R and d . These clusters weakly bind together to form the large aggregates seen in Figure 4.3 and Figure 4.4. Additionally, this association-dissociation event is reversible – once agitation is stopped, very large aggregates were observed again. The association in a small cell cluster is based on CD44-HA interactions between the membrane and HA-containing cell-adhesive region. Binding between clusters to form large aggregates are much weaker, and is likely based on non-selective interactions between cells and the outer face of the backpack (which contains some or all of the hydrogen-bonded release region). These non-selective interactions are weak enough to be compromised with even mild agitation. Binding interactions in the small cell clusters, however, are not compromised by even very harsh agitation (maximum stir bar rotation).

Nylon Mesh Filtering: A Model for Extravasation

To further test how strongly backpacks are attached to B cells in clusters and aggregates, aliquots of cells and backpacks ($R=0.33$, $d=7\mu\text{m}$) were collected and passed through nylon mesh filters of varying aperture size. In the body, immune system cells must undergo extravasation, the process by which these cells leave the circulatory system and enter tissue. This process requires the cells to squeeze through very tightly apposed endothelial cells²⁰, exerting shear forces on the surface and challenging the adherence of any attached object.

The average diameter of a B cell is $\sim 17\mu\text{m}$, and four mesh sizes were chosen to challenge the aggregate association strength as well as the cell-backpack interaction. Figure 4.10 shows that for mesh opening sizes of 11, 20, 30, and $60\mu\text{m}$, a significant number of cell-backpack complexes remain after filtering. Consistent with the agitation-dependant, reversible aggregation behavior seen above, aggregates are dissociating into smaller aggregates or cell clusters (i.e., cells attached to a backpack via strong CD44-HA interactions) while passing through the mesh. (The total number of cells in the filtrate is comparable to the pre-filtered aliquot, indicating that very few clusters or aggregates are actually removed during filtering.) After this dissociation, small aggregates and clusters are then free to reform larger aggregates. The size of the remade aggregates decreases with decreasing mesh size, since the original large aggregate is broken down into smaller clusters or aggregates. This demonstrates that the size of the temporary small aggregate or cluster created immediately after filtering influences the final remade aggregate size.

The $11\mu\text{m}$ pore size case is of particular interest since it is less than the average diameter of a B cell. Clusters in the filtrate are very small – primarily, cells are associated with only one backpack. This result suggests that even though a cell was forced to deform as it passed through the pore, the backpack remained on the surface. While this does not directly correlate to the active, receptor-mediated process of extravasation²⁰, it does suggest that the cell-backpack association is sufficient to resist moderately strong mechanical challenges.

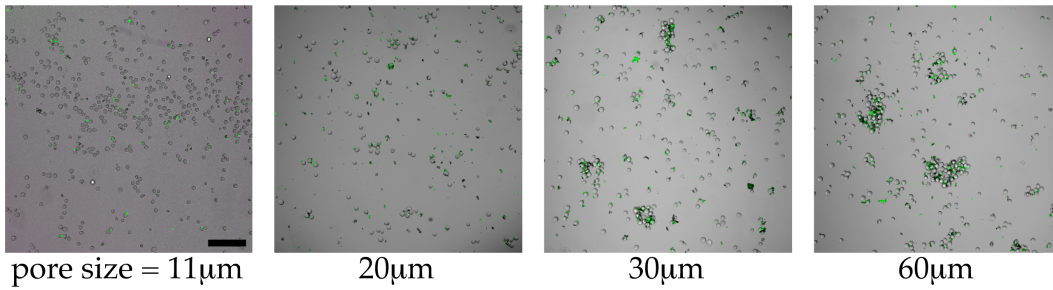


Figure 4.10: Confocal microscopy images of aggregates seen after filtering an $R=.33$, $d=7\mu\text{m}$ aliquot through the indicated mesh pore sizes. As the mesh size decreases, so do the resulting aggregate size.

Conclusions

Cellular backpacks may be used to create aggregates of a model B-lymphocyte cell line. Two variables were examined to affect the size of the aggregates: the ratio of cells to backpacks, and the backpack diameter. By decreasing the ratio R of cells to backpacks, we increase the size of the aggregate. As the diameter of the backpack increases (for the same R), so does the aggregate size. Flow cytometry results indicate that for $R=0.1$ and $d=7\mu\text{m}$, greater than 65% of cells will be associated with a backpack. When d increases to $15\mu\text{m}$ at $R=0.1$, greater than 45% of cells will remain attached to a backpack. When aggregates formed with $d=7\mu\text{m}$ backpacks are forced through a mesh filter for varying pore sizes, aggregates will dissociate and re-associate. As the pore size decreases, the final aggregate size decreases as well. For the smallest pore size, $11\mu\text{m}$, backpacks remain associated with cells even though this is less than the diameter of the cell, suggesting a strong interaction between the cell and backpack.

Experimental Details

Materials. Poly(methacrylic acid) (PMAA, PolySciences, M=100kDa), poly(vinylpyrrolidone) (PVPON, Aldrich, M=1.3MDa), poly(diallyldimethylammonium chloride) (PDAC, Aldrich, M=200-350kDa in 20% aqueous solution), poly(styrene sulfonate) (SPS, Aldrich, M=70kDa), hyaluronic acid (HA, Fluka, from *Streptococcus equi*, Fluka, M~145kDa by intrinsic viscosity²¹), low MW chitosan (CHI, Sigma, DS=.85, M~390kDa by intrinsic viscosity²²), and poly(lactide-*co*-glycolide) (PLGA, Sigma, M_w = 5-15kDa) were used without purification. Cells were passaged and maintained in RPMI with L-glutamine (Mediatech), Penicillin/Streptomycin (P/S, Mediatech), and fetal calf serum (characterized FCS, Mediatech). 3,3'-dioctadecyloxycarbocyanine perchlorate (DiO, Molecular Probes), which fluoresces at the same wavelengths as fluorescein isothiocyanate (FITC), was used to stain the PLGA backpack. Iron oxide magnetic nanoparticles (MNP, Fe₃O₄, 10nm diameter, Ferrotec EMG 705) stabilized with an anionic surfactant were used. Hank's Balanced Salt Solution (Gibco) was used to wash cells, and propidium iodine (PI, Calbiochem) was used as a viability dye.

Backpack fabrication. We used a previously described⁷ aqueous-based layer-by-layer technique to deposit the polymer films. One significant exception is the PLGA region of the backpack in the current study, which was assembled using a spray technique. A solution of PLGA (1mg/mL) and DiO (1mg/mL) in chloroform was sprayed (10mL/min for 30s, substrate 15cm from Badger 105 air brush powered with nitrogen) onto the surface of a (PMAA2.0/PVPON2.0)_{20.5} multilayer atop a patterned photoresist layer. The resulting thickness was ~10nm, as observed by spraying PLGA onto Si wafers and measuring using spectroscopic ellipsometry²³. Chloroform does not dissolve the developed photoresist. Substrates were then coated by the layer-by-layer technique to build the rest of the heterostructured, functional backpack. The following formula describes all backpacks used in this work:

(PMAA2.0/PVPON2.0)_{20.5}(PLGA+DiO) (PAH3.0/MNP4.0)₁₀(CHI3.0/HA3.0)₃, where the number following each LbL deposited species indicates the solution pH and subscripts are the number of bilayers (where a half bilayer is indicated .5). We included a (PAH3.0/MNP4.0)₁₀ layer to increase the mechanical integrity of the backpack; we found that backpacks built identically but without the (PAH3.0/MNP4.0)₁₀ region were compromised during acetone sonication as indicated by a lack of DiO signal. The (CHI/HA) region was built with 100mM NaCl added to each polymer solution. To detach backpacks from the glass substrate, 1mL of PBS was pipetted onto the surface and a cell scraper was used to gently remove the backpacks. The backpacks in PBS were collected with a pipette and passed through a 27 μ m nylon mesh (McMaster Carr) to remove any large aggregates or backpacks that had not correctly undergone acetone liftoff.

Cell Culture. CH27 B lymphocytes were maintained at 37°C, 5% CO₂ and passaged in RPMI 1640 cell culture media (Mediatech) supplemented with 10% FCS, 1% penicillin/streptomycin, and 25mM HEPES.

Backpack Attachment. Cells were washed once with HBSS and resuspended at 10⁶ cells/mL in complete RPMI media. Backpacks were pelleted down (2000rpm for 5min) and resuspended in PBS at 10⁷ backpacks/mL (as measured by a hemacytometer). For imaging and laser diffraction experiments, backpacks were introduced at the indicated ratio to the cell suspension in 4 or 8 well LabTek chambers (Nunc) and agitated at ~100rpm at 37°C and 5% CO₂ for 15 min, incubated for 15min in the same conditions, and this cycle was repeated once more. Cells were allowed to sediment down for ~30min before imaging. For flow cytometry experiments, the concentration of cells in complete media was 10⁶ cells/mL, and the backpack concentration in PBS was 6x10⁶ backpacks/mL. Backpacks were introduced to the cells in 35mm Petri dishes, which were agitated as described above. Cell-backpack aliquots were transferred to 15mm tubes and chilled on ice.

Flow Cytometry and Confocal Microscopy. Aliquots of cell-backpack complexes were analyzed on a BD FACS Canto II flow cytometer. The cell viability marker propidium iodide (PI, 50 μ g/ml PBS) was added during backpack attachment at

40 μ L/10⁶ cells (i.e., a final 2 μ g/mL PI concentration with 10⁶ cells/mL). Data sets of 1x10⁵ events were gated so that only sufficiently large objects were analyzed (i.e., above the FSC value for a B cell), and further gated on a low PI signal (i.e., only live cells). Confocal laser scanning microscopy images were collected on an inverted Zeiss LSM 510 using 4 or 8 well LabTek chambers and a 10x air objective under ambient conditions. Since the exact shape and structure of each aggregate is of less interest than the overall size and frequency, most microscopy data is shown at low magnification so that multiple aggregates may be seen in each field of view. These images are an overlay of brightfield and fluorescence signals, and the reader is directed to note the green aggregates. Though green fluorescence arises from the DiO co-sprayed with PLGA, FITC detectors were used on the flow cytometer and confocal microscope and data is thus labeled "FITC" throughout this work.

Particle Size Measurement by Laser Diffraction. Cell-backpack complexes were analyzed using a Horiba LA-950V2 laser diffraction system. Cell-backpack aliquots at the indicated ratio were gently added to 18mL pH 7.4 PBS in a quartz cuvette. Data were collected before and after gentle agitation using the built-in magnetic stir bar. All data shown were collected following agitation. Data analysis was performed using a Fraunhofer model²⁴ which does not require the input of a refractive index.

Nylon mesh filtering. Backpacks were attached to cells at $R=0.33$, and 0.5mL aliquots were passed through 25mm diameter nylon mesh filters of three different opening sizes (20 μ m, 30 μ m, and 60 μ m; Millipore) using a reusable syringe filter (Pall). These aliquots were placed in 4 well LabTek chambers and observed using confocal microscopy.

References

- (1) Yoshida, M.; Roh, K. H.; *et al.* Structurally Controlled Bio-hybrid Materials Based on Unidirectional Association of Anisotropic Microparticles with Human Endothelial Cells *Advanced Materials* **2009**, *21*, 4920.
- (2) Feinberg, A. W.; Feigel, A.; *et al.* Muscular Thin Films for Building Actuators and Powering Devices *Science* **2007**, *317*, 1366.
- (3) Ebara, M.; Yamato, M.; *et al.* Temperature-Responsive Cell Culture Surfaces Enable "On-Off" Affinity Control between Cell Integrins and RGDS Ligands *Biomacromolecules* **2004**, *5*, 505.
- (4) Okajima, S.; Sakai, Y.; *et al.* Development of a Regenerable Cell Culture System That Senses and Releases Dead Cells *Langmuir* **2005**, *21*, 4043.
- (5) Kriha, O.; Becker, M.; *et al.* Connection of Hippocampal Neurons by Magnetically Controlled Movement of Short Electrospun Polymer Fibers—A Route to Magnetic Micromanipulators *Advanced Materials* **2007**, *19*, 2483.
- (6) Cheng, H.; Kastrup, C. J.; *et al.* Nanoparticulate Cellular Patches for Cell-Mediated Tumorotropic Delivery *ACS Nano* **2010**, *4*, 625.
- (7) Swiston, A. J.; Cheng, C.; *et al.* Surface Functionalization of Living Cells with Multilayer Patches *Nano Letters* **2008**, *8*, 4446.
- (8) Suematsu, S.; Watanabe, T. Generation of a synthetic lymphoid tissue-like organoid in mice *Nature Biotechnology* **2004**, *22*, 1539.
- (9) ShaikhMohammed, J.; DeCoster, M. A.; *et al.* Micropatterning of Nanoengineered Surfaces to Study Neuronal Cell Attachment in Vitro *Biomacromolecules* **2004**, *5*, 1745.
- (10) ShaikhMohammed, J.; DeCoster, M. A.; *et al.* Fabrication of Interdigitated Micropatterns of Self-Assembled Polymer Nanofilms Containing Cell-Adhesive Materials *Langmuir* **2006**, *22*, 2738.
- (11) Cho, J.; Char, K.; *et al.* Fabrication of Highly Ordered Multilayer Films Using a Spin Self-Assembly Method *Advanced Materials* **2001**, *13*, 1076.
- (12) Izquierdo, A.; Ono, S. S.; *et al.* Dipping versus Spraying: Exploring the Deposition Conditions for Speeding Up Layer-by-Layer Assembly *Langmuir* **2005**, *21*, 7558.
- (13) Krogman, K. C.; Lowery, J. L.; *et al.* Spraying asymmetry into functional membranes layer-by-layer *Nat Mater* **2009**, *8*, 512.
- (14) Schlenoff, J. B.; Dubas, S. T.; *et al.* Sprayed Polyelectrolyte Multilayers *Langmuir* **2000**, *16*, 9968.
- (15) Dubas, S. T.; Schlenoff, J. B. Factors Controlling the Growth of Polyelectrolyte Multilayers *Macromolecules* **1999**, *32*, 8153.
- (16) Kharlampieva, E.; Sukhishvili, S. A. Hydrogen-Bonded Layer-by-Layer Polymer Films *Polymer Reviews* **2006**, *46*, 377
- (17) Shiratori, S. S.; Rubner, M. F. pH-Dependent Thickness Behavior of Sequentially Adsorbed Layers of Weak Polyelectrolytes *Macromolecules* **2000**, *33*, 4213.
- (18) Anderson, J. M.; Shive, M. S. Biodegradation and biocompatibility of PLA and PLGA microspheres *Advanced Drug Delivery Reviews* **1997**, *28*, 5.

- (19) Schild, H. G.; Tirrell, D. A. Microcalorimetric detection of lower critical solution temperatures in aqueous polymer solutions *The Journal of Physical Chemistry* **2002**, *94*, 4352.
- (20) Schenkel, A. R.; Mamdouh, Z.; *et al.* CD99 plays a major role in the migration of monocytes through endothelial junctions *Nature Immunology* **2002**, *3*, 143.
- (21) Mendichi, R.; Soltes, L.; *et al.* Evaluation of Radius of Gyration and Intrinsic Viscosity Molar Mass Dependence and Stiffness of Hyaluronan *Biomacromolecules* **2003**, *4*, 1805.
- (22) Mohammad R. Kasaai, J. A. G. C. Intrinsic viscosity-molecular weight relationship for chitosan *Journal of Polymer Science Part B: Polymer Physics* **2000**, *38*, 2591.
- (23) Tompkins, H. G.; Irene, E. A. *Handbook of ellipsometry*; William Andrew Publishing and Springer-Verlag GmbH & Co.: Norwich, NY and Heidelberg, Germany, 2005, pages
- (24) Agrawal, Y. C.; McCave, I. N.; *et al.* *Principles, Methods, and Applications of Particle Size Analysis*; Cambridge University Press: Cambridge, 1991, pages 119-128.

Chapter 5: All-Biopolymer Multilayer Systems

Multilayer films based on biologically derived polymers are an attractive candidate for cellular backpacks. Biocompatibility, bioresorbability, and bioactivity are all enabled or enhanced using biopolymers rather than synthetic polymers.

To create such backpacks, several electrostatically-charged biopolymer multilayer systems were built and tested. Four biopolymers were investigated: hyaluronic acid (HA), alginate (ALG), carboxymethylcellulose (CMC), and chitosan (CHI). HA, ALG, and CMC are polyanions, and CHI is a polycation. Each of these polymers is naturally found or formed from minimal processing of natural precursors. The chemical structures for each are found in Figure 5.1.

HA/CHI Multilayers*

Hyaluronic acid (HA) was chosen for its bioactive properties, namely the ability to bind to the cell-surface protein CD44¹. This natural receptor-ligand interaction is used to attach the backpack to the surface of immune cells. In addition to our cellular attachment and immobilization work, other groups have studied this

* The results in this section were in collaboration with Fernando C. Vasconcellos, School of Chemical Engineering, Department of Thermofluidynamics, State University of Campinas, Campinas, Brasil.

film system for biocompatibility^{2,3}, exponential growth behavior⁴, and encapsulation⁵.

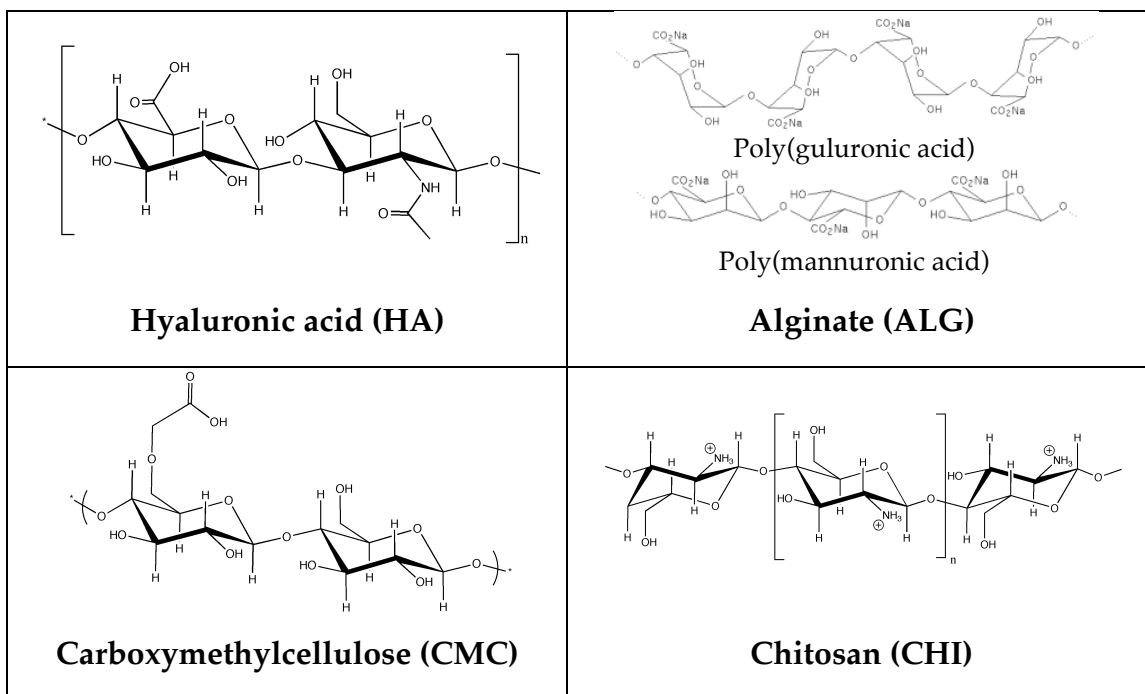


Figure 5.1: The chemical structures of hyaluronic acid (HA), alginate (ALG, a random copolymer of guluronic and mannuronic acids), carboxymethylcellulose (CMC), and chitosan (CHI).

The polycation CHI is formed from the base-catalyzed deacetylation of chitin, an abundant structural polymer found in crustacean shells. CHI is a linear copolymer of β -(1,4) linked 2-amino-2-deoxy-D-glucose and 2-acetoamido-2-deoxy-D-glucose, the ratio of which is referred to as the degree of deacetylation (DD). The DD determines the number of cationically ionizable primary amines on the polymer, and has been shown to affect properties such as cellular cytotoxicity and metabolism⁶. Upon deacetylation, CHI contains a primary amine with a solution $pK_a \sim 6.5$.

Many studies have focused on how deposition variables such as salt⁷ and pH⁸ changes film morphology and biological characteristics, and how the resulting presentation of the film affects its interaction with adherent cells^{5,9-16}. However, we are aware of no reports that show how these characteristics vary with pH and NaCl concentration during HA/CHI PEM film deposition for non-adherent cells.

We studied how HA/CHI PEMs can be used to immobilize non-adherent B lymphocyte to a surface, using the versatile, conformal layer-by-layer coating process. Deposition parameters such as salt (0 or 100mM), pH (3 or 5) and final polymer deposited (HA versus CHI) were systematically adjusted to optimize binding efficiency (i.e., the total number of cells attached to the film in a given area) via CD44-HA interactions. This PEM film is the basis for all backpack cell-adhesive regions used in this thesis.

This work shows two important conditions for successfully attaching B cells to HA-containing PEM films. First, HA is required for the proposed CD44-mediated binding, as shown by the alginate (ALG) controls and antagonistic binding by soluble HA and ALG. However, the total amount of HA in a film does not determine B cell binding capability. Second, HA deposition conditions that favor loops and tails, such as low pH and with added salt, can result in more available CD44-binding ligands and thus greater B cell attachment. These two conditions emphasize that the most important factor affecting cell binding potential is the presentation and configuration of HA on a surface, conditions controllable in PEM film assembly by changing solution deposition conditions (such as salt and pH).

Multilayer Assembly

The pK_a of HA (in salt free solution) is about 2.9, and CHI's pK_a is about 6.0 (in 0.1 M acetic acid solution)¹⁷⁻¹⁹. Above pH 6, CHI is not soluble in water. We chose to initially focus on solution pH values of 3.0 and 5.0. Low molecular weight CHI was used in this study since faster PEM growth has been observed for low MW chitosan⁴. To promote uniform multilayer assembly, glass and silicon wafer substrates were pre-coated with a uniform charged multilayer thin film composed of the strong polyelectrolytes PDAC and SPS. The (PDAC4/SPS4)_{15.5} precursor film used in this study had an approximate thickness of 57 nm and an RMS roughness of about 2 nm, as measured by profilometry. Biopolymer PEM deposition was initiated by the adsorption of HA on the positively charged PDAC surface followed by alternate depositions of CHI and HA. In addition to variations in solution pH (pH 3 versus 5), the ionic concentration of the deposition solutions was also varied (0 versus 100 mM NaCl). In all cases, film thickness increased exponentially with the number of deposition steps. These results corroborate the findings of Picart and co-workers⁴, who attributed this exponential growth mechanism to CHI's ability to diffuse in and out of the entire HA/CHI film at each deposition step. These authors also reported that HA was found to be a non-diffusing species.

Table 5.1 presents thickness and roughness values for 3 and 3.5 bilayer HA/CHI PEMs deposited under the different assembly conditions examined. Multilayer films with 3.0 bilayers have CHI as the outermost layer and films with 3.5 bilayers have HA as the last deposited layer. As expected⁷, the addition of 100 mM salt to the dipping solutions generally resulted in an increase in overall

multilayer film thickness. In addition to charge screening effects, added salt can promote inter-diffusion and mobility of oppositely charged polymers within a film^{2,20}, which leads to thicker films according to the diffusion-based film growth model⁴. Finally, films assembled at pH 5 tended to be thicker and rougher than those prepared at pH 3.

<i>Biopolymer Film</i>	<i>Salt Condition (mM NaCl)</i>	<i>Thickness (nm)</i>	<i>RMS Roughness (nm)</i>
(HA3.0/CHI3.0) ₃	0	17	2
(HA3.0/CHI3.0) _{3,5}	0	37	4
(HA3.0/CHI3.0) ₃	100	27	2
(HA3.0/CHI3.0) _{3,5}	100	42	3
(HA5.0/CHI5.0) ₃	0	42	7
(HA5.0/CHI5.0) _{3,5}	0	43	8
(HA5.0/CHI5.0) ₃	100	39	5
(HA5.0/CHI5.0) _{3,5}	100	49	10

Table 5.1: Thickness and roughness values of 3-3.5 bilayer HA/CHI films. Each value is the average of 7 independent measurements.

CH27 B-Cell Binding

Figure 5.2 summarizes B lymphocyte binding trends on uniform (HA/CHI) films prepared under the pH and salt conditions outlined above. Optical micrographs of B-cells adhering to select PEM films can be found in Figure 5.3. For PEMs prepared at pH 3, the salt concentration and polymer deposited last modulates B lymphocyte binding over a relatively wide range. In contrast, multilayer films assembled at pH 5 exhibited overall lower binding efficiency that was less sensitive to the pH, salt, and final polymer deposited. High binding efficiencies were found with either HA (at 1850 ± 150 cells/mm²) or CHI (1840 ± 50

cells/mm²) terminated films assembled at pH 3; here, salt and final polymer deposited determined binding efficiency. This means that even though CHI is deposited last, there is a similar presentation of accessible binding ligands available on the surface. The two least efficient cell-binding films, (HA3.0/CHI3.0)_{3,5} deposited without salt and (HA3.0/CHI3.0)₃ deposited with 100mM NaCl, bound cells at 1200 ± 200 cells/mm² and 770 ± 25 cells/mm², respectively. These results demonstrate that significant variations in B-cell binding to CHI/HA multilayers can be realized through changes in easily controlled multilayer processing parameters (such as pH, salt, and final polymer deposited).

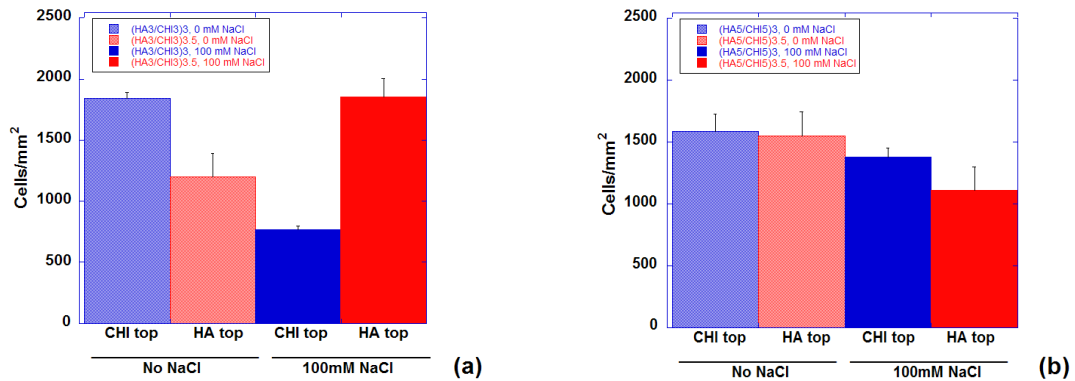


Figure 5.2: B lymphocyte binding to (a) (HA3.0/CHI3.0)_{3,x} and (b) (HA5.0/CHI5.0)_{3,x} films, for x=0 or 5. Error bars correspond to the standard error for 7 independent measurements.

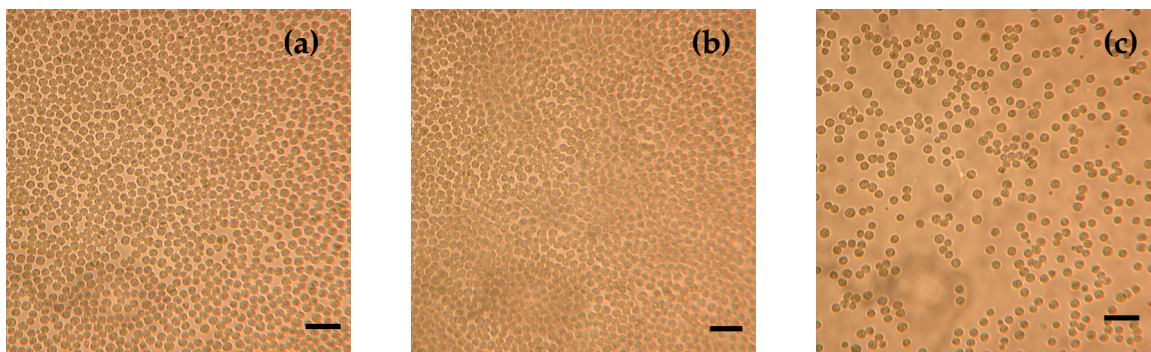


Figure 5.3: Optical micrographs of B cells adhered to a (a) $(\text{HA3.0/CHI3.0})_{3.5}$ film made with 100 mM NaCl (the best lymphocyte binding PEM), (b) $(\text{HA3.0/CHI3.0})_{3.0}$ film made with no NaCl (the second best binding motif), and (c) $(\text{HA3.0/CHI3.0})_{3.0}$ film made with 100 mM NaCl (least effective binding PEM). Scale bars = 50 μm .

Lymphocyte Binding to PEM Arrays

In addition to uniform PEMs, patterned film arrays of 7 μm posts (Figure 5.4) were fabricated via a photolithographic lift-off technique^{9,21,22}. The compositions of these films were: $(\text{MNP4/FITC-PAH3})_{9.5}(\text{CHI3.0/HA3.0})_x$ for $x=3$ or 3.5. Both the (MNP/FITC-PAH) and (CHI/HA)_x regions remain intact during the photoresist lift-off step and both maintain their functionality post-fabrication. The (MNP/FITC-PAH) region was chosen for its usefulness in imaging and our experience with patterning these films⁹.

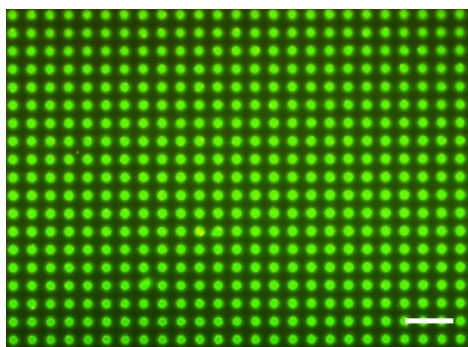


Figure 5.4: Fluorescent image of a $(\text{MNP4.0/FITC-PAH3.0})_{9.5}(\text{CHI3.0/HA3.0})_3 + 100 \text{ mM NaCl}$ patterned slide. Scale bar = 50 μm .

B lymphocytes in 37°C RPMI media were gently pipetted onto slides with patterned posts and incubated for 1 or 2 hours with intermittent gentle agitation. The cell array was washed with Hank's balanced salt solution (HBSS) following cell seeding and incubation. Figure 5.5 presents typical examples of B lymphocytes adhered to arrays of HA and CHI-terminated multilayers deposited with and without NaCl.

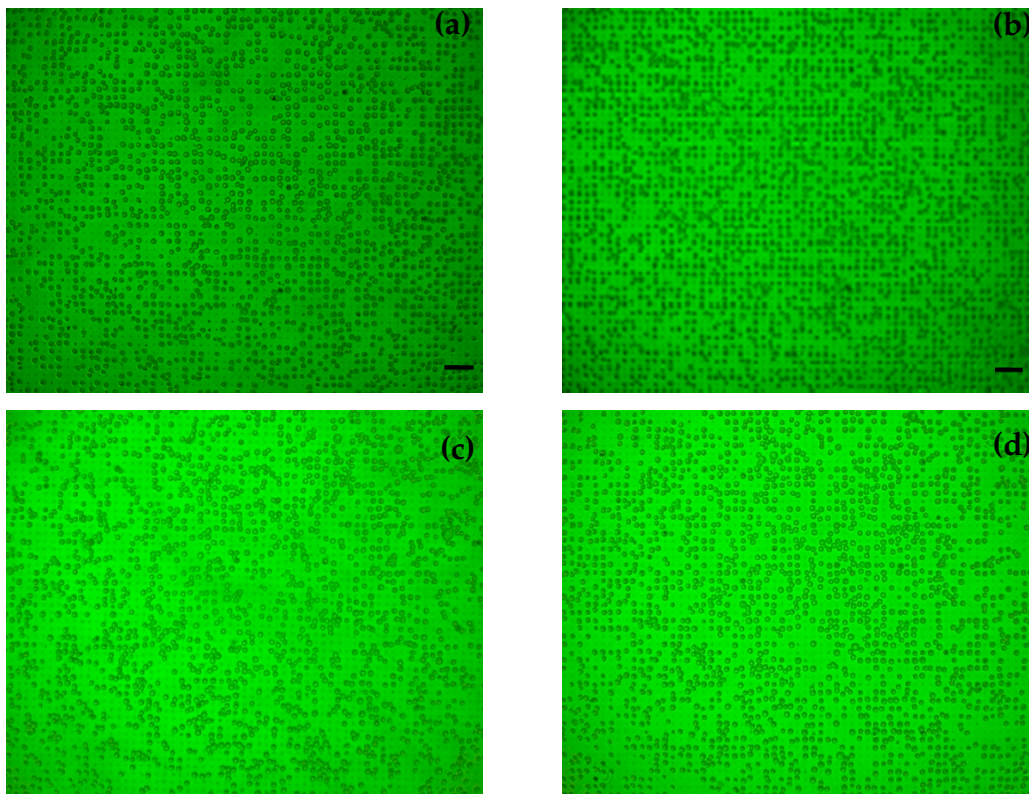


Figure 5.5: B lymphocytes arrays on (a) (CHI3.0/HA3.0)₃ (~57% occupancy), (b) (CHI3.0/HA3.0)₃ +100 mM NaCl (~71% occupancy), (c) (CHI3.0/HA3.0)_{3,5} (~54% occupancy), and (d) (CHI3.0/HA3.0)_{3,5} +100 mM NaCl (~56% occupancy) after 1 hr of agitation and incubation. Scale bars = 50 μm.

Figure 5.5 shows arrays with roughly the same occupancy (~55%) except for (CHI3.0/HA3.0)₃ fabricated with 100 mM NaCl, for which ~71% of array sites were occupied. For all films tested, even greater array occupation could be

achieved by increasing the seeding time from 1 to 2 hours, as seen in Figure 5.6a. Although well-ordered B lymphocyte arrays were generally observed, other arrangements were also seen: lymphocytes aggregated in interstitial spaces, more than one cell on a PEM array sites, and empty sites. The interstitial space is a cationic PDAC-terminated surface. B cells seeded on a uniform $(\text{PDAC4}/\text{SPS4})_{15.5}$ surface showed an attachment density of approximately 310 cells/ mm^2 , which explains why we observe limited attachment on non-array position (see Figure 5.6b).

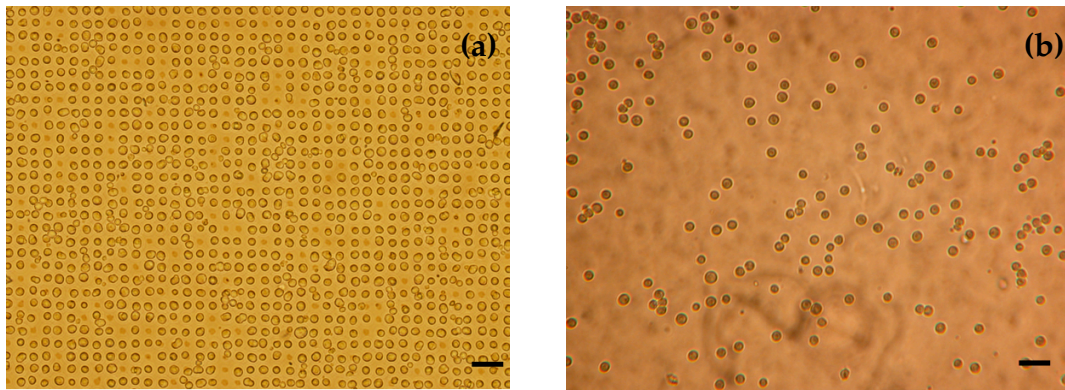


Figure 5.6: (a) B lymphocyte arrays on $(\text{CHI3.0}/\text{HA3.0})_3 + 100 \text{ mM NaCl}$ (~ 97% occupancy) after 2 hrs of agitation and incubation. (b) B lymphocytes adhered non-specifically to a $(\text{PDAC4}/\text{SPS4})_{15.5}$ film, which is the background (i.e., interstitial) surface. Scale bars = 50 μm .

From the above arrays, different cell-attachment scenarios were measured, including available sites occupied by B cells, the number of sites shared by two cells, and the number of cells adhered off array sites. These results are presented in Table 5.2.

	HA-topped (built without NaCl) (Figure 5.5a)	HA-topped (built with NaCl) (Figure 5.5b)	HA-topped (built with NaCl) (Figure 5.6a)
	cells seeded for 1h		cells seeded for 2h
occupied array sites (%)	56.9	71.1	96.7
two cells sharing a site (%)	0.7	0.9	1.9
cells off array sites (%)	2.2	2.7	2.5

Table 5.2: Quantification of the different cell-attachment scenarios as a function of film deposition conditions and seeding time. Total array occupancy increases with seeding time, but the number of cells off array sites is constant, indicating that off-array attachment is non-specific.

Given that B-cell binding to CHI/HA multilayers is facilitated by a CD44 receptor interaction with HA chain segments¹, then the above results point to specific assembly conditions that enrich the multilayer surface in accessible, cell binding HA segments. Two tests confirmed that HA is responsible for B-cell binding. First, HA was replaced in the multilayer with the very similar, non-cell binding polysaccharide alginic acid (ALG). CHI/ALG multilayers with 3 and 3.5 bilayers were built under pH 3 conditions in the absence of NaCl. In this case, no B lymphocyte binding was observed with either CHI or ALG as the top layer. This finding shows that HA is critical to B lymphocyte binding mediated by CD44-HA interactions and that the positive charge of CHI alone is insufficient to provide efficient cell binding to the multilayer. The second test used soluble HA and ALG as antagonists for cell binding. B cells were seeded onto patterned HA or CHI-topped films built with and without 100mM NaCl, respectively, and soluble HA or ALG was added to competitively bind with CD44 or CHI (see Table 5.3 and Table 5.4). ALG was used as control that would electrostatically bind to CHI but not CD44. Soluble HA caused a significant decrease in array

occupancy, dropping 60% and 12% for the CHI and HA-topped films, respectively. Furthermore, soluble ALG (which would complex with cationic CHI) did not release any cells from the backpack array, indicating that the anionic cell membrane is not electrostatically attaching to CHI-topped films. These results are consistent with our previous finding that adding soluble HA to a B-cell suspension prior to exposure to a patterned CHI/HA multilayer dramatically decreases cell binding due to saturation of the cell's CD44 receptors with soluble HA⁹. These three experiments lead to the conclusion that CD44-HA interactions are the dominant binding mode in all HA-containing films - even those assembled with CHI in the final deposition step.

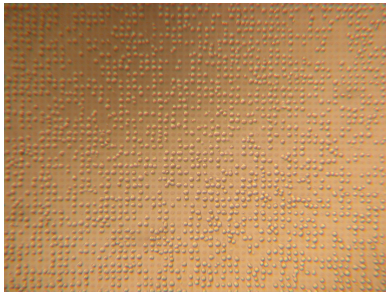
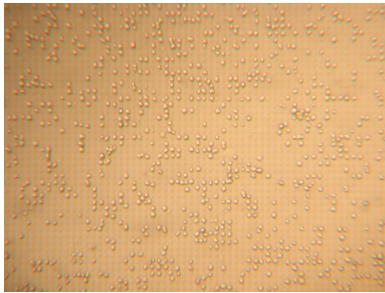
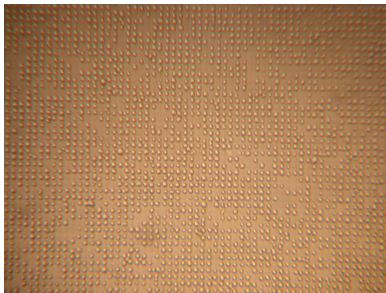
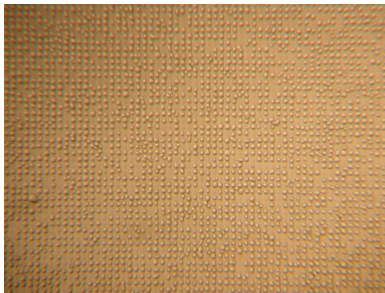
HA-topped film (deposited with 100mM NaCl)	Before exposure	After exposure
Soluble HA $(\Delta = - 11.82\%)$	 <p style="text-align: center;">71.5%</p>	 <p style="text-align: center;">63.0%</p>
Soluble ALG $(\Delta \approx 0\%)$	 <p style="text-align: center;">91.0%</p>	 <p style="text-align: center;">91.1%</p>

Table 5.3: Micrographs of B cells attached to $(\text{CHI}3.0/\text{HA}3.0)_3$ film arrays and the percentage of array occupancy. B cells were found to attach very effectively after 4, 15min incubation/agitation cycles. (The before exposure, soluble HA image is lower than expected because of more vigorous washing than other slides. The identical film washed less vigorously is shown in Figure 5.2.). Soluble HA was found to remove cells from the array, while soluble ALG did not: HA reduced array occupancy by 12%, while ALG did not seem to change the occupancy rate.

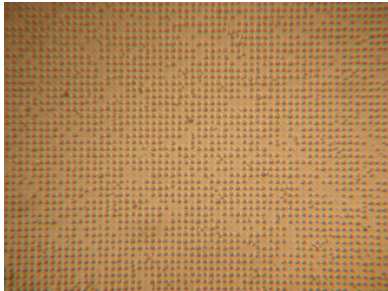
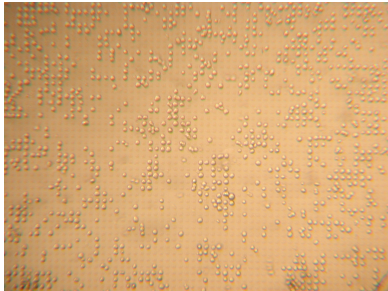
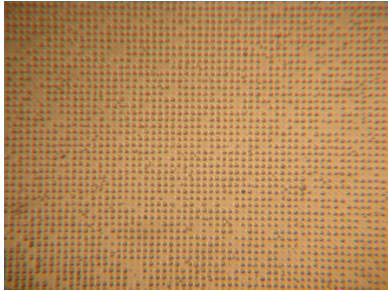
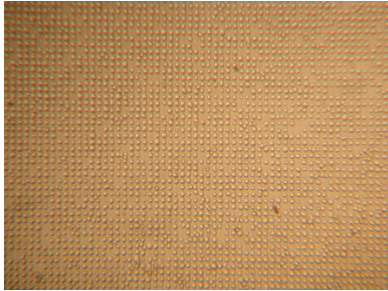
CHI-topped film (deposited without NaCl)	Before exposure	After exposure
Soluble HA ($\Delta = - 60.31\%$)	 93.3%	 37.0%
Soluble ALG ($\Delta \approx + .69\%$)	 92.2%	 92.9%

Table 5.4: Micrographs of B cells attached to (CHI3.0/HA3.0)_{3,5} film arrays and the percentage of array occupancy. B cells were found to attach very effectively after 4, 15min incubation/agitation cycles. Soluble HA was found to remove cells from the array, while soluble ALG did not: HA reduced array occupancy by 60%, while ALG did not seem to change the occupancy rate.

Determination of HA Carboxylates and CHI Amines

To indirectly explore changes in the amount of non-complexed HA chain segments presented under different assembly conditions, we used specific dyes known to bind to charged HA and CHI functional groups. These dyes have been shown to stain only free, non-paired amine or carboxylic acid groups and do not titrate electrostatically-paired groups²³. Free carboxylic acid groups of HA were

stained with alcian blue, a tetracationic dye that shows a high degree of specificity for polyanionic substances such as hyaluronic acid^{24,25}. Staining with rose bengal, an anionic dye, was used to evaluate the presence of free amine groups of CHI.

Alcian blue staining results are shown in Figure 5.7. Figure 5.7a and Figure 5.7b represent data for pH 3 and the pH 5 assembly conditions, respectively.

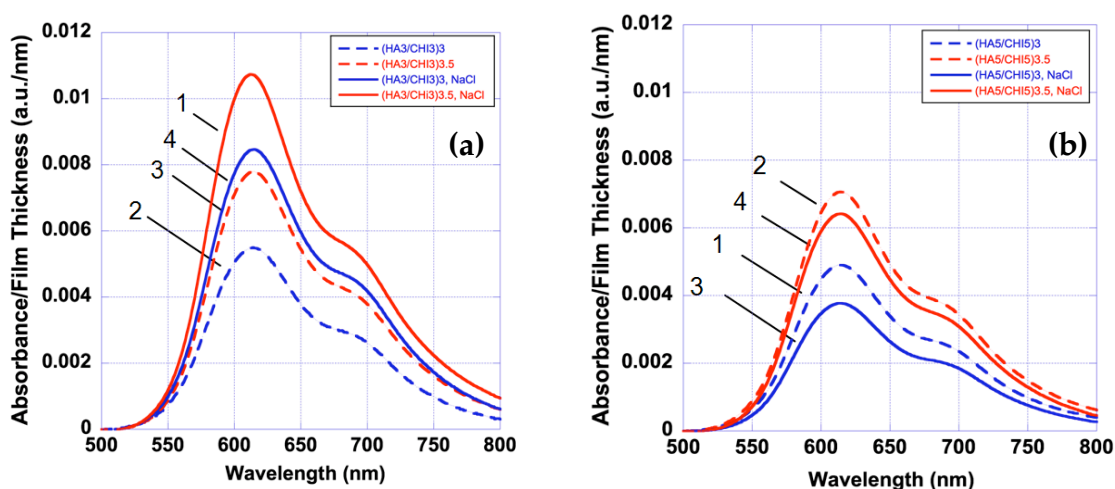


Figure 5.7: Alcian blue absorbance for (a) (HA3.0/CHI3.0) and (b) (HA5.0/CHI5.0) films normalized by film thickness. The numbers 1 to 4 correspond to films with greatest to the least lymphocyte binding capability.

All films were stained by both dyes regardless of the final polymer deposited. This suggests that these are highly intermixed multilayers with the ionic functional groups of both polymers available at or near the surface (depending on multilayer swellability and diffusion times, dyes can penetrate and access free ionic functional groups deeper into the multilayer) and that no assembly conditions produced an outermost layer arrangement capable of blocking the uptake of an oppositely charged dye²³.

Figure 5.7a shows that PEMs prepared at pH 3 with NaCl and regardless of final polymer deposited display the highest two alcian blue absorbance curves and thus have the most free HA chain segments. Preparing a film at pH 3 with NaCl increases its absorbance value over a film prepared without salt. These trends were not observed under pH 5 deposition conditions (Figure 5.7b), where the two highest alcian blue absorbance values were found for HA-terminated films regardless of salt condition, and preparing a film without NaCl increases its absorbance value over a film prepared with salt.

Rose bengal staining of free cationic charges is shown in Figure 5.8. CHI-terminated films assembled at pH 3 (labeled 2 and 4 in Figure 5.8a) have many free amines since it has overcompensated negative surface charges on the previously HA-capped surface. It follows that HA-terminated films would then have the lowest number of free amines, as seen by the curves labeled 1 and 3 in Figure 5.8a. Salt also reduces the number of free amines by encouraging HA adsorption (see curves 1 and 4 in Figure 5.7a). These trends were seen only under pH 3 deposition conditions; at pH 5, the free amine concentration is insensitive to deposition conditions (final polymer deposited and salt).

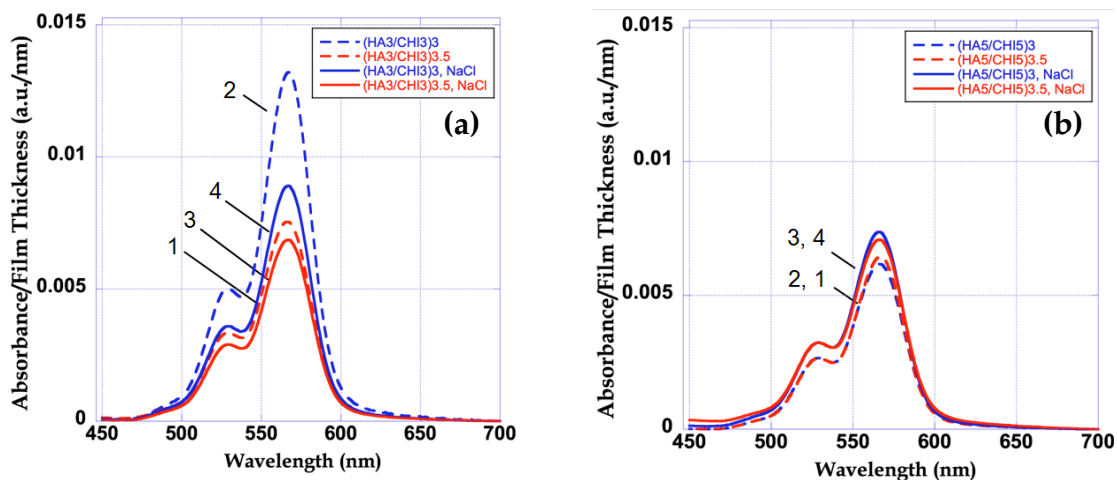


Figure 5.8: Rose bengal absorbance per film thickness for (a) (HA3.0/CHI3.0) and (b) (HA5.0/CHI5.0) films. The numbers 1 to 4 correspond to films with greatest to the least lymphocyte binding capability.

Quartz Crystal Microbalance

HA/CHI film buildup at pH 3 was monitored by *in situ* QCM-D, shown in Figure 5.9. Here, a frequency decrease is proportional to the mass deposited on the surface, and an increase in dissipation energy indicates a decrease in the film's shear elastic modulus. Deposition with salt seems to encourage polymer desorption and leads to less mass adsorbed per bilayer, contrary to previous findings for CHI/HA films⁷. (These studies considered well beyond the first 3 bilayers, and depositions were completed at pH 5.) Interestingly, films built with salt seem to be mechanically unaffected by HA adsorption, exhibiting a drop in elastic modulus upon only CHI exposure. Films built without salt show a decrease in modulus with each adsorption step. During the first three bilayers in both the salt and salt-free cases, each deposition cycle results in a larger downward frequency shift indicating an ever-increasing mass uptake per bilayer. This is consistent with reported initial exponential growth behavior in the HA/CHI system²⁶. Absolute values for thickness from QCM-D analysis are

higher than those from profilometry, as QCM-D includes the mass of solvent (i.e., water) bound to the polymer chain. In this analysis, we assume HA and CHI are similarly hydrated, and use thickness ratios to factor out solvent mass.

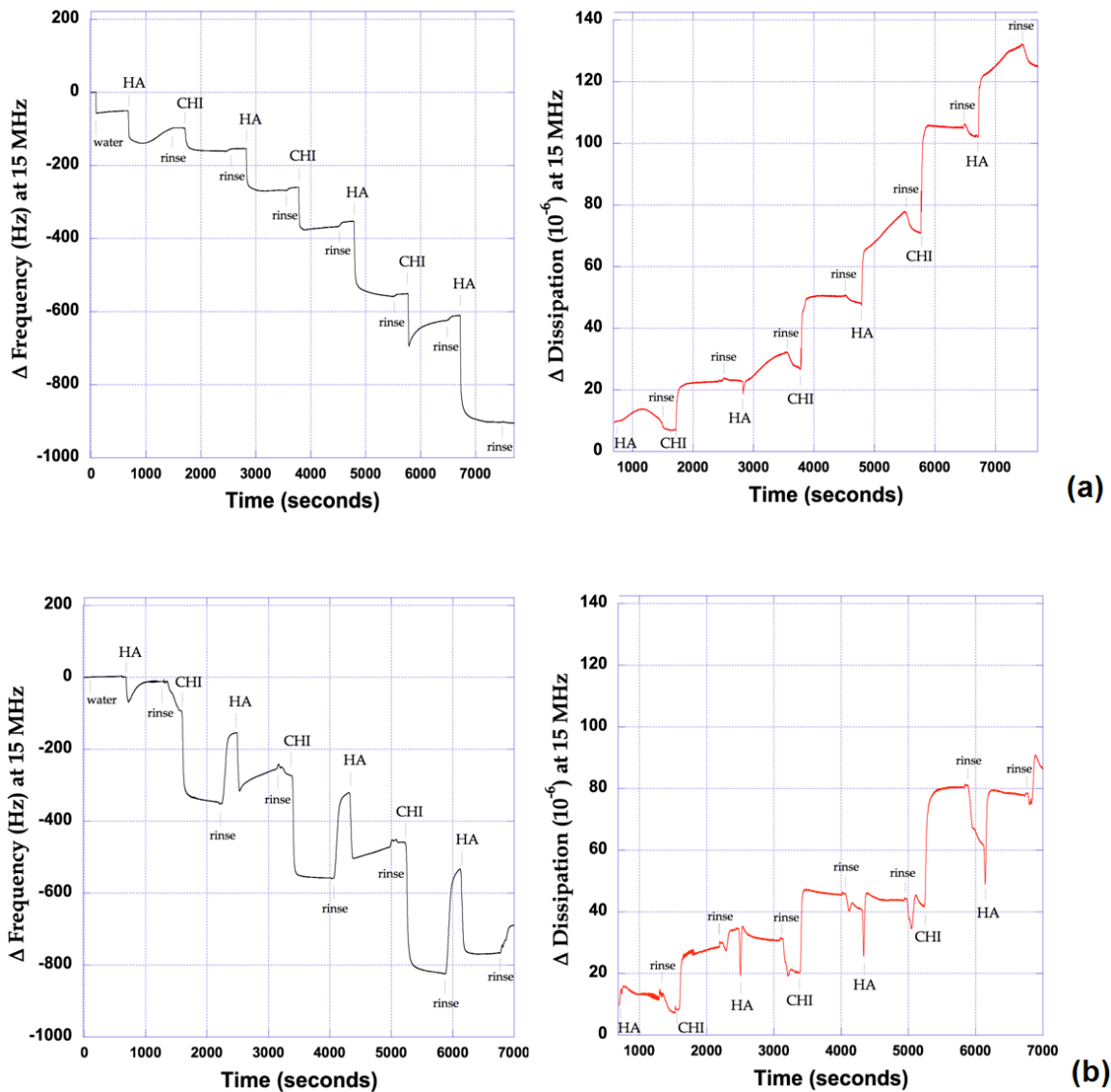


Figure 5.9: Raw QCM-D frequency shift and dissipation data for (HA3.0/CHI3.0) films deposited with (a) 0 mM NaCl and, (b) 100 mM NaCl in the polymer solutions.

QCM-D results were analyzed using the QTools software provided with the equipment. Fitting the data to a Voigt model (more details can be found in the

Experimental Details section), the thickness for each deposition step was determined. These thickness values were then added to give a *total* thickness for each polymer (t_{HA} or t_{CHI}). If the density for CHI and HA are assumed to be equal and constant, t_{HA} and t_{CHI} are directly proportional to the total mass of each polymer in the film. Total thickness values and the ratio t_{HA}/t_{CHI} are shown in Table 5.5.

	<i>HA thickness</i> t_{HA} (nm)	<i>CHI thickness</i> t_{CHI} (nm)	t_{HA}/t_{CHI}
(HA3.0/CHI3.0) ₃	76.78	58.22	1.32
(HA3.0/CHI3.0) _{3,5}	148.78	58.22	2.55
(HA3.0/CHI3.0) ₃ + 100mM NaCl	39.42	56.70	0.69
(HA3.0/CHI3.0) _{3,5} + 100mM NaCl	71.20	56.70	1.26

Table 5.5: Values for the total thickness contributed by each polymer (t_{HA} or t_{CHI}) and their ratio. Since the density of HA and CHI are nearly equal, t_{HA} or t_{CHI} represent the total amount of each polymer in the final film.

The ratio t_{HA}/t_{CHI} reveals how much of each polymer is present in the final film; values greater than 1 are “HA rich” (or “CHI poor”) films, and values less than 1 are “HA poor” (or “CHI rich”). As might be expected, depositing HA last leads to a greater t_{HA}/t_{CHI} value for a given salt condition. Also, using salt seems to reduce the amount of HA contained in a film by a factor of 2, but does not seem to affect the total amount of CHI. Considered with the absorbance data, it seems that though salt decreases the total amount of HA in the film, it leaves more HA groups free to bind alcian blue (curves 1 and 4 in Figure 5.7a).

CHI content can also be interpreted with regard to the spectroscopic absorption data. Following from above, films with CHI as the outermost layer are CHI rich and have lower t_{HA}/t_{CHI} values at a given salt condition – these films show greater

rose bengal dye uptake as well. Salt seems to make films CHI rich, but decreases the number of primary amines able to bind to rose bengal (curves 1 and 4 in Figure 5.8a).

Like the absorbance data, no clear relationship exists between total HA and cell-binding capability. For instance, the film with the highest t_{HA}/t_{CHI} value (2.55) was not the film with greatest cell-binding efficiency. This further emphasizes that sheer quantity of HA does not determine the ability to bind to CD44, but rather how CD44-binding ligands are presented on the surface.

Discussion on HA/CHI Multilayers

HA and CHI-containing PEMs are interesting for a host of biological applications because of their well-established biocompatible and biodegradable properties^{4,12,27}. In the specific case of immune system engineering, a six-sugar sequence of HA is a natural ligand for the CD44 surface receptor found in many immune system cells¹. To take full advantage of this potentially powerful cell-polymer interaction, it is necessary to create molecular assemblies that present their critical binding functional groups in an optimal arrangement. To accomplish this goal, we examined how deposition conditions influenced molecular-level blending⁸ of these two polymers during multilayer assembly, resulting in thin films which could be used to control the binding of B-cells. Three deposition variables were studied in depth: the presence of NaCl in the polymer solutions (0 or 100mM), the pH of the polymer solutions (3 or 5), and the final polymer deposited (HA or CHI).

HA is required for successful B cell attachment as shown by two ALG controls. ALG is structurally very similar to HA, yet ALG/CHI films were unable to bind lymphocytes. Soluble ALG was also unable to antagonistically bind and release cells that had already been attached to HA-containing films. Soluble HA, on the other hand, was able to release up to 60% of formerly attached cells. The two most efficient B cell binding films terminated in either HA or CHI, differing by the presence of NaCl in the polymer deposition solutions (no NaCl for the CHI-topped film, 100mM NaCl for the HA-topped film). The pronounced difference in the number of cells released from a HA vs. CHI-topped film (12% vs. 60%, respectively; see Table 5.3 and Table 5.4) by soluble HA indicates that the adhesion between the cell and a CHI-topped film is considerably less strong. We hypothesize that the additional CHI layer complexes with surface HA, reducing the number of available CD44 ligand sites and weakening the adhesive force between the cell and film but not affect the binding efficiency (i.e., number of cells attached).

The ability to terminate a film in either HA or CHI and achieve similar binding efficiency may be of particular interest for some applications. If application requirements dictate a need for particular functional groups on the surface (carboxylates on HA, amines on CHI), then either HA or CHI may be used without impairing B cell binding capability. For instance, CHI's primary amines are known to be antibacterial²⁸, which may be a desirable property of the outermost layer before B cells are attached.

Film deposition conditions that favor loops and tails, rather than sheer quantity of HA, lead to more efficient cell binding. While the film that showed the best

lymphocyte binding - (HA3.0/CHI3.0)_{3,5} with 100 mM NaCl – also displayed the greatest alcian blue staining of free carboxylic acid groups, the total amount of HA seems uncorrelated to binding efficacy. As the amount of free HA decreases, the B cell binding capacity increases (curves 2-4 in Figure 5.7a). (HA3.0/CHI3.0)₃ deposited without salt displayed the least free HA and the greatest amount of free cationic groups of CHI (curve 2 in Figure 5.8a), yet bound to cells with similar efficiencies as the HA-terminated film deposited with salt. This result shows that even with CHI deposited last there are sufficient free HA-binding ligands available to attach to CD44. Presentation of HA binding ligands, not the total quantity of HA, is far more important for efficient CD44 binding, a fact further supported by quartz crystal microbalance studies (see above).

The ability to precisely pattern B cells onto a surface may be critical to biosensing and tissue engineering applications. We found that adding NaCl during deposition at pH 3 and longer cell seeding times favor high fidelity cell arrays. The number of cells attached off the array sites is insensitive to film processing and seeding time, indicating that this cell-surface interaction is non-specific, and is mostly likely based upon a weak electrostatic attraction between the anionic cell surface and cationic slide. This cell patterning method offers binding efficiency that is competitive with existing techniques²⁹ while not requiring covalent coupling or uniform decoration of the cell surface with an attachment group such as biotin. Furthermore, the natural interaction between CD44 and HA could initiate cell signaling cascades and prompt behavior desirable for biosensing, an application that originally motivated this work³⁰.

Conclusions and Future Work on HA/CHI Multilayers

Biopolymer multilayers comprised of hyaluronic acid and chitosan successfully immobilize non-adherent B lymphocytes. These films bind to B lymphocytes via a native CD44-hyaluronate interaction, ensuring their viability and function following attachment. We were able to maximize binding efficiency of the PEMs by systematically adjusting solution deposition variables such as ionic strength and pH. From all the biopolymer multilayer systems studied, the greatest lymphocyte binding was found for the HA-terminated (HA3.0/CHI3.0)_{3,5} film deposited with 100 mM NaCl. Very similar binding levels were found for the CHI-terminated (HA3.0/CHI3.0)₃ film deposited without salt. Lymphocytes bind to photolithographically patterned HA/CHI film arrays, corroborating previous findings.

This work demonstrates two important conditions for successfully attaching B cells to HA-containing PEM films. First, HA is essential for CD44-mediated binding, as shown by the ALG controls and antagonistic binding by soluble HA and ALG. However, as the absorbance data shows, the total amount of HA in a film does not determine B cell binding capability. Second, HA deposition conditions that favor loops and tails, such as low pH and with added salt, can result in greater B cell attachment by making more CD44-binding ligands available. These two conditions emphasize how HA is presented on a surface is the most important factor determining cell binding potential. PEM film technology is especially well suited for controlling polymer configurations, since adjusting solution deposition conditions (salt, pH) can dramatically affect how polymer chains adsorb. We believe the ability to easily produce CD44-binding

thin films with tunable binding affinity will find numerous applications in biosensing, biomaterials, and tissue and immune system engineering applications.

This work provides a model for optimizing the B cell binding abilities of thin polymer films; however, we do not have a mechanistic understanding of why certain conditions lead to greater binding. The absorbance and QCM-D data shows no clear trend in polymer content and cell-binding ability, but do not give any evidence for what *does* lead to efficient cell binding. Surface analysis techniques, such as XPS and Auger spectroscopy, could lead to better insights into exactly which functional groups are present on the outermost part of the cell-adhesive region. Scattering techniques with labeled polymers (such as deuterated HA) and direct surface measurement methods like AFM could also give information about how CD44 ligands are presented on the surface. These studies could give us valuable information for how to develop new cell-adhesive regions based not only on CD44, but a range of cell surface adhesion proteins.

CMC/CHI Multilayers

Biocompatibility of the linear polysaccharides carboxymethylcellulose (CMC) and chitosan (CHI) has long encouraged their use in biological applications. CMC is a cellulose derivative formed from the reaction between chloroacetic acid and cellulose; this reaction introduces carboxylic acid moieties along the polymer backbone, rendering CMC a polyanion with a solution $pK_a \sim 4$.^{31 31}. The degree of

substitution of carboxylic acid groups is controllable and quantifiable, and is commonly between 50% and 100%. CMC is found in a host of personal care products, and is FDA approved for ocular applications such as lubricating eye drops. Details on CHI may be found above on page 128. The chemical structures of both CMC and CHI may be found in Figure 5.1.

We were motivated to build CMC/CHI films to produce an ultra-thin, anti-fouling film for optical device applications. We chose a fluoro-silicone containing poly(acrylate) material (Equalens II ®, also named oprifocon A) that models the hydrophobic material commonly used for gas-permeable hard contact lenses. A hydrogel film coating must be mechanically robust (patients wear the device constantly and will blink every few seconds), optically transparent, biocompatible, and must not decrease oxygen permeability. This final requirement is critical since the cornea is the only tissue that obtains oxygen from the environment rather than through respiration.

Addressing these design parameters, we built (CMC/CHI) multilayer films on the surface of Equalens II discs and Si wafers, and investigated *in vitro* thickness and swelling behavior. While electrostatic interactions between the polyanion CMC and polycation CHI provide the mechanism for film growth, films were covalently crosslinked using EDC/NHS chemistry to increase mechanical durability and robustness in physiological conditions.

We used a simple abrasion test to evaluate the mechanical durability of these films, as well as the adhesion to the hydrophobic Equalens material. Films could

be vigorously abraded in isotonic, neutral solutions, and the (CMC/CHI) films remained on the surface, as indicated by continued superhydrophilicity.

Growth Behavior and Crosslinking

As expected from other biopolymer systems (such as HA/poly(lysine)³² and CHI/ALG)³³, (CMC/CHI) multilayers grow exponentially with the number of bilayers. The growth profiles for (CMC4.0/CHI4.0) as a function of bilayers and EDC/NHS crosslinking may be found in Figure 5.10. A refractive index of 1.46 for the (CMC/CHI) film was found to fit the experimental ellipsometry data.

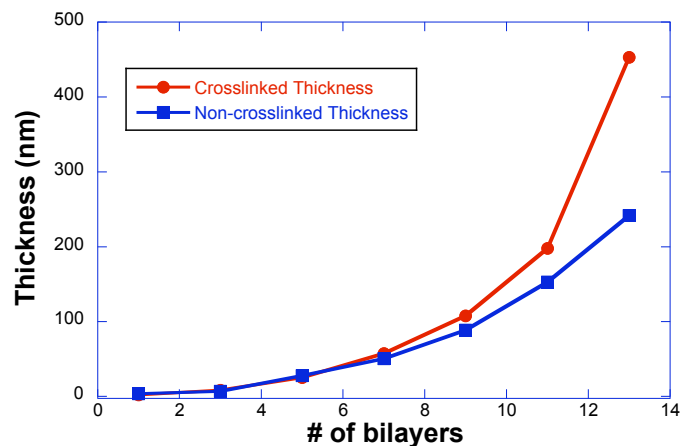


Figure 5.10: (CMC4.0/CHI4.0) thickness vs. number of bilayers for as-deposited and EDC/NHS crosslinked films, as determined by ellipsometry ($n=1.46$).

It is generally accepted that hydrophilicity and film swelling are two dominant factors in reducing non-specific macromolecule adsorption^{34,35}. A highly swollen hydrogel comprises mostly water molecules, and thus macromolecules have little free energy benefit in adsorbing to a hydrogel structure versus remaining in solution. To quantify the swelling behavior of the (CMC/CHI) PEM, we

measured the swelling behavior's dependence on the number of bilayers (thickness) and the solvent (pure water or PBS). For all solvent and crosslinking conditions, the swelling ratio increases with film thickness then plateaus. The onset of this plateau depends on film crosslinking – a non-crosslinked film plateaus after 7 bilayers, whereas crosslinked films plateau after 11. Further, the magnitude of this plateau swelling ratio depends on crosslinking – the maximum swelling ratio of crosslinked films is ~120%, whereas non-crosslinked films swell up to ~160%.

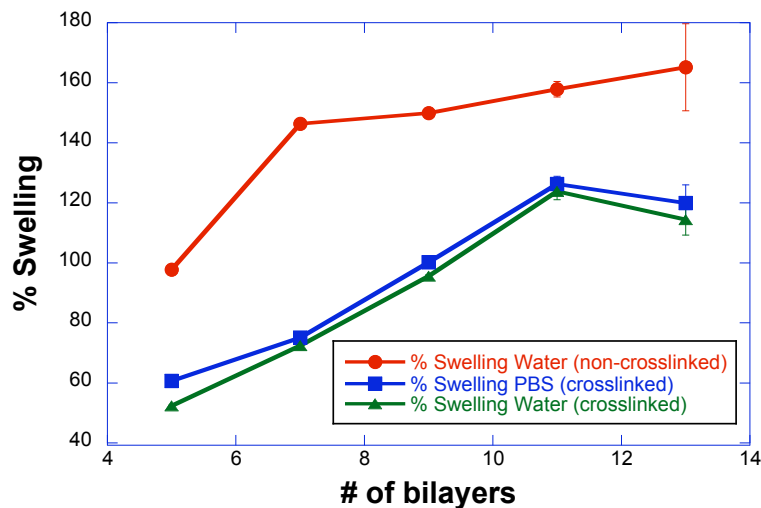


Figure 5.11: Swelling ratio for (CMC4.0/CHI4.0) films as a function of number of bilayers, crosslinking status, and solvent. All films exhibit a monotonic increase in swelling with film thickness, followed by a plateau. Error bars reflect the standard deviation of at least three film measurements.

Hydrophilicity and Mechanical Robustness

The need for a highly swollen hydrogel film must be balanced with mechanical robustness. A film that swells several hundred percent would not be able to withstand the continuous mechanical abrasion of blinking in ocular device applications. Mechanical coating failure may occur in two ways – the film may

slowly erode away at the surface between the eyelid and the film, or the entire film may delaminate from the surface of the lens. The first scenario is unlikely, given the highly entangled and covalently crosslinked (CMC/CHI) film. Failure is most likely to occur because of a poor anchoring of the coating to the lens surface. To improve this attachment, we used an initial PAH polymer solution comprised of a binary 50% (by volume) isopropanol/pH3 water solvent. Since the Equalens II material is primarily polyanionic PMAA, fully-charged PAH (due to the pH3 water) will readily bind via electrostatic interactions. The isopropanol-containing solvent swells the lens (~3% by mass) so that PAH can copiously interpenetrate into the surface; PAH reptation into the lens introduces physical entanglements that strongly anchor the film to the lens surface. All following deposition and rinse steps are done in aqueous solvents, during which the lens will contract to its original volume. Following the PAH/isopropanol/water step, an adhesion layer of (SPS4.0/PAH4.0)₅ was deposited. This layer renders the lens uniformly charged and provides an adhesive surface for all subsequent depositions.

To test the (CMC/CHI) film's mechanical integrity, (CMC4.0/CHI4.0)_{10.5} films were attached to polished, planar Equalens II discs and crosslinked as above. These discs were submerged in pure water, weights were applied to the disc normal to the coated surface, and the disc plus weights were abraded against the surface of a clean, soft metallurgical polishing cloth (DP-Nap, Struers) for 1 meter. Water contact angle was used to indicate the presence of the film – the contact angle of the bare lens, (SPS4.0/PAH4.0), and (CMC4.0/CHI4.0)₁₀, is 110°, ~60°, and <5° in .5s, respectively (see Figure 5.12). Coated discs were abraded

against the polishing cloth with variable amounts of weight applied, and up to the maximum weight available, 200g, the coated disc had a contact angle of $<5^\circ$. We can conclude that for up to 200g applied mass during abrasion, the (CMC4.0/CHI4.0)₁₀ film does not delaminate from the lens surface and is still intact. These conditions may not perfectly mimic those found in the eye, but do show that for significantly harsher mechanical stresses, the hydrogel layer is not removed.

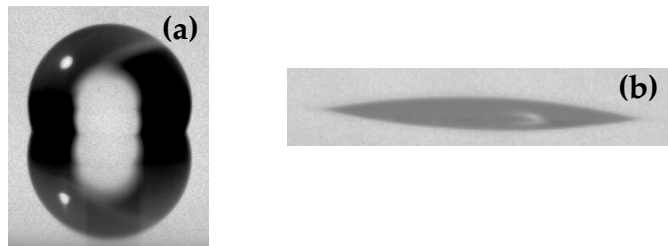


Figure 5.12: Advancing water contact angles for (a) the bare Equalens II material, $\sim 110^\circ$, and (b) (CMC4.0/CHI4.0)₁₀, $\sim 5^\circ$ in .5s.

Transparency of CMC/CHI Films

Optical transparency across the visible spectrum is a primary requirement for any optical coating, especially one that may be worn on the surface of the eye. To test for optical clarity, CMC/CHI films were assembled on glass substrates and transmittance behavior was measured.

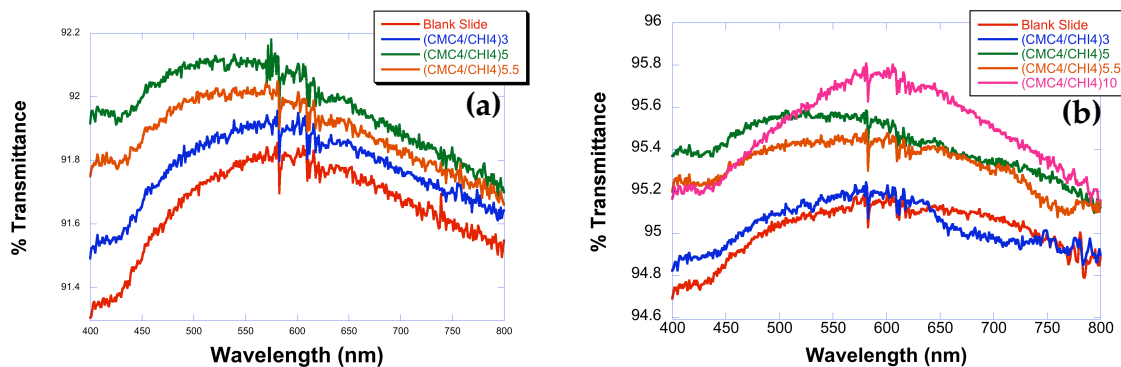


Figure 5.13: Optical transmission behavior of various CMC/CHI films assembled on glass. (a) shows the transmission in dry (CMC/CHI) films, while (b) shows films that had been soaked in distilled water immediately before measurement. Notice that the films show similar or greater transmission than through an uncoated glass slide.

Conclusions and Future Work on CMC/CHI films

CMC and CHI effectively assemble via the layer-by-layer technique to form hydrophilic, swellable films. Since CMC and CHI are biopolymers, the resultant film should be highly biocompatible. While the original application in mind – using CMC/CHI films for ocular device coatings – will require a clinical partner to test safety and efficacy, the CMC/CHI system has found application in anti-fogging coatings for optical components. The superhydrophilic surface may also be effective in any water collecting application, such as those proposed for patterned superhydrophilic/superhydrophobic surfaces³⁶.

The CMC/CHI system offers particularly attractive possibilities for studying wicking and wetting behavior related to anti-fogging applications. Film properties such as porosity and density can be changed with crosslinking treatments, both polymers are very hydrophilic, and films seem to be mechanically and chemically robust to remain anti-fogging over time. A great deal of work remains to explain why this system is particularly well suited to anti-fogging applications, including the mechanism by which water interacts

with the film. The original medical device coating application remains unexplored clinically, and initial tests of how protein adsorbs to the film surface may provide proof-of-concept evidence for this purpose. Certainly CMC/CHI films hold a great deal of potential for practical applications as well as fundamental studies on how fluids interact with surfaces.

ALG/CHI Multilayers*

Both chitosan and alginate have shown promising potential in pharmaceutical release³⁷, protein encapsulation, elution barriers, muccoadhesives, waste water treatment, and biocompatible coatings. Alginate is a water-soluble linear polysaccharide composed of alternating blocks of (1,4) linked α -L-guluronic ($pK_a \sim 3.6$) and β -D-mannuronic ($pK_a \sim 3.4$) acid components. At physiological pH, alginate is a fully charged polyanion due to unprotonated carboxylate groups.

We investigated chitosan/alginate films as a potential candidate for use in cellular backpacks. Specifically, the morphology of LbL assembled chitosan/alginate films was controlled by varying the ionic concentration (using the divalent salt CaCl_2) and pH value of the washing solutions during deposition. Such morphological control may be used to tune mechanical properties and elution barrier behavior when integrated into a multi-region

* The results in this section were in collaboration with Marisa M. Beppu, School of Chemical Engineering, Department of Thermofluidynamics, State University of Campinas, Campinas, Brasil.

heterostructured backpack. Using atomic force microscopy (AFM), we found that films could be created ranging from compact to highly porous, making these films candidates for controlling the release of payload materials from the backpack.

Atomic Force Microscopy (AFM)

The use of divalent cations, such as Ca^{2+} , Br^{2+} , and Sr^{2+} , to crosslink alginate's guluronic groups³⁷ has been used to increase the density of chitosan-alginate thin films. This has been shown to subsequently inhibit the release of insulin^{38,39} and B2⁴⁰ from chitosan-alginate microcapsules. We used a similar approach by exposing (CHI/ALG) films to a CaCl_2 solution after each deposition cycle. Further, we exposed the film to an acetic acid rinse step, which would encourage chitosan solubility. These treatments were found to significantly affect film morphology, as seen in Table 5.6.

Conclusions and Future Work on CHI/ALG Films

CHI/ALG films are attractive for any application requiring a biocompatible multilayer system. The structure of these films has been found to be tunable by adjusting the deposition rinse conditions. CHI's limited solubility below pH 6 and ALG's ability to crosslink with divalent cations allow for unique film morphologies. Future efforts could focus on how this morphology could be leveraged to create controllable elution barriers for the backpack's payload region. For instance, CHI/ALG films could be deposited atop drug or particle laden payload regions. Release of the payload could then be monitored as a

function of CHI/ALG deposition conditions. This practical use could lead to basic insights into methods for controlling backpack dissolution, a characteristic critical to any clinical application.

	$(\text{CHI}/\text{ALG})_5$	
Water		
Acid		
CaCl₂		
Acid&CaCl₂		

Table 5.6: AFM images of $(\text{CHI}/\text{ALG})_5$ films assembled under the various conditions indicated. Notice the significant coarsening of the film morphology with exposure to CaCl_2 rinse solutions.

Conclusions

Several all-biopolymer PEMs were prepared for different applications. HA/CHI films were studied in depth as a cell-adhesive PEM. HA is the ligand for a cell surface receptor named CD44, which many immune system cells express constitutively. PEM deposition variables, such as pH and salt concentration, were adjusted to maximize B lymphocyte binding. Interestingly, neither the total amount of HA nor the amount of free, non-complexed HA was not found to affect B cell binding capacity; rather, how HA was presented on the surface was the determining factor for successful cell attachment.

PEMs based on CMC/CHI were fabricated to be an ultra-swellable, protein-resistant coating for medical device applications. These films are superhydrophilic (i.e., with a water contact angle $<5^\circ$ in .5s), and have been found to be excellent candidates for anti-fogging purposes. Mechanically and chemically robust, these films have the potential to be applied in a number of practical areas as well as provide a basis for fundamentally understanding how liquids interact with surfaces. Finally, PEMs based on the biopolymers CHI and ALG were built as a candidate for a biocompatible cell backpack payload region. When these films were deposited with certain acid or salt rinses, the resulting film morphology ranged from dense to highly porous. The ability to tune a film's morphology so widely using rinses during deposition could lead to elution barriers useful in controlling a backpack's payload release.

Experimental Details

Materials. Hyaluronic acid sodium salt (HA, from *Streptococcus equi* sp, MW $\approx 1.63 \times 10^6$ g/mol), chitosan (CHI, low molecular weight $\sim 5 \times 10^4$ g/mol, 75-85 % deacetylated), alginate (ALG, in the form of alginic acid sodium salt, low molecular weight), carboxymethylcellulose (CMC, Sigma, MW=250kDa, DS=0.7), poly(diallyldimethylammonium chloride (PDAC, medium molecular weight, 20 wt % in water solution), poly(sodium 4-styrene-sulfonate) (SPS, MW $\approx 7 \times 10^4$ g/mol) and fluorescein isothiocyanate-labeled poly(allylamine hydrochloride) (FITC-PAH) were purchased from Sigma-Aldrich (USA). All polyelectrolytes were used without further purification. Anionic, superparamagnetic nanoparticles (MNPs, Fe₃O₄ EMG 705, 10nm diameter) were purchased from FerroTec (USA). Ethyl-3-(3-dimethylaminopropyl)carbodiimide hydrochloride (EDC) and N-hydroxysuccinimide (NHS) were purchased from Pierce. Fetal calf serum (FCS) was purchased from Hyclone (USA). Hank's Balanced Salt Solution (HBSS) was purchased from Gibco, Invitrogen (USA). The positive photoresist S-1813 and MF-319 developing solution were purchased from MicroChem.

HA/CHI Film Deposition. Before use, VWR glass slides were sonicated for 15 minutes in a 3% detergent (Micro 90) aqueous solution followed by a 10 min wash in 1 M NaOH and 2 consecutive 5 minute rinses in Milli-Q water. All samples were air dried. Si wafers were cut to the desired sample size, wiped with ethanol, O₂ plasma cleaned, and air dried before use. The LbL technique was used to deposit the heterostructured polymer and nanoparticle films. The notation that is used for each bilayer of complementary polymers or nanoparticles is: (Poly₁X/Poly₂Y)_n. Poly₁ and Poly₂ refer to the polymers or nanoparticles, X and Y refer to the solution pH, and *n* is the number of bilayers deposited. A "half bilayer" is represented when *n* = x.5, where x is any integer. A (PDAC4/SPS4)_{15.5} pre-layer was deposited on all substrates using an automatic dipping procedure with a Zeiss HMS™ Series Programmable Slide Stainer. Clean glass or Si wafer slides were alternately immersed in PDAC (pH 4, 100 mM NaCl) and SPS (pH 4, 100 mM NaCl) solutions, each followed by two

consecutive Milli-Q water (pH ~ 5.7) rinse steps of 2 and 1 minutes, respectively. PDAC and SPS solutions were prepared at 10^{-2} M (based on the repeat unit molecular weight) in 100 mM NaCl. CHI, HA, and ALG solutions were prepared by dissolving the respective polymer in water at concentrations of 1 mg/mL and gently stirring the solution overnight. The CHI solution was prepared with 100 mM glacial acetic acid (HAc). HA, CHI, and ALG solutions were prepared both with and without 100 mM NaCl. The pH of all solutions was adjusted with 1 M HCl and 1 M NaOH solutions. MNP solutions were prepared at a concentration of 0.005% w/v at pH 4.0. HA/CHI bilayers were deposited with a StratoSequence VI spinning dipper running StratoSmart v6.2 software from nanoStrata Inc. (USA). HA and CHI polyelectrolyte deposition steps were performed without stirring for 10 minutes. The three consecutive rinse steps (2, 1, and 1 minutes) with Milli-Q water were performed while spinning the substrate within the solutions at a frequency of approximately 100 rpm.

CH27 B Lymphocyte Culture. CH27 B lymphocytes were cultured and passaged (1:10 every 3 days) in RPMI-1640 media containing 10% fetal calf serum (FCS), and 1% streptomycin/ penicillin (P/S). Cell cultures were maintained at 37°C and 5% CO₂. Adhesion experiments were performed with cell aliquots at 10⁶ cells/mL. Cells were washed in HBSS 3 times prior to attachment.

B Lymphocyte attachment to PEMs. B lymphocyte suspensions (2mL) were gently pipetted directly onto the prepared HA/CHI multilayered surfaces in Petri dishes. These dishes were placed on a vibratory platform (IKA Vibrax) inside an incubator. Samples were incubated for 15 minutes, followed by a gentle agitation for 15 minutes. This procedure was repeated twice (for a total time of 1 or 2 hours), to promote cell adhesion. Immediately after the incubation/agitation steps, samples were gently washed in fresh HBSS to remove unbound cells, then placed in complete RPMI-1640 media and analyzed.

UV-Visible Spectroscopy. Free HA carboxylic acid groups were stained by first immersing the film in an alcian blue solution (0.001 M, pH 3) for 15 minutes. Slides were then rinsed extensively in pH 3 Milli-Q water twice for 2 min. Films were dried with N₂ and immediately analyzed in a Cary 5E UV-Vis

spectrophotometer. Alcian blue peaks were observed at 617 nm. Free CHI amine groups were stained by immersing the PEM in a rose bengal solution (0.001 M, pH 7) in RPMI media (with 25 mM HEPES, without FCS, phenol red, or S/P) for 15 minutes. The slides were then rinsed extensively in Milli-Q water twice for 2 min each. Films were dried with N₂ and absorbance was immediately measured. Peaks for rose bengal were observed at 567 nm. Films were also immersed overnight in Milli-Q water with the same pH as their respective build-up pH conditions (pH 3 and pH 7) and measured again. Measurements include absorption from multilayers on both sides of the substrate.

B Lymphocyte Binding Efficiency. Uniform films and patterned film arrays with adhered CH27 B lymphocytes were analyzed with an Olympus IX-81 inverted optical microscope. At least 7 images for each sample were analyzed and either the total number of cells attached per unit area (for uniform films) or the percentage of patterned array sites occupied with a cell was determined.

Quartz crystal microbalance (QCM-D) Analysis. QCM-D provides useful information about the film build-up mechanism.⁴¹ A Q-Sense D300 was used for all measurements. Quartz crystals were washed in 1M HCl, dried under N₂, and O₂ plasma cleaned for 30 minutes. They were subsequently coated with a (PDAC4/SPS4)_{15,5} film utilizing the same protocol mentioned above. The film on the electrodes side of the crystal was removed with HCl and Milli-Q water. Crystals were then submersed in Milli-Q water with the same pH as the respective QCM-D planned run (pH 3 or pH 5), and allowed to equilibrate for several hours. Polymer and rinsing solutions were flowed over the crystals at a flow-rate of 1.50 mL/min (non-turbulent flow). For each polymer deposition step, the polymer and rinsing solutions were flowed over the crystals for 11 and 4 minutes, respectively. All frequency and dissipation signals were measured at the 15 MHz, $\nu = 3$ overtone of the crystal. Analysis was carried out using the QTools software provided with the instrument.

PEM Film Patterned Arrays. The patterning method of McShane and co-workers^{42,43} and Swiston *et al*⁹ was used to create patterned multilayer heterostructure assemblies. Briefly, this process uses a traditional lift-off

photolithographic approach to pattern ultrathin polymer films. These assemblies were fabricated with a (MNP4.0/FITC-PAH3.0)_{9.5} region between the pre-layer and cell adhesion regions. Deposition of the (MNP4.0/FITC-PAH3.0)_{9.5} region on the (PDAC4/SPS4)_{15.5} pre-layer was performed by a Zeiss HMS static dipper. Two consecutive pH 3 Milli-Q water rinse steps were performed after each deposition step. After 9.5 bilayers were deposited, samples were allowed to dry in ambient conditions, and stored away from light. To build the cell adhesive region, CHI was deposited first on the negatively charged MNP surface. The same pH, NaCl, and top layer variations, as studied for uniform films, were performed to evaluate B lymphocyte binding to these arrays.

Competitive binding with ALG and HA. Patterned film arrays were built with HA or CHI-terminated films as described before. Arrays were imaged, then 200 μ g/mL soluble HA or ALG was added to the media. The samples were agitated for 15 min, incubated for 15 min, and this agitation/incubation cycle was repeated 3 more times, for a total of 2 hours. Arrays were imaged again, and the occupied sites on the array were counted and compared to the before exposure images.

CMC/CHI Film Deposition. PEMs were deposited onto Si wafers and Equalens II[®] discs using an automated dipping procedure detailed previously. The substrate was first immersed in the polycation solution for 15 minutes, followed by two Milli-Q water rinse steps (2 and 1 minutes). The substrate was then immersed in the polyanion solution and rinsed in a similar manner. The rinse baths following CHI deposition were Milli-Q water adjusted to pH3 using HCl.

ALG/CHI Film Deposition. Low molecular weight chitosan (CHI, degree of acetylation = 16.7%), alginic acid (ALG) were purchased from Sigma. Glacial acetic acid (HAc), and sodium acetate (analytical grade) were purchased from Sigma and used without purification. Polymer solutions were made in concentrations of .2% (2 mg/ml). Chitosan was dissolved in a .25M acetic acid / .25M sodium acetate buffer (pH~4.4). Alginic acid was dissolved in water and the pH was measured to be 6.7. Films were built using a Strato Sequence VI dipping machine (NanoStrata Inc.). The number and duration of deposition

cycles was regulated using the provided StratoSmart software. The different deposition routines were as follows:

Water Rinse	Acid Rinse	CaCl ₂ Rinse	Acid & Ca Rinse
CHI – 15min	CHI – 15min	CHI – 15 min	CHI – 15 min
Water – 2min	.25M HAc – 2min	Water – 2min	.25M HAc – 2min
Water – 1min	.25M HAc – 1min	Water – 1min	.25M HAc – 1min
Water – 1min	.25M HAc – 1min	Water – 1min	.25M HAc – 1min
ALG – 15min	ALG – 15min	ALG – 15min	ALG – 15min
Water – 2min	Water – 2min	Water – 1 min	Water – 2min
Water – 1min	Water – 1min	.1M CaCl ₂ – 2min	.1M CaCl ₂ – 1min
Water – 1min	Water – 1min	Water – 1min	Water – 1min

Film Thickness. All thicknesses reported for CMC/CHI films were measured from films built on Si wafers. A Woolham Co. VASE spectroscopy ellipsometer was used to determine film thickness, and data analysis was performed with the included WVASE32 software. Measurements were performed from 400 to 2000nm at a 70° angle of incidence. Data was fit using a Cauchy model. For HA/CHI films, dry film thickness and RMS roughness measurements were measured using a P-16+ stylus profilometer (KLA Tencor Corporation, USA) with the following parameters: 0.50 mg applied force, 200 Hz sampling rate, 50 μm/sec scan speed, 131/0.0781 Å range/resolution.

Swelling. Films were loaded into a quartz ellipsometry cell that allows *in-situ* thickness measurements of a submerged film⁴⁴. Since the film is tethered to a substrate and cannot expand in two principal directions, swelling is found from the ratio of hydrated to dry thickness (dimension orthogonal to the substrate). Mathematically, swelling is defined as

$$\%Swelling = \left(\frac{h}{h_0} - 1 \right) \times 100$$

where h and h_0 is the submerged and dry thickness, respectively.

References

- (1) Underhill, C. CD44: the hyaluronan receptor *Journal of Cell Science* **1992**, *103*, 293.
- (2) Richert, L.; Engler, A. J.; *et al.* Elasticity of Native and Cross-Linked Polyelectrolyte Multilayer Films *Biomacromolecules* **2004**, *5*, 1908.
- (3) Thierry, B.; Kujawa, P.; *et al.* Delivery Platform for Hydrophobic Drugs: Prodrug Approach Combined with Self-Assembled Multilayers *Journal of the American Chemical Society* **2005**, *127*, 1626.
- (4) Richert, L.; Lavalle, P.; *et al.* Layer by Layer Buildup of Polysaccharide Films: Physical Chemistry and Cellular Adhesion Aspects *Langmuir* **2004**, *20*, 448.
- (5) Hillberg, A. L.; Tabrizian, M. Biorecognition through Layer-by-Layer Polyelectrolyte Assembly: In-Situ Hybridization on Living Cells *Biomacromolecules* **2006**, *7*, 2742.
- (6) Mao, J. S.; Cui, Y. L.; *et al.* A preliminary study on chitosan and gelatin polyelectrolyte complex cytocompatibility by cell cycle and apoptosis analysis *Biomaterials* **2004**, *25*, 3973.
- (7) Dubas, S. T.; Schlenoff, J. B. Factors Controlling the Growth of Polyelectrolyte Multilayers *Macromolecules* **1999**, *32*, 8153.
- (8) Shiratori, S. S.; Rubner, M. F. pH-Dependent Thickness Behavior of Sequentially Adsorbed Layers of Weak Polyelectrolytes *Macromolecules* **2000**, *33*, 4213.
- (9) Swiston, A. J.; Cheng, C.; *et al.* Surface Functionalization of Living Cells with Multilayer Patches *Nano Letters* **2008**, *8*, 4446.
- (10) Croll, T. I.; O'Connor, A. J.; *et al.* A Blank Slate? Layer-by-Layer Deposition of Hyaluronic Acid and Chitosan onto Various Surfaces *Biomacromolecules* **2006**, *7*, 1610.
- (11) Decher, G. Fuzzy Nanoassemblies: Toward Layered Polymeric Multicomposites *Science* **1997**, *277*, 1232.
- (12) Thierry, B.; Winnik, F. M.; *et al.* Bioactive Coatings of Endovascular Stents Based on Polyelectrolyte Multilayers *Biomacromolecules* **2003**, *4*, 1564.
- (13) Chua, P.-H.; Neoh, K.-G.; *et al.* Surface functionalization of titanium with hyaluronic acid/ chitosan polyelectrolyte multilayers and RGD for promoting osteoblast functions and inhibiting bacterial adhesion *Biomaterials* **2008**, *29*, 1412.
- (14) Schneider, A.; Richert, L.; *et al.* Elasticity, biodegradability and cell adhesive properties of chitosan/hyaluronan multilayer films *Biomedical Materials* **2007**, S45.
- (15) Berg, M. C.; Yang, S. Y.; *et al.* Controlling Mammalian Cell Interactions on Patterned Polyelectrolyte Multilayer Surfaces *Langmuir* **2004**, *20*, 1362.
- (16) Richert, L.; Lavalle, P.; *et al.* Cell Interactions with Polyelectrolyte Multilayer Films *Biomacromolecules* **2002**, *3*, 1170.
- (17) Rinaudo, M.; Pavlov, G.; *et al.* Influence of acetic acid concentration on the solubilization of chitosan *Polymer* **1999**, *40*, 7029.

- (18) Denuziere, A.; Ferrier, D.; *et al.* Chitosan-chondroitin sulfate and chitosan-hyaluronate polyelectrolyte complexes. Physico-chemical aspects *Carbohydrate Polymers* **1996**, *29*, 317.
- (19) Lapčik, L.; De Smedt, S.; *et al.* Hyaluronan: Preparation, Structure, Properties, and Applications *Chemical Reviews* **1998**, *98*, 2663.
- (20) Schlenoff, J. B.; Dubas, S. T. Mechanism of Polyelectrolyte Multilayer Growth: Charge Overcompensation and Distribution *Macromolecules* **2001**, *34*, 592.
- (21) ShaikhMohammed, J.; DeCoster, M. A.; *et al.* Micropatterning of Nanoengineered Surfaces to Study Neuronal Cell Attachment in Vitro *Biomacromolecules* **2004**, *5*, 1745.
- (22) ShaikhMohammed, J.; DeCoster, M. A.; *et al.* Fabrication of Interdigitated Micropatterns of Self-Assembled Polymer Nanofilms Containing Cell-Adhesive Materials *Langmuir* **2006**, *22*, 2738.
- (23) Yoo, D.; Shiratori, S. S.; *et al.* Controlling Bilayer Composition and Surface Wettability of Sequentially Adsorbed Multilayers of Weak Polyelectrolytes *Macromolecules* **1998**, *31*, 4309.
- (24) Whiteman, P. The quantitative measurement of Alcian Blue-glycosaminoglycan complexes *Biochemical Journal* **1973**, *131*, 343.
- (25) Fagnola, M.; Pagani, M. P.; *et al.* Hyaluronic acid in hydrophilic contact lenses: Spectroscopic investigation of the content and release in solution *Contact Lens and Anterior Eye* **2009**, *32*, 108.
- (26) Porcel, C.; Lavalle, P.; *et al.* Influence of the Polyelectrolyte Molecular Weight on Exponentially Growing Multilayer Films in the Linear Regime *Langmuir* **2007**, *23*, 1898.
- (27) Etienne, O.; Schneider, A.; *et al.* Degradability of Polysaccharides Multilayer Films in the Oral Environment: an in Vitro and in Vivo Study *Biomacromolecules* **2005**, *6*, 726.
- (28) Kumar, M. N. V. R.; Muzzarelli, R. A. A.; *et al.* Chitosan Chemistry and Pharmaceutical Perspectives *Chemical Reviews* **2004**, *104*, 6017.
- (29) Kim, H.; Doh, J.; *et al.* Large Area Two-Dimensional B Cell Arrays for Sensing and Cell-Sorting Applications *Biomacromolecules* **2004**, *5*, 822.
- (30) Rider, T. H.; Petrovick, M. S.; *et al.* A B Cell-Based Sensor for Rapid Identification of Pathogens *Science* **2003**, *301*, 213.
- (31) Nevell, T. P.; Zeronian, S. H. *Cellulose chemistry and its applications*; E. Horwood; Halsted Press: Chichester, West Sussex, England, 1985, pages
- (32) Picart, C.; Mutterer, J.; *et al.* Molecular basis for the explanation of the exponential growth of polyelectrolyte multilayers *Proceedings of the National Academy of Sciences of the United States of America* **2002**, *99*, 12531.
- (33) Garza, J. M.; Schaaf, P.; *et al.* Multicompartment Films Made of Alternate Polyelectrolyte Multilayers of Exponential and Linear Growth *Langmuir* **2004**, *20*, 7298.
- (34) Ratner, B. D. New ideas in biomaterials science - a path to engineered biomaterials *Journal of Biomedical Materials Research* **1993**, *27*, 837.
- (35) Yang, Z.; Galloway, J. A.; *et al.* Protein Interactions with Poly(ethylene glycol) Self-Assembled Monolayers on Glass Substrates: Diffusion and Adsorption *Langmuir* **1999**, *15*, 8405.
- (36) Zhai, L.; Berg, M. C.; *et al.* Patterned Superhydrophobic Surfaces: Toward a Synthetic Mimic of the Namib Desert Beetle *Nano Letters* **2006**, *6*, 1213.

- (37) George, M.; Abraham, T. E. Polyionic hydrocolloids for the intestinal delivery of protein drugs: Alginate and chitosan -- a review *Journal of Controlled Release* **2006**, *114*, 1.
- (38) Ye, S.; Wang, C.; *et al.* New loading process and release properties of insulin from polysaccharide microcapsules fabricated through layer-by-layer assembly *Journal of Controlled Release* **2006**, *112*, 79.
- (39) Hara, M.; Miyake, J. Calcium alginate gel-entrapped liposomes *Materials Science and Engineering: C* **2001**, *17*, 101.
- (40) Bajpai, S. K.; Tankhiwale, R. Investigation of dynamic release of vitamin B2 from calcium alginate/chitosan multilayered beads: Part II *Reactive and Functional Polymers* **2006**, *66*, 1565.
- (41) Marx, K. A. Quartz Crystal Microbalance: A Useful Tool for Studying Thin Polymer Films and Complex Biomolecular Systems at the Solution-Surface Interface *Biomacromolecules* **2003**, *4*, 1099.
- (42) Shaikh Mohammed, J.; DeCoster, M. A.; *et al.* Fabrication of Interdigitated Micropatterns of Self-Assembled Polymer Nanofilms Containing Cell-Adhesive Materials *Langmuir* **2006**, *22*, 2738.
- (43) Shaikh Mohammed, J.; DeCoster, M. A.; *et al.* Micropatterning of Nanoengineered Surfaces to Study Neuronal Cell Attachment in Vitro *Biomacromolecules* **2004**, *5*, 1745.
- (44) Brunner, H.; Vallant, T.; *et al.* Formation of Ultrathin Films at the Solid-Liquid Interface Studied by In Situ Ellipsometry *Journal of Colloid and Interface Science* **1999**, *212*, 545.

Chapter 6: Cellular Backpacks as Functional Phagocytosis-Resistant Materials

The delivery of active synthetic materials via cellular backpacks requires that the body not clear the backpack prematurely. One of the principal mechanisms for large ($>0.5\mu\text{m}$) foreign bodies to be swept from the body is a process known as phagocytosis¹. This innate immune response is primarily performed by antigen-presenting cells (such as macrophages and dendritic cells), which internalize foreign objects, digest them, then present fragments of the object on their surface to elicit a more significant response from the rest of the immune system. Often, phagocytosis is a significant barrier to drug delivery², as drug-laden, spherical microparticles have limited circulation times *in vivo*³. Internalization depends on a number of factors, including object size, shape, and surface chemistry (including ligands for specific phagocytosis receptors)⁴. Object shape has only recently begun to be explored and understood as an internalization-determining criterion⁵⁻⁸, and particle shape can be engineered to either promote or avoid phagocytosis.

Mitragotri *et al*^{2,9-11} have shown how the local curvature of a particle will determine if a phagocyte will internalize it¹⁰. Even if particles contained a phagocytosis receptor – namely, IgG opsonized particles, which interact with the Fc receptor on a phagocyte's surface – particle shape and curvature at the initial point of contact ultimately determined its internalization fate.

These design rules grant a great deal of insight into a designing a general particle system that resists clearance by phagocytes. Cellular backpacks allow for exciting ways to apply this work for clinical purposes; namely, backpacks possess an ideal curvature (i.e., $\Omega=90^\circ$, or a flat disc) to resist internalization and may be loaded with a wide range of synthetic materials. Indeed, because of the different backpacks methods developed (see Figure 3.1b, page 86), we can guarantee that the curvature at the initial point of contact is 90° . This combines a “stealthy” microparticle with functional payloads that may be therapeutically or diagnostically useful. Such particles may be attached to a phagocyte’s (such as a monocyte) membrane and remain on the surface while that cell traffics to inflammation or tumor sites in the body¹² where they selectively accumulate. Triggered release of anti-inflammatory drugs with much greater precise spatial resolution may be possible, since a cell is selectively trafficking the backpack rather than relying on passive release by a particulate drug carrier. If chemotherapy agents or particles capable of ablation via RF heating (i.e., gold or iron oxide) are loaded into a backpack and attached to a monocyte being recruited into a solid tumor, such cytotoxic materials could enter the relatively inaccessible hypoxic region of a tumor¹³. Such a strategy has been adopted for gold nanoparticles with promising results¹⁴.

We present initial observations on the phagocytosis-resistance of cell backpacks for two phagocyte cell lines: DC2.4 dendritic cells and J774 macrophages. Not only is the backpack shape ideal for the phagocytosis-resistance design rules specified by Mitragotri¹⁰, but also the surface chemistry may be tuned to include specific ligands such as hyaluronic acid, known to be a phagocytosis receptor¹⁵.

The concurrent control over shape, approach angle, and surface chemistry makes cellular backpacks an unique system to investigate the basic mechanisms of shape-induced phagocytosis-resistance and surface chemistry.

Phagocytosis-Resistance by Dendritic Cells

The first phagocyte used to test internalization resistance was the dendritic cell line DC2.4. (An introduction to dendritic cells may be found on page 95.) DC2.4 cells were sedimented overnight onto thermally-released backpacks of the following composition: (PMAA3.0/PNIPAAm3.0)_{80.5}(FITC-PAH3.0/Fe₃O₄NP4.0)₁₀ with an optional (CHI3.0/HA3.0)₃ layer as noted. The temperature was lowered to 4°C, releasing the backpacks from the surface. Backpacks with and without a (CHI3.0/HA3.0)_{3.5} cell-adhesive region were attached to cells, which were allowed to attach to a polystyrene dish (Figure 6.1) or a PDAC-terminated glass slide (Figure 6.2). Backpacks with the (CHI3.0/HA3.0)_{3.5} outer face (Figure 6.1a and Figure 6.2a) were incubated on the cell surface for ~2h longer than the MNP-terminated backpacks (Figure 6.1b and Figure 6.2b).

Figure 6.1 and Figure 6.2 show representative examples of backpacks on dendritic cells. Among the few dozen cells examined, there was no clear example of internalization. Interestingly, regardless of the nature of the outer face of the backpack (i.e., with or without HA), internalization seems to be prevented. A time course image was collected to see how backpacks interact with cells over time, and representative images are shown in Figure 6.3.

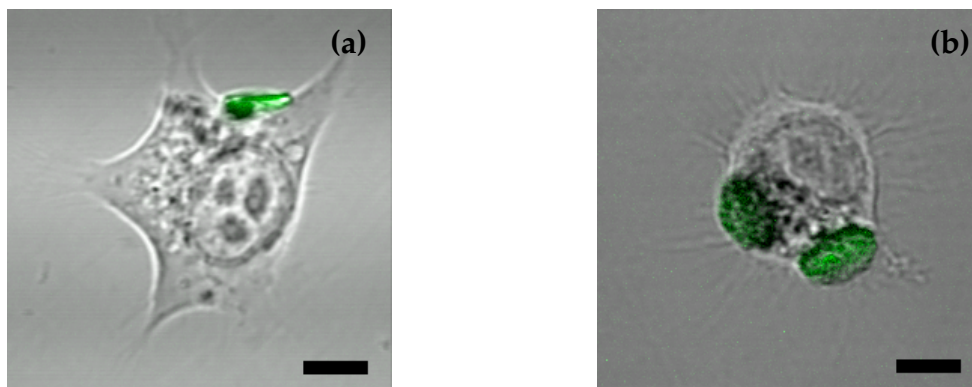


Figure 6.1: Confocal micrographs (with overlaid fluorescence signal from FITC-labeled PAH in the payload region) of backpacks attached to DC2.4 dendritic cells adhered to a polystyrene dish. (a) shows a backpack with an (CHI3.0/HA3.0)_{3,5} cell-adhesive region. (b) does not have an (HA/CHI) outer face and terminates with (PAH/MNP). Scale bars = 10 μ m.

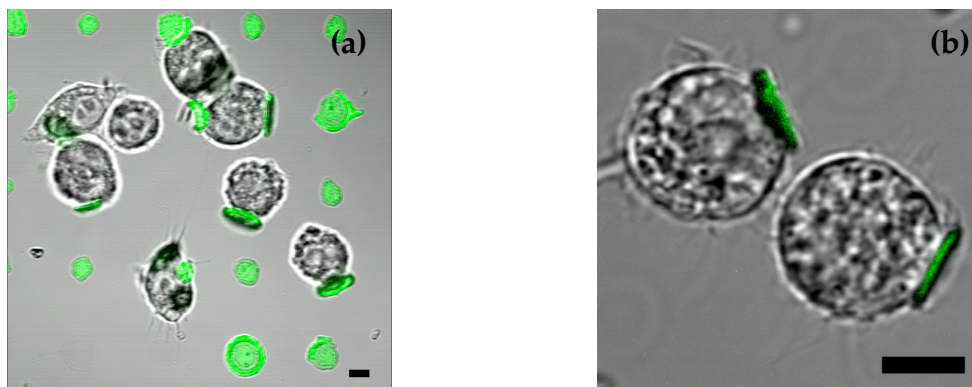


Figure 6.2: Confocal micrographs (with overlaid fluorescence signal from FITC-labeled PAH in the payload region) of backpacks attached to DC2.4 dendritic cells above a PDAC-terminated glass slide. (a) shows backpacks with an (CHI3.0/HA3.0)_{3,5} cell-adhesive region. (b) does not have an (HA/CHI) outer face and terminates with (PAH/MNP). Scale bars = 10 μ m.

Two interesting behaviors were seen during this time course. First, backpacks resist rapid internalization as might be expected for a phagocyte¹⁰. Indeed, backpacks seem able to reversibly associate with the cells, as seen by the release of a backpack at 41 min. Second, backpacks are able to move around on the surface of the cell indicating that the cell is interacting with the backpack, but unable to engulf and phagocytose it.

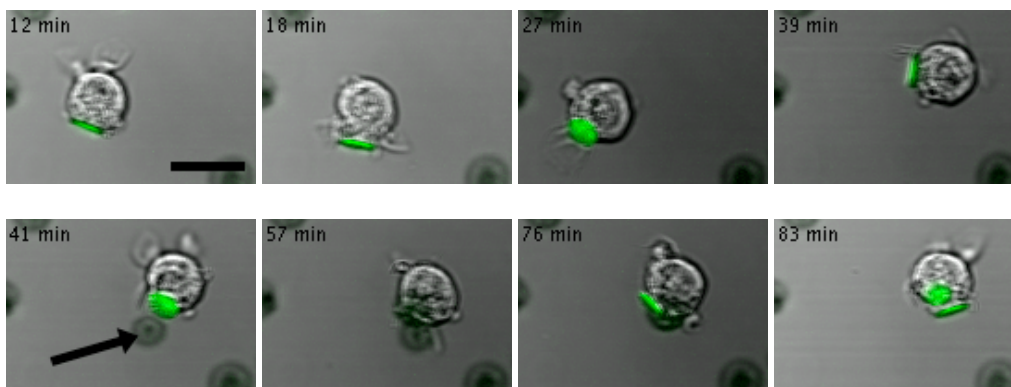


Figure 6.3: Select images of a time course; the time from the beginning of imaging is shown in the upper left. These backpacks do not have an (CHI/HA) outer face. While the dendritic cell interacts with the backpack, and at times seems to attempt phagocytosis (18 min), the backpack is never internalized. In fact, a backpack (indicated by the arrow) attached to the bottom of the cell (and outside of the confocal image plane), is released at 41 min and picked up again at 57 min. At 83 min, both backpacks are clearly seen on the cell surface. Scale bar = 20 μm .

These promising results led us to further investigate backpack phagocytosis-resistance using a model macrophage cell in collaboration with the Mitragotri group at the University of California Santa Barbara.

Phagocytosis-Resistance by Macrophages*

The J774 macrophage cell line, a model phagocyte, was used to investigate the phagocytosis-resistant behavior of backpacks with the following compositions: $(\text{PMAA}3.0/\text{PNIPAAm}3.0)_{80.5}(\text{FITC-PAH}3.0/\text{MNP}4.0)_{10}$ and $(\text{PMAA}3.0/\text{PNIPAAm}3.0)_{80.5}(\text{FITC-PAH}3.0/\text{MNP}4.0)_{10}(\text{PAH}3.0/\text{SPS}4.0)_{30}$. Both types of backpacks were tested with and without a $(\text{CHI}3.0/\text{HA}3.0)_3$ outer layer.

* I acknowledge the collaboration of Nishit Doshi, UCSB, in performing the experiments described in this section.

Optical videomicroscopy and scanning electron microscopy (SEM) were used to confirm that backpacks were not internalized over a 3h period. SEM of fixed macrophages (Figure 6.4) shows that even after 3h of exposure, backpacks were not internalized (Figure 6.4a and Figure 6.4b) while PS spheres of similar size and with a (CHI3.0/HA3.0)₃ outer layer were phagocytosed (Figure 6.4c).

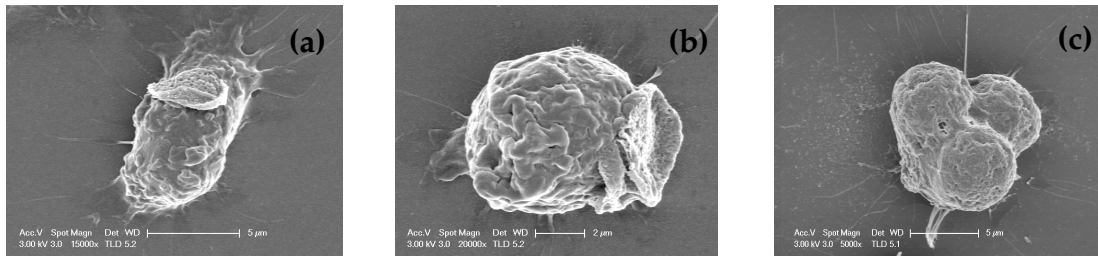


Figure 6.4: Scanning-electron micrographs of macrophages exposed to (CHI3.0/HA3.0)₃ coated (a) and (b) 7µm backpacks and (c) 6µm PS spheres. These backpacks and spheres were exposed to cells for 3 hours.

Videomicroscopy further confirms that macrophages do not phagocytose backpacks. Interestingly, the outermost (CHI3.0/HA3.0)₃ layer did not affect whether a backpack was internalized, even though CD44 is known to be a phagocytosis receptor¹⁵. Both HA and non-coated backpacks were found to resist internalization. A videomicroscopy time course of HA-coated backpacks is shown in Figure 6.5. Within the field of view, only one backpack was phagocytosed over the 50 min observation time, much longer than the ~3 min required for internalization observed previously¹⁰.

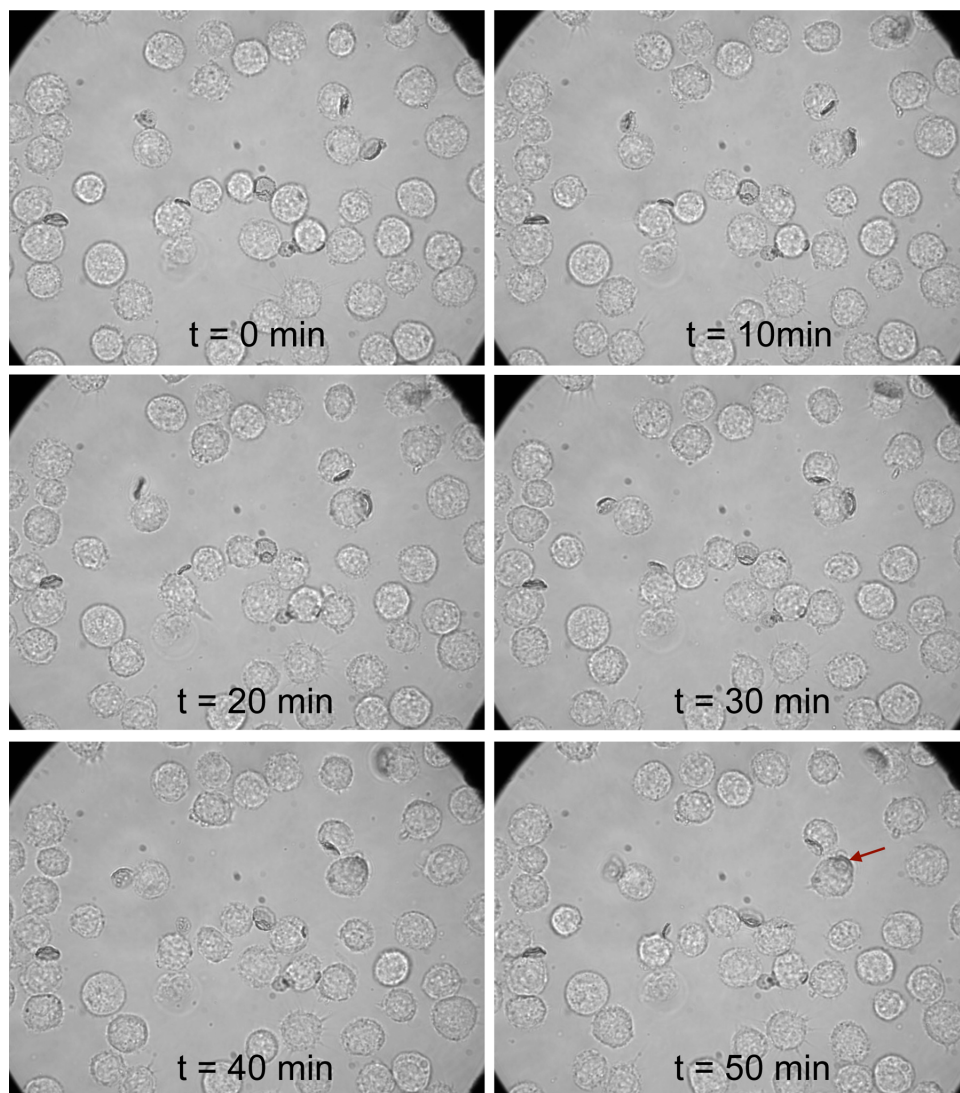


Figure 6.5: Optical microscopy images showing backpacks exposed to macrophages without being internalized. The arrow at 50min shows the only internalized backpack in the field of view.

To investigate how the size, shape, and surface chemistry may determine whether a backpack is phagocytosed, internalization frequency was quantified for $7\mu\text{m}$ diameter HA-coated backpacks, $6\mu\text{m}$ diameter HA-coated spheres, and $6\mu\text{m}$ diameter amine-functionalized spheres. As Figure 6.6 shows, size does not prevent backpack internalization – $\sim 75\%$ of amine-functionalized PS beads of the

same diameter are internalized. Similarly, the HA-coating does not seem to prevent phagocytosis, since ~35% of (CHI3.0/HA3.0)_{3.0}-coated PS spheres are internalized. This result leads us to conclude that the unique shape and aspect ratio of the backpack strongly influences its phagocytosis-resistance, and that size and surface chemistry are much less influential criteria, in good agreement with previous IgG-opsonized particle and dimensionless volume analyses¹⁰.

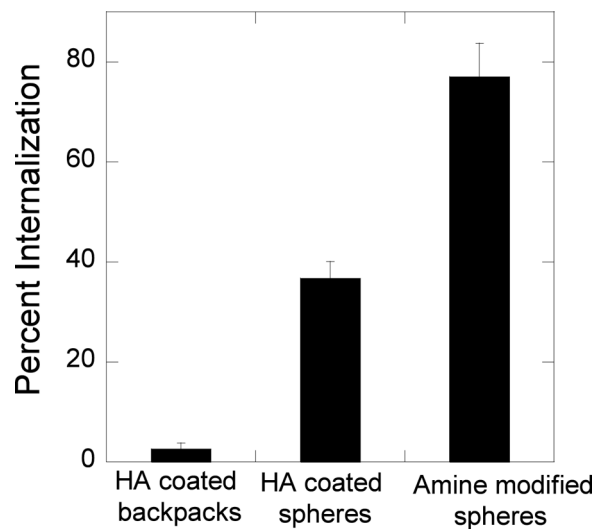


Figure 6.6: Measurement of how many 7 μ m diameter HA-coated backpacks, 6 μ m diameter HA-coated spheres, and 6 μ m diameter amine-functionalized spheres were internalized by macrophages.

Conclusions

The use of shape to discourage internalization is a relatively new and unexplored field. Combining the power of geometry-induced phagocytosis-resistance with functional materials is a significant step towards creating active therapeutics based on this phenomenon. We have found that two types of phagocytes – dendritic cells and macrophages – do not internalize functional backpacks.

Preliminary results suggest that surface chemistry (with or without an HA-containing film) and size do not lead to phagocytosis-resistance, but rather the shape and angle at the point of contact (namely, $\Omega=90^\circ$). A statistical analyses shows that HA-coated backpacks are internalized far less frequently than HA-coated or amino-functionalized spheres of a similar size. These initial findings suggest that backpacks obey the previously-discovered phagocytosis-resistance design rules, but with the ability to include a broad palette of functional materials. The combination of synthetic functionality and resistance to internalization may lead to new long-lasting diagnostic or therapeutic tools or the ability to functionalize the surface of phagocytes without material loss via phagocytosis.

Experimental Details

Backpack Fabrication and Cell Attachment. Backpacks were fabricated as described in Chapter 2 (see page 75). Exact compositions are as noted in the text. DC2.4 and J774 cells were seeded onto a backpack-laden slide and incubated at 37°C and 5% CO₂ for 15 min. Slides were then agitated at ~100s⁻¹ for 15min, and this incubation/agitation cycle was repeated once more. Slides were washed in serum-free RPMI media to remove non-adhered cells, and placed into 4°C complete media. Cells were agitated for 30min at 4°C to encourage film dissolution and lift-off.

Cell Culture. DC2.4 cells were maintained and passaged as described in Chapter 3 (see page 101). The J774 mouse monocyte macrophage cell line (ECACC products, Sigma Aldrich, St. Louis, MO, USA) was used in this study. Cells were cultured in Dulbecco Eagle media (ATCC, Manassas, VA, USA) supplemented with 1% penicillin/streptavidin (Sigma Aldrich, St. Louis, MO, USA) and 10% fetal bovine serum (Invitrogen, Carlsbad, CA, USA). Cells were grown in standard culture conditions (37°C and 5% CO₂).

Optical and Fluorescence Microscopy. Confocal laser scanning microscopy (CLSM) was used to image DC2.4 cells. High-resolution images of live cell-backpack complexes were imaged using CLSM at ambient conditions on a Zeiss 510 upright microscope (40x water immersion objective). For J774 macrophages, cells were cultured overnight in glass bottom delta T dishes (Bioprotech, PA) at a density of ~10⁵ cells per dish (3.8 cm²). Cells were washed with PBS the following day and the media was replaced with HEPES (Sigma Aldrich, MO) containing media (DMEM + 25mM HEPES) to maintain pH regardless of carbon dioxide levels. Control experiments with polystyrene spheres used a 5 particle per cell concentration. Cells were incubated with particles (polystyrene spheres or backpacks) for 1h prior to imaging. Cells were imaged on an Axiovert 25 microscope using a Neo-Fluor oil immersion objective (100x, 1.3 NA) (Zeiss, NY).

A constant 37°C temperature was maintained using a Delta T temperature controller (Biopetechs) fitted to the microscope. Brightfield images were taken using a cooled CCD camera (CoolSnap_{HQ}, Roper Scientific, GA). Images of J774 macrophages were collected at 20s intervals and compiled into a timelapse video using Metamorph software (Molecular Devices, PA).

Scanning Electron Microscopy (SEM). Experimental conditions were identical to that described in the optical microscopy section above, except cells were incubated with particles (polystyrene spheres or backpacks) for 3h prior to imaging. After incubation, unbound particles were washed away and cells were fixed with 2.5% glutaraldehyde. Cells were washed with increasing concentrations of ethanol (up to 100%), vacuum dried and coated with palladium (Hummer 6.2 Sputtering System, Anatech Ltd., Union City, CA). Cells were imaged with a Sirion 400 SEM (FEI Company, Hillsboro, OR) at an acceleration voltage of 2 kV.

Quantification of Internalized Particles. Optical micrographs were analyzed for the number of particles in a field of view, and whether each was interior or exterior to the cell membrane. One hundred cells were counted and measured for internalization.

References

- (1) Aderem, A.; Underhill, D. M. Mechanisms of Phagocytosis in Macrophages *Annual Review of Immunology* **1999**, *17*, 593.
- (2) Champion, J. A.; Mitragotri, S. Shape Induced Inhibition of Phagocytosis of Polymer Particles *Pharmaceutical Research* **2009**, *26*, 244.
- (3) Storm, G.; Belliot, S. O.; *et al.* Surface modification of nanoparticles to oppose uptake by the mononuclear phagocyte system *Advanced Drug Delivery Reviews* **1995**, *17*, 31.
- (4) Hu, L.; Mao, Z.; *et al.* Colloidal particles for cellular uptake and delivery *Journal of Materials Chemistry* **2009**, *19*, 3108.
- (5) Decuzzi, P.; Ferrari, M. The adhesive strength of non-spherical particles mediated by specific interactions *Biomaterials* **2006**, *27*, 5307.
- (6) Decuzzi, P.; Ferrari, M. The Receptor-Mediated Endocytosis of Nonspherical Particles *Biophysical Journal* **2008**, *94*, 3790.
- (7) Geng, Y.; Dalhaimer, P.; *et al.* Shape effects of filaments versus spherical particles in flow and drug delivery *Nature Nanotechnology* **2007**, *2*, 249.
- (8) Muro, S.; Garnacho, C.; *et al.* Control of Endothelial Targeting and Intracellular Delivery of Therapeutic Enzymes by Modulating the Size and Shape of ICAM-1-targeted Carriers *Molecular Therapy* **2008**, *16*, 1450.
- (9) Champion, J. A.; Katare, Y. K.; *et al.* Particle shape: A new design parameter for micro- and nanoscale drug delivery carriers *Journal of Controlled Release* **2007**, *121*, 3.
- (10) Champion, J. A.; Mitragotri, S. Role of target geometry in phagocytosis *Proceedings of the National Academy of Sciences of the United States of America* **2006**, *103*, 4930.
- (11) Champion, J. A.; Walker, A.; *et al.* Role of Particle Size in Phagocytosis of Polymeric Microspheres *Pharmaceutical Research* **2008**, *25*, 1815.
- (12) Kelly, P. M.; Davison, R. S.; *et al.* Macrophages in human breast disease: a quantitative immunohistochemical study *British Journal of Cancer* **1988**, *57*, 174.
- (13) Primeau, A. J.; Rendon, A.; *et al.* The Distribution of the Anticancer Drug Doxorubicin in Relation to Blood Vessels in Solid Tumors *Clinical Cancer Research* **2005**, *11*, 8782.
- (14) Choi, M. R.; Stanton-Maxey, K. J.; *et al.* A Cellular Trojan Horse for Delivery of Therapeutic Nanoparticles into Tumors *Nano Letters* **2007**, *7*, 3759.
- (15) Vachon, E.; Martin, R.; *et al.* CD44 is a phagocytic receptor *Blood* **2006**, *107*, 4149.

Chapter 7: Summary and Future Work

Thesis Summary

This thesis investigated the enormous potential of patterned polymer multilayers as functional cellular backpacks. Below is a brief summary of the major points presented in this thesis, followed by suggestions for future efforts.

Chapter 1 reviewed current work in polymer multilayer thin films and the functionalization of living cells. The layer-by-layer deposition affords a number of benefits over other polymer thin film techniques, and these are presented and discussed. Because of the enormous tunability of these polymer systems, they are natural candidates for functional coatings. Past work on cellular functionalization has relied upon covalent chemistry, metabolism of non-native sugars, and other techniques that may have unintended effects. Furthermore, cell backpacks do not occlude the entire cell surface, allowing the cell to continue interacting with its surrounding environment.

Chapter 2 presented fundamental work on fabrication of a heterostructured, multi-functional backpack system. Using photolithographic techniques, a multi-region film can be patterned without sacrificing the capabilities of the constituent materials. A number of hydrogen-bonded multilayers were developed as a release region, which tethers the backpack to the fabrication substrate and dissolves upon a given temperature and/or pH condition. Next, functional

materials, such as quantum dots, fluorescent polymers, and nanoparticles, were deposited to create the backpacks payload region. Finally, a non-cytotoxic cell-adhesive region, which anchors the backpack to the cell membrane, was developed based on the natural CD44-hyaluronic acid interaction. These fundamental fabrication studies provided the basis for the rest of the thesis.

Chapter 3 discusses how backpacks interact with several types of immune system cells, including B, T, and dendritic cells. The toxicity of backpack attachment is of utmost importance, and B cells were found to remain viable for up to 72h (approximately the life time of this cell line) following backpack attachment. Further studies on T cells show that migration, a natural behavior, was not encumbered by an attached backpack. Finally, dendritic cells were activated, as seen by an increased expression of characteristic CD surface receptors, upon attachment of backpack coated with LPS and MPLA. This last result shows that backpacks need not be passive bodies attached to cell surfaces, but could affect desirable behaviors in the attached cell. This holds promise for creating synergistic bio-hybrid devices based on cells and functional backpacks.

Chapter 4 covers the aggregation behavior of injectable backpacks with B cells. The ratio of cells to backpacks and backpack diameter were two variables found to heavily influence the size of aggregates formed, which was shown by confocal microscopy, flow cytometry, and laser diffraction. Large aggregates were found to dissociate upon agitation, leaving smaller cell clusters that usually included 2-3 cells attached to a backpack. The large aggregates were found to reform when agitation was stopped, indicating reversibly associating aggregates, which may be of great use in injectable tissue engineering.

Chapter 5 presents the various all-biopolymer multilayer films investigated as candidate films for backpacks. Any backpack system must be biocompatible and biopolymers are a natural material choice. The adhesion between hyaluronic acid-containing PEMs and cell surface CD44 is characterized and systematically optimized in terms of PEM deposition conditions.

Carboxymethylcellulose/chitosan and alginate/chitosan films were also investigated as potential backpack components.

Carboxymethylcellulose/chitosan films in particular were found to be superhydrophilic, and are currently being employed in anti-fogging applications.

Chapter 6 presents preliminary observations on the phagocytosis-resistance of backpacks. Using previous design rules of the Mitragotri group at the University of California at Santa Barbara has led to promising results showing that functional backpacks are resistant to internalization by macrophages. We have begun collaborating with the Mitragotri group to pursue the use of cell backpacks to functionalize the surface of phagocytic cells.

Future Research Directions

Cell backpacks are a new concept in single-cell functionalization, combining the power of functional polymeric and nanomaterials with the incredible power of well-hewn biological systems. Future efforts in this work can be broken down to focusing on the materials science of the backpack itself, and biological aspects, such as interfacing with the cell, *in vivo* behavior, and choosing impactful

biological issues that the backpack might address. These two thrusts are symbiotic, and require constant communication and feedback from both camps.

First, the materials science of the backpack fabrication process is still not fully understood, and some significant drawbacks exist for the current methods.

Specifically, the final acetone sonication step is chemically and mechanically very harsh for a highly flexible, mechanically weak polymer system. The specific requirements required for successful acetone liftoff are not fully understood. For instance, the ratio of multilayer film and resist thickness, and the diameter of the backpack, must be within a very precise range that is a function of film mechanical properties. Last, particular polymer systems – such as homopolymer systems soluble in acetone – cannot be used in the backpack. Developing a method that replaces or completely eliminates this acetone step would lead to greater processing ease, higher throughput, and increase the palette of materials that can be integrated into the backpack. A top-down “ablation” type fabrication method, such as UV-ozone, could begin to address these issues. Other lithographic approaches should also be considered, such as using water-based developers and liftoff solutions (as opposed to MF319 and acetone, respectively)^{1,2} and / or different types of photoresists^{2,3}.

Another materials science project to be considered is increasing the number of therapeutically or diagnostically useful materials that can be included in a backpack, such as RF-heating nanoparticles, chemokines for chemoattractive studies, or controllably degrading polymers such as PLGA. PLGA is a very attractive candidate for further work, because of a wealth of existing information, FDA approval, and its finely tunable degradation properties. A number of drugs

could be loaded into a PLGA matrix, and measuring the release of such functional molecules from a backpack should be a very high priority for future efforts.

There exists a very interesting basic science story in the polymer physics of the release region. We have shown that the release region displays a critical thickness, and this is due to diffusion of the polycation from the release region. The factors influencing this diffusion are not understood, but I hypothesize molecular weight, hydrophobicity, and charge density will determine the critical thickness required for release and the amount of the hydrogen-bonded film attached to a released backpack. A mechanistic understanding of this phenomenon would be valuable to any application employing polymer multilayers.

The prospect of functionalizing both faces of the backpack opens interesting tissue engineering possibilities. Two adhesive faces could lead to well-controlled cell clusters, as shown theoretically^{4,5}. Combining the “stickiness” of a backpack with colloidal ordering techniques such as dielectrophoresis⁶ could yield well-ordered cellular structures that mimic natural tissue. One-dimensional cellular “polymers” could be made where a cell is the “monomer” and the backpack serves as a bifunctional linker. Two-dimensional cellular sheets or three-dimensional clusters may serve as the basis for a new class of tissue engineering constructs assembled from cellular constituents rather than polymeric scaffolds.

Finally, using the current three region backpack system, the release region is included in the released backpack (see Chapter 2, page 52). This may be either a

liability or benefit. Since this outer face is the one presented to the environment, it may elicit or prevent an immune response, control release of a molecule from the backpack, or attach to particular types of tissue *in vivo*. At present, we have no control over exactly what is presented on this surface. Being able to precisely tailor this surface could lead to “stealthier” backpacks (by using PEG), better targeting (antibodies), or adhesive backpacks (hyaluronic acid, RGD tripeptides, etc.).

Understanding the interaction between biological systems and backpacks should be pursued concurrently with the above materials science efforts. Only in doing the biological studies will the materials development be meaningful – for instance, knowing which drugs to incorporate into the backpack. This thesis made extensive use of a hardy B cell line, but a great deal of insight will be granted in moving to primary cells (i.e., ones isolated from a live animal). In addition to greater clinical relevance (i.e., mimicking adoptive immunotherapy methods), primary cells are more variable than cell lines and thus more indicative of *in vivo* performance.

The phagocytosis-resistance work introduced in this thesis is an extremely exciting research vector. Leveraging the previous findings of the Mitragatori group for phagocytosis-resistance particle designs with functional materials could lead to an entirely new class of therapeutic and diagnostic particles. Backpacks could lead to either longer-lasting particles that resist clearance from the body, or could be used to functionalize phagocytes that traffic to areas of interest, such as solid tumors. *In vivo* work should be conducted as soon as possible to see if the behaviors observed with an *in vitro* macrophage cell line

continue to hold. The interplay between backpack surface chemistry (over which we have good control on one surface), aspect ratio, and the cell angle of approach are only beginning to be understood, and a great deal of fundamental insight will follow. Furthermore, this work may be one of the first therapeutic embodiments of the cell backpack concept, and is worthy of continued and increased effort.

Finally, affecting the backpacked cell's behavior has only barely begun to be explored. Originally, we envisioned a cell as a passive backpack carrier – that is, the cell would not change its behavior based on the backpack, nor would the cell negatively affect the backpack. The dendritic cell activation work discussed in Chapter 3 shows that backpacks might be able to elicit desired behaviors. No longer does the backpack need to be a “ghost-like” particle, but could engage with the cell. For instance, the backpack might elute a drug that caused the cell's migration to speed up or slow down, or begin expressing a quiescent surface receptor. This approach could even be used for a cytotoxic payload: freely suspended, injected backpacks could attach to a specific type of tissue (for example, to CD44⁺ tumor cells via a (HA/CHI) film) that needs to be removed. A great deal of work remains on understanding and engineering this interaction if a truly synergistic bio-hybrid type device is going to be made.

References

- (1) Nolte, A. J.; Takane, N.; *et al.* Thin Film Thickness Gradients and Spatial Patterning via Salt Etching of Polyelectrolyte Multilayers *Macromolecules* **2007**, *40*, 5479.
- (2) Dubas, S. T.; Schlenoff, J. B. Polyelectrolyte Multilayers Containing a Weak Polyacid: Construction and Deconstruction *Macromolecules* **2001**, *34*, 3736.
- (3) Minsk, L. M.; Smith, J. G.; *et al.* Photosensitive polymers. I. Cinnamate esters of poly(vinyl alcohol) and cellulose *Journal of Applied Polymer Science* **1959**, *2*, 302.
- (4) Glotzer, S. C. Some Assembly Required *Science* **2004**, *306*, 419.
- (5) Zhang, Z. L.; Glotzer, S. C. Self-Assembly of Patchy Particles *Nano Letters* **2004**, *4*, 1407.
- (6) Gupta, S.; Alargova, R. G.; *et al.* On-Chip Dielectrophoretic Coassembly of Live Cells and Particles into Responsive Biomaterials *Langmuir* **2009**, *26*, 3441.

Appendix A: Photolithography Photomask Designs

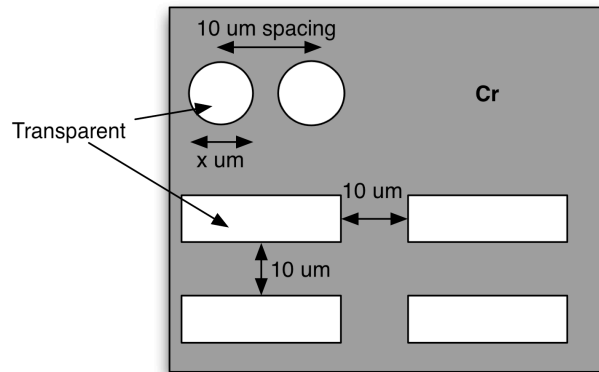
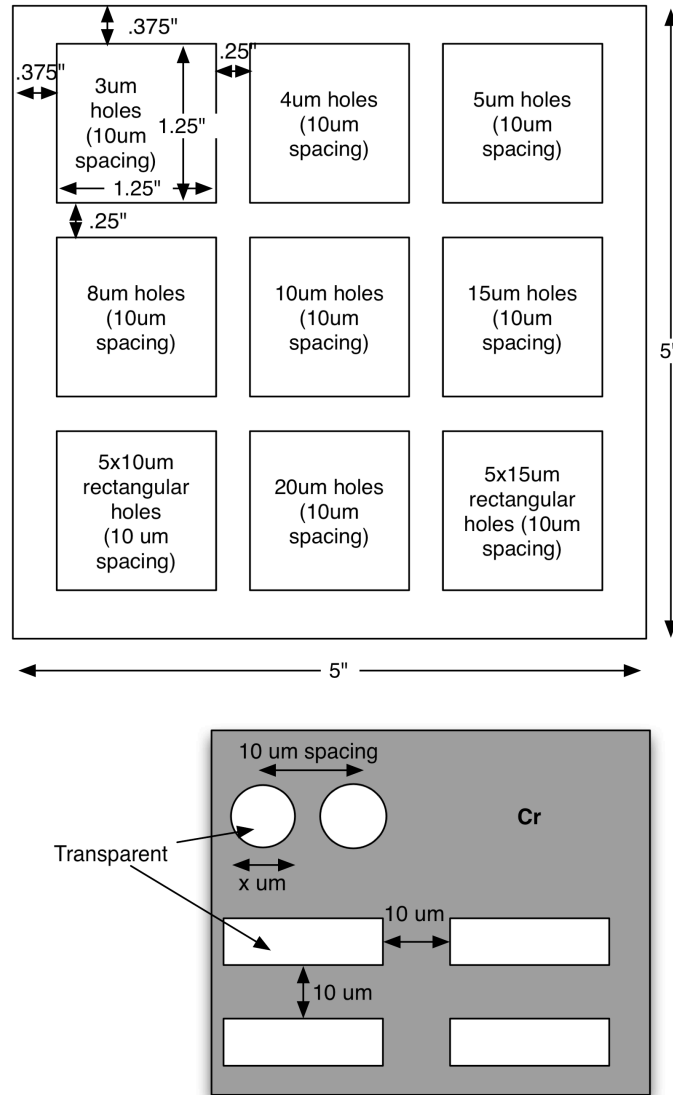


Figure A.1: "Swiston Mask 1" design.

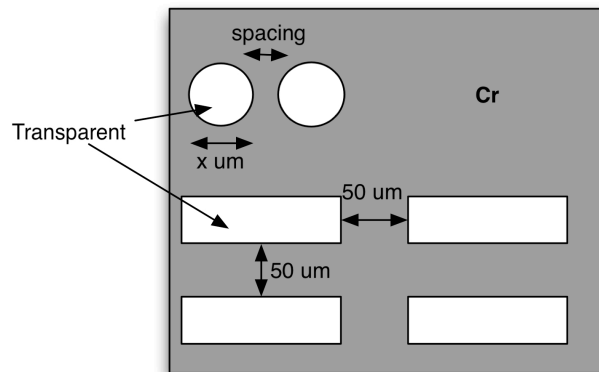
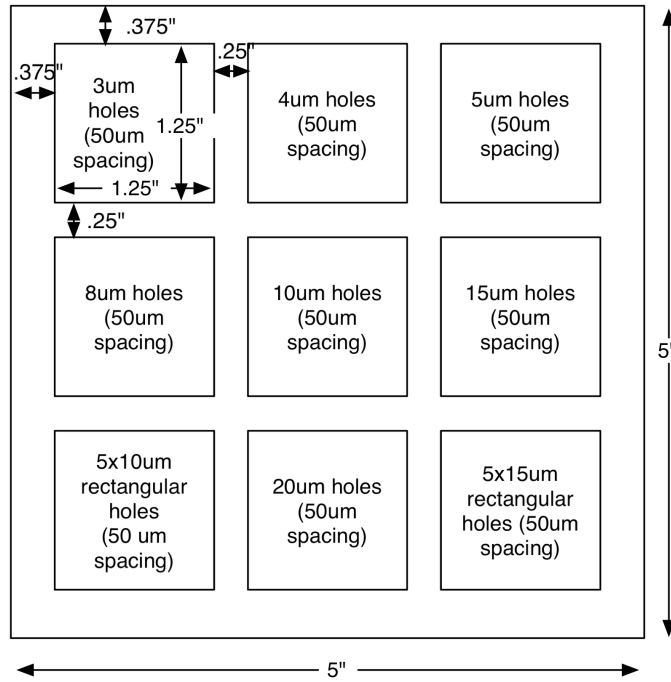


Figure A.2: "Swiston Mask 2" design.

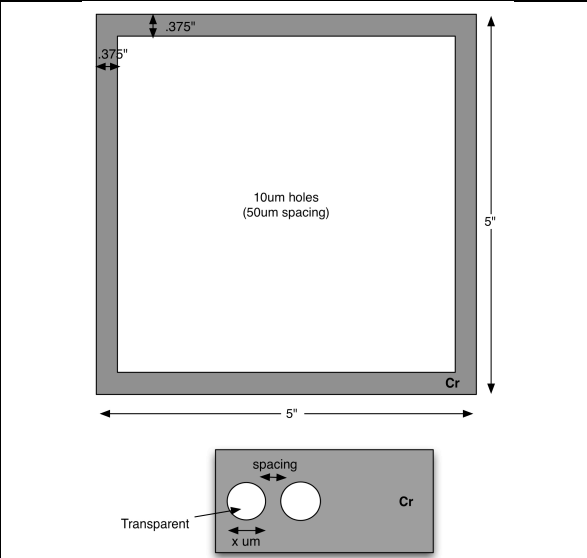


Figure A.3: "Swiston Mask 3" design.

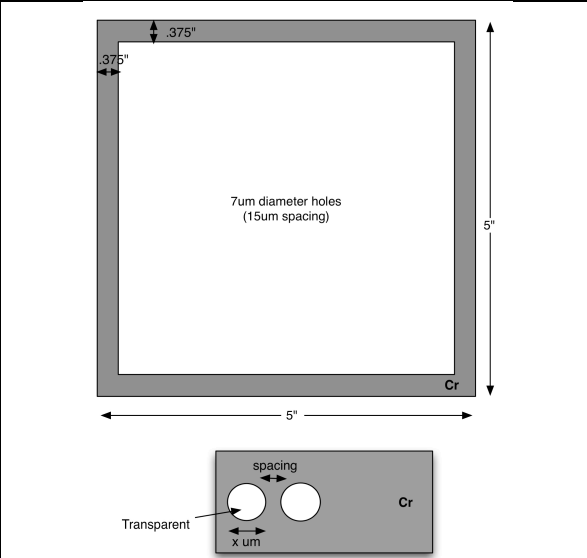


Figure A.4: "Swiston Mask 4" design.

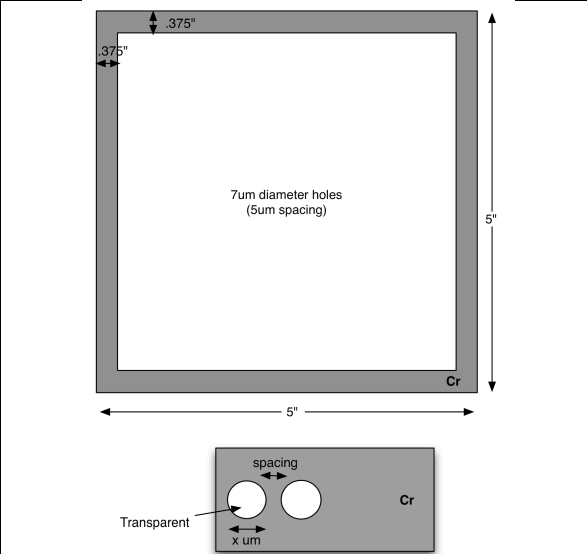


Figure A.5: "Swiston Mask 5" design.

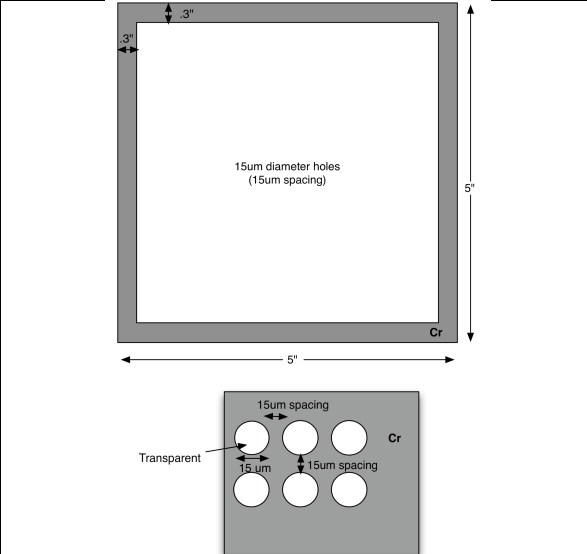


Figure A.6: "Swiston Mask 6" design.

Appendix B: Batch ID Definitions

Below is a list of Batch ID codes used throughout this work (but not in this written thesis), and the corresponding multilayer systems to which they refer.

Brief comments and notes are also included.

<i>Batch ID</i>	<i>Film</i>	<i>Comments and Notes</i>
L1	(PAH) ₁ (PAA3/PAAm3) ₁₀ (HA3/FITC-CHI) ₃	Exposure time = 4min 60s acetone liftoff
L2	(PAA3/PAAm3) ₁₀ (HA3/FITC-CHI) ₃	2min dip for CHI
L3	(PDAC4/SPS4) _{15.5} slide (PAA3/P4VP3) _{10.5} (HA3/FITC-CHI) _{3.5}	All 15,2,1,1 dips, pH3 water rinses P4VP 200k MW, 10mM
L4	(PDAC4/SPS4) _{15.5} slide (PAA/PEG) ₁₀ (HA3/FITC-CHI) _{3.5}	PEG .1% (1g/L) 20k MW PAA 90k MW
L5	(PDAC4/SPS4) _{15.5} slide (PAA/PEG) ₂₀ (HA3/FITC-CHI) _{3.5}	PAA = 90k MW PEG 20k MW
L6	(PDAC4/SPS4) _{15.5} slide (PAA/PEG) ₁₀ (HA3/FITC-CHI) _{3.5}	PAA = 450k MW, .01M PEG = 20k MW, .1%
L7	(PDAC4/SPS4) _{15.5} slide (PAA/PEG) _{10.5} (PAH3/SPS3) _{5.5} (HA3/FITC-CHI) _{3.5}	PAA = 450k MW incubated with CH27 cells, removed with PBS
L8	(PDAC4/SPS4) _{15.5} slide (PAA/PEG) _{10.5} (PAH3/SPS3) _{5.5} (HA3/FITC-CHI) _{7.5}	
L9	(PDAC4/SPS4) _{15.5} slide (PAA/PEG) _{10.5} (PAH3/SPS3) _{7.5} (HA3/FITC-CHI) _{7.5}	
L10	(PEG-silane glass slide) (PAA/PEG) _{10.5} (PAH3/SPS3) _{5.5} (HA3/FITC-CHI) _{3.5}	
L11	(PDAC4/SPS4) _{15.5} slide (PAA/PEG) _{10.5} (PAH3/SPS3) _{9.5} (HA3/FITC-CHI) _{3.5}	
L12	Si wafers treated with .5% PEG-silane in meOH (pg89,Notebook3) for 1h (PAA/PEG) _{10.5} (PAA/PEG) _{10.5} (PAH3/SPS3) _{5.5}	Removed half of slides to deposit (PAH/SPS), do ellipsometry on both
L13	(PDAC4/SPS4) _{15.5} slides (PAA/PEG) _{25.5} (PAH3/SPS3) _{9.5} (HA3/FITC-CHI) _{3.5}	Fantastic lift-off in PBS
L14	Plain glass slide (PDAC4/SPS4) _{15.5} (PAA/PEG) _{25.5} (HA3/FITC-CHI) _{3.5}	To test if diffusion layer needed to test PEG-silane treatment post-dep.
L15	(PDAC4/SPS4) _{15.5} slides and (PDAC4/SPS4) _{15.5} Si wafers glass slides: (PAA/PEG) _{x.5} (PAH3/SPS3) _{9.5} (HA3/FITC-CHI) _{3.5} Si wafers: (PAA/PEG) _{x.5}	X = 12,14,16,18,20,22 to test x needed for lift-off Zeiss dipper
L16	Plain glass slides (PDAC4/SPS4) _{15.5} (PAA/PEG) _{25.5} (PAH3/SPS3) _{9.5} (HA3/FITC-CHI) _{3.5}	to test PEG-silage treatment post-dep.

L17	(PDAC4/SPS4) _{15.5} Si wafers (PAA/PEG) _{x.5}	X = 12,13,14,15,16,17,18,19,20 Made in Spin dipper
L18	(PDAC4/SPS4) _{15.5} slides (PAA/PEG) _{20.5} (PAH3/SPS3) _{9.5} (HA3/FITC-CHI) _{3.5}	Made in spin dipper Some pre-mature lift-off during acetone step
L19	Plain glass slides (PDAC4/SPS4) _{15.5} (PAA/PEG) _{20.5} (PAH3/SPS3) _{9.5} (HA3/FITC-CHI) _{3.5}	Made in static dipper, except for HA/CHI stack
L20	(PDAC4/SPS4) _{15.5} slides (PAA/PEG) _{20.5} (PAH3/SPS3) _{9.5} (HA3/FITC-CHI) _{3.5}	For cell work, 7/5/07
L21	Plain glass slides (PDAC4/SPS4) _{15.5} (PAA/PEG) _{x.5} (PAH3/SPS3) _{9.5} (HA3/FITC-CHI) _{3.5}	For lift-off experiments, post dep. PEG-silane treatment
L22	(PDAC4/SPS4) _{15.5} slides (PAA/PEG) _{20.5} (PAH3/SPS3) _{x.5} (HA3/FITC-CHI) _{3.5}	For cell lift-off experiments Variable # of diffusion barrier layers x=[1,9]
L23	Plain glass slides, air plasma treated after lithographic develop. (PDAC4/SPS4) _{15.5} (PAA/PEG) _{x.5} (PAH3/SPS3) _{9.5} (HA3/FITC-CHI) _{3.5}	200mTorr air pressure, 15s, HI setting for lift-off experiments, like L21 x = [15,20]
L24	PEG-silane coated slides, patterned, then plasma cleaned to remove PS (PDAC4/SPS4) _{15.5} (PAA/PEG) _{20.5} (PAH3/SPS3) _{9.5} (HA3/FITC-CHI) _{3.5}	150mTorr air pressure, 15s, HI setting for cell experiments
L25	Plain glass slides, air plasma treated after lithographic develop. (PDAC4/SPS4) _{15.5} (PAA/PEG) _{20.5} (PAH3/SPS3) _{x.5} (HA3/FITC-CHI) _{3.5} + PEG-Silane (0.5% in meOH for 1h)	For variable diffusion layer liftoff exp
L26	Plain glass slides, air plasma treated after lithographic develop. (PDAC4/SPS4) _{15.5} (PAA/PEG) _{20.5} (PAH3/SPS3) _{9.5} (HA3/FITC-CHI) _{3.5} + PEG-Silane (0.5% in meOH for 1h)	For PBS liftoff timecourse
L27	PEG-silane coated slides, patterned, then plasma cleaned to remove PS (PDAC4/SPS4) _{15.5} (PAA/PEG) _{20.5} (FITC-PAH3/SPS3) _{9.5}	For cell experiments w/ streptavidin-biotin, also to check lift-off of L24
L28	(PDAC4/SPS4) _{15.5} slides (PAA/PEG) _{20.5} (PAH3/SPS3) _{15.5} (SPS3/FITC-PAH3) ₅ (PAA/PEG) _{20.5} (PAH3/SPS3) _{15.5} (SPS3/FITC-PAH3) ₁₀ (SPS/PAH-biotin) _{3.5}	For cell experiments w/ streptavidin-biotin
L29	Plain glass slides plasma ashed, patterned (PDAC4/SPS4) _{15.5} (dry) (PAA/PEG) _{25.5} (dry) (FITC-PAH3/SPS3) _{15.5} (CHI3.0/HA3.0) ₃	
L30	(PDAC4/SPS4) _{15.5} slides 1 slide: (PDAC4/SPS4) _{15.5} (PAA/PEG) _{25.5} (FITC-PAH3/SPS3) ₁₀ (PAH-biotin3/SPS3) _{5.5} 2 slides: (PDAC4/SPS4) _{15.5} (PAA/PEG) _{25.5} (FITC-PAH3/SPS3) ₁₀ (CHI3.0/HA3.0) ₃	Used spin dipper to deposit 10% substituted PAH-biotin+100mM NaCl

L31	(PDAC4/SPS4) _{15.5} slides 3 slides: (PAH3/SPS3) _{5.5} (CMC4/CHI4) ₁₅ (FITC-PAH3/SPS3) ₁₀ (PAH-biotin3/SPS3) _{5.5} 2 slides: (PAH3/SPS3) _{5.5} (CMC4/CHI4) ₁₅ (FITC-PAH3/SPS3) ₁₀ (CHI3.0/HA3.0) ₃	To test liftoff via enzymatic degradation of CMC w/ cellulase Used spin dipper to deposit 10% substituted PAH-biotin+100mM NaCl
L32	(PDAC4/SPS4) _{15.5} slides 3 slides: (CMC4/CHI4) ₁₅ (FITC-PAH3/SPS3) ₁₀ (CHI3.0/HA3.0) ₃	Premature liftoff during acetone sonication – do NOT soak in water before this step
L33	(PDAC4/SPS4) _{15.5} slides (PAA/PEG) _{30.5} (FITC-PAH3/SPS3) _{10.5} (CHI3.0/HA3.0) ₃	Repeat of L30 expt
L34	(CMC4/CHI4) _{9.5} (FITC-PAH3/SPS3) ₁₀ (CHI3.0/HA3.0) ₃	
L35	(PDAC4/SPS4) _{15.5} slides 4 slides: (PAA/PEG) _{20.5} (dry 30min) (FITC-PAH3/SPS3) _{10.5} (CHI3.0/HA3.0) ₄	
L36	Plain glass slides plasma ashed, patterned, ashed 15s (PDAC4/SPS4) _{15.5} (PAA/PEG) _{20.5} (dry) (FITC-PAH3/SPS3) ₁₀ (CHI3.0/HA3.0) ₃	Timecourse
L37	Plain glass slides plasma ashed, patterned, ashed 15s (PDAC4/SPS4) _{15.5} (PAA/PEG) _{20.5} (dry)(FITC-PAH3/SPS3) ₁₀	Baking Expt
L38	(PDAC4/SPS4) _{15.5} slides (PAA/PEG) _{20.5}	
L39	(PDAC4/SPS4) _{15.5} slides (PAA/PEG) _{25.5}	
L41	(PDAC4/SPS4) _{15.5} slides (PAA/PEG) _{x.5} (FITC-PAH3/SPS3) ₁₀ (CHI3.0/HA3.0) _{3.5}	PEG 400k X = [8:2:16]
L42	(PDAC4/SPS4) _{15.5} slides (PAA/PEG) _{12.5} (FITC-PAH3/SPS3) ₁₀	PEG 400k Fell off bar during dipping
L43	(PDAC4/SPS4) _{15.5} slides (PAA/PEG) _{x.5}	PEG 100k X = [14:2:22]
L44	(PDAC4/SPS4) _{15.5} slides (PAA/poly1) _{15.5}	
L45	(PDAC4/SPS4) _{15.5} slides (PAA/poly1) _{10.5} (FITC-PAH5.1/SPS5.1) ₁₀	
L46	(PDAC4/SPS4) _{15.5} slides (PAA/PEG) _{15.5} (FITC-PAH3/SPS3) ₁₀	PEG 100k
L47	(PDAC4/SPS4) _{15.5} slides (PMAA/PEG) _{x.5} (FITC-PAH3/SPS3) ₁₀	PMAA = poly(methacrylic acid) PEG 100k X = [20:2:28] and [5:2:13]
L48	(PDAC4/SPS4) _{15.5} slides (PMAA/PEG) _{7.5} (FITC-PAH3/SPS3) ₁₀ (CHI3.0/HA3.0) _{3.5}	Tried varying EDC xlinking []'s: 1,10,100mM for 5 min
L49	(PDAC4/SPS4) _{15.5} slides (PMAA/PEG) _{x.5} (FITC-PAH3/SPS3) ₁₀	X = [6,8,9,10]
L50	(PDAC4/SPS4) _{15.5} slides (PMAA/PEG) _{10.5} (FITC-PAH3/SPS3) ₁₀	100mM EDC xlinking for 5,15,30,60,300min
L51	(PDAC4/SPS4) _{15.5} slides (PMAA/PEG) _{7.5} (FITC-PAH3/SPS3) ₁₀ (CHI3.0/HA3.0) ₃	
L52	(PDAC4/SPS4) _{15.5} slides (PMAA/PEG) _{7.5} (FITC-PAH3/MNP4) ₁₀ (CHI3.0/HA3.0) ₃	FerroTec 705 anionic nanoparticles at pH4 D~10nm. Used .5ml in 400mL H2O, approx .005% (w/v)

L53	(PDAC4/SPS4) _{15.5} slides (PMAA/PEG) _{7.5} (FITC-PAH3/MNP4) ₁₀ (CHI3.0/HA3.0) ₅	
L54	(PDAC4/SPS4) _{15.5} slides (PMAA/PEG) _{7.5} (FITC-PAH3/MNP4) ₁₀ (CHI3.0/HA3.0) ₅	Mask 1 pattern
L55	(PDAC4/SPS4) _{15.5} slides (PMAA5/PVCL5) _x	For x=[10:10:50]
L56	(PDAC4/SPS4) _{15.5} slides (PMAA5/PVCL5) _{70.5} (FITC-PAH3/MNP4) ₁₀ (CHI3.0/HA3.0) ₃	PVCL = 1.8kDa
L57	(PDAC4/SPS4) _{15.5} slides (PMAA5/PVCL5) _{50.5}	PVCL = 1.8kDa
L58	(PDAC4/SPS4) _{15.5} slides (PMAA5/PVCL5) _{x.5}	PVCL = 6h synthesized X = [43.5,45.5:5:60.5]
L59	(PDAC4/SPS4) _{15.5} slides (PMAA2/PVCL2) _{x.5} (FITC-PAH3/MNP4) ₁₀	PVCL from polysciences, MW=354kDa X=[15.5:5:35.5] Made in the static dipper
L60	(PDAC4/SPS4) _{15.5} slides (PMAA3/PNIPAAm) _{x.5} (FITC-PAH3/MNP4) ₁₀	Release region Made in the spin dipper-
L61	(PDAC4/SPS4) _{15.5} slides (PMAA3/PNIPAAm) _{x.5} (FITC-PAH3/MNP4) ₁₀	Release region made in spin dipper X = 70.5, 80.5, & 90.5
L62	(PDAC4/SPS4) _{15.5} slides (PMAA3/PNIPAAm) _{40.5} (Amino QD5/SPS5) ₆₀	5/14/08
L63	(PDAC4/SPS4) _{15.5} slides (PMAA3/PNIPAAm) _{x.5} (FITC-PAH3/MNP4) ₁₀	X=62,64,66,68

Table B.1: List of Batch IDs and the corresponding multilayer film system built.